

Campbell, Eimear (2018) *Applications of ultrasonic technology: an investigation into the impact on fluid saturated rock*. PhD thesis.

<https://theses.gla.ac.uk/8782/>

Copyright and moral rights for this work are retained by the author

A copy can be downloaded for personal non-commercial research or study, without prior permission or charge

This work cannot be reproduced or quoted extensively from without first obtaining permission in writing from the author

The content must not be changed in any way or sold commercially in any format or medium without the formal permission of the author

When referring to this work, full bibliographic details including the author, title, awarding institution and date of the thesis must be given

APPLICATIONS OF ULTRASONIC  
TECHNOLOGY: AN INVESTIGATION INTO  
THE IMPACT ON FLUID SATURATED ROCK

Eimear Campbell

A thesis for the degree of Doctor of Philosophy (PhD)

Submitted to the College of Science and Engineering,  
University of Glasgow

February 2018



# Abstract

With dwindling worldwide petroleum supplies, there is an ever increasing pressure on the oil industry to develop new reservoir recovery mechanisms or maximise the effectiveness of those currently utilised. Fluctuations of reservoir recovery as a result of nearby seismic activity has been observed, initiating a range of studies into what is causing this effect. The generation of ultrasonic wave fields due to the dispersion of seismic wave fields as they travel through saturated porous rock has been shown, both analytically and experimentally. The feasibility of these generated ultrasonic waves being capable of this observed modification to reservoir is investigated. For the initial stage of this research, the feasibility of changing the behaviour of fluid in rock using an ultrasonic field is considered.

Research into the interaction between acoustic waves, the porous rock and the pore fluid indicates two key areas of permeability enhancement - increasing rock permeability and modifying the fluid behaviour within the pores. By increasing the permeability of the rock, previously unobtainable sources may be recovered and less energy would be necessary to obtain these reserves. Cavitation erosion or localised rock weakening due regions of high stress resulting from complex internal wave interactions are the two mechanisms proposed to increase permeability.

Modification of the relative fluid behaviours within the rock as a result of mechanical agitation of the fluid from peristaltic transport and cavitation bubbles generated due to the acoustic field was explored.

Sandstone cores saturated partially with tap water were placed in a degassed fluid and a low or high acoustic field applied. Tensile strength measurements are taken following exposure to the acoustic field and measurements compared to control samples. Samples were weighed prior to and following testing to determine fluid and gas motion between the surrounding fluid and pore volume.

Samples exposed to the low amplitude acoustic pressure field showed no change in tensile strength when compared to control samples. The high pressure acoustic field caused samples to have an increase of strength when compared to the control batch of samples. The partial saturation of the samples exposed to the acoustic pressure field showed an increased in mass following exposure. An exchange of gas bubbles trapped within the pores and fluid with the surrounding degassed water explains this mass increase during testing.

# Contents

<b>Abstract</b>	<b>i</b>
<b>Nomenclature</b>	<b>1</b>
<b>1 Introduction and Aim of Thesis</b>	<b>1</b>
1.1 Introduction . . . . .	1
1.2 The Petroleum Reservoir . . . . .	2
1.2.1 Reservoir Rock . . . . .	2
1.2.2 Petroleum generation . . . . .	3
1.2.3 Migration . . . . .	3
1.2.4 Petroleum constituents . . . . .	4
1.3 Oil and gas recovery . . . . .	4
1.3.1 Primary recovery . . . . .	4
1.3.2 Secondary Recovery . . . . .	7
1.3.3 Tertiary Recovery . . . . .	8

1.4	An ideal reservoir . . . . .	9
1.4.1	Reservoir Rock . . . . .	9
1.4.2	Reservoir Fluid . . . . .	11
1.5	Basis for research . . . . .	14
1.5.1	Waves and Reservoirs . . . . .	14
1.6	The Acoustic Wave . . . . .	15
1.6.1	Wave properties . . . . .	17
1.6.2	Wave Linearity . . . . .	19
1.6.3	Ultrasonic Waves . . . . .	20
1.6.4	Seismic Waves . . . . .	20
1.6.5	Generation of Ultrasonic waves from Seismic waves . . . . .	22
1.7	Previous Laboratory Research . . . . .	23
1.7.1	Reservoir Testing . . . . .	25
1.8	Summary . . . . .	25
<b>2</b>	<b>Ultrasonic Generated Mechanisms</b>	<b>32</b>
2.1	Stress Generated Fragmentation . . . . .	32
2.1.1	Background . . . . .	33
2.2	Cavitation . . . . .	39
2.2.1	Cavitation Generation . . . . .	41

2.2.2	Cavitation effects in Reservoir applications . . . . .	49
2.3	Ultrasonic Setup . . . . .	50
2.4	Summary . . . . .	52
<b>3</b>	<b>Material Properties</b>	<b>54</b>
3.1	Acoustic and Mechanical properties . . . . .	54
3.1.1	Material Properties . . . . .	55
3.1.2	Acoustic Properties . . . . .	57
3.1.3	Material Failure . . . . .	58
3.2	Physical Properties . . . . .	65
3.2.1	Porosity . . . . .	65
3.2.2	Permeability . . . . .	66
3.3	Fluid Properties . . . . .	67
3.3.1	Fluid Density and Buoyancy . . . . .	69
3.3.2	Surface Tension and Inter-facial Tension . . . . .	69
3.3.3	Reservoir Rock and Sandstone Samples . . . . .	70
3.4	Summary . . . . .	72
<b>4</b>	<b>Sample Testing</b>	<b>73</b>
4.1	Sample Characterisation . . . . .	73
4.1.1	Compressive Strength Test . . . . .	73

4.1.2	Tensile Strength Test . . . . .	76
4.1.3	Young's Modulus . . . . .	78
4.1.4	Poisson's Ratio . . . . .	78
4.2	Physical Property Testing . . . . .	79
4.2.1	Permeability . . . . .	80
4.3	Measured Sample Parameters . . . . .	86
4.4	Summary . . . . .	87
<b>5</b>	<b>Finite element analysis and Model Validation</b>	<b>88</b>
5.1	Finite Element Analysis . . . . .	88
5.1.1	FEA Assumptions . . . . .	90
5.2	The Model . . . . .	90
5.2.1	Material Properties . . . . .	91
5.2.2	Boundary Conditions . . . . .	96
5.3	FEA Model Validation . . . . .	99
5.3.1	Vibration analysis . . . . .	103
5.3.2	The Hydrophone . . . . .	110
5.3.3	Acoustic Characterisation . . . . .	117
5.3.4	Cavitation . . . . .	119
5.4	Chapter Summary . . . . .	126

<b>6</b>	<b>Results</b>	<b>127</b>
6.1	Statistical Significance . . . . .	127
6.1.1	Significance Testing . . . . .	128
6.2	Discussion . . . . .	132
6.2.1	Mass Lost . . . . .	135
6.3	Conclusions . . . . .	138
6.3.1	Tensile Strength Measurements . . . . .	138
6.3.2	Pore Fluid Loss . . . . .	140
6.3.3	Conclusion . . . . .	141
<b>7</b>	<b>Further Work</b>	<b>144</b>
7.1	Fluid behaviour with a Cavitation Field . . . . .	144
7.1.1	Background . . . . .	144
7.1.2	Reservoir Fluids and Saturation Fluids . . . . .	145
7.2	Visual Observations . . . . .	146
7.3	Findings . . . . .	151
7.3.1	Further Work . . . . .	153
	<b>References</b>	<b>154</b>

# List of Tables

1.1	Oil densities . . . . .	14
3.1	Material properties of Sandstone . . . . .	71
3.2	Material properties of Dolomite . . . . .	71
3.3	Material properties of Limestone . . . . .	71
3.4	Material properties of Reservoir Rock . . . . .	71
4.1	Material properties calculated from compression test for the Locharbriggs sandstone in accordance with ASTM standard . . . . .	87
5.1	Material properties used in FEA . . . . .	95
5.2	Element size used for FEA . . . . .	96
6.1	Data Analysis for Tensile strength of the samples treated with 5 $\mu\text{m}$ ultrasonic pressure field compared to the control . . . . .	134
6.2	Statistical Output for Data Analysis for Tensile strength of the samples treated with 5 $\mu\text{m}$ ultrasonic pressure field compared to the control . . . . .	134
6.3	Data Analysis for Tensile strength of the samples treated with 2.5 $\mu\text{m}$ amplitude ultrasonic pressure field compared to the control . . . . .	134



6.4	Statistical Output for Data Analysis for Tensile strength of the samples treated with 2.5 $\mu\text{m}$ amplitude ultrasonic pressure field compared to the control . . .	135
6.5	Data Analysis for Mass Lost of the samples treated with with 5 $\mu\text{m}$ amplitude ultrasonic pressure field compared to the control . . . . .	136
6.6	Statistical Output for Data Analysis for Mass Lost of the samples treated with with 5 $\mu\text{m}$ ultrasonic pressure field compared to the control . . . . .	136
6.7	Data Analysis for mass gain of the samples treated with 2.5 $\mu\text{m}$ amplitude ultrasonic pressure field compared to the control . . . . .	138
6.8	Statistical Output for Data Analysis for Mass gain of the samples treated with 2.5 $\mu\text{m}$ amplitude ultrasonic pressure field compared to the control . . . . .	138
7.1	Fluid properties of light and heavy mineral oils . . . . .	146
7.2	Fluid properties of the saturation fluids used for testing at room temperature	146
7.3	Rapeseed oil saturated sandstone sample behaviour when exposed to a cavitation bath over time . . . . .	148
7.4	Comparison of response of various fluid saturated samples with time . . . . .	148

# List of Figures

1.1	Material segregation within a reservoir . . . . .	5
1.2	Comparison between grain sizes for porosity . . . . .	10
1.3	Response of oil and water wet rock to an oil droplet . . . . .	12
1.4	Surface tension at a fluid interface . . . . .	13
1.5	Disturbance orientation and resulting wave progression for a longitudinal and transverse wave . . . . .	27
1.6	Response of matter to a sinusoidal acoustic wave . . . . .	28
1.7	Wave propagation in terms of time and distance . . . . .	29
1.8	Wave travelling from one medium into another . . . . .	30
1.9	Comparing the progression of a linear and non-linear wave . . . . .	31
2.1	Typical shock wave pressure field created with time . . . . .	34
2.2	Compressive, tensile and shear stress generation as a result of the angle of force application . . . . .	35
2.3	Process of spallation . . . . .	37
2.4	Process of circumferential Squeezing . . . . .	38

2.5	Comparison of the generation and behaviour of stable and transient cavitation	40
2.6	Phase diagram of an ideal fluid [1]	43
2.7	Contact angle associated with Heterogeneous Cavitation, taken from [1]	45
2.8	Forces experienced by a cavitation bubble within a sinusoidal acoustic field	46
2.9	Comparison between Focused and Planar ultrasonic transducer face and resulting wave field	50
2.10	Ultrasonic horn types	51
2.11	Comparison between focused and planar transducer	51
2.12	General transducer, ultrasonic transducer and horn configuration	52
3.1	Forces applied during confined and unconfined testing	60
3.2	Shear and Normal stresses generated in a sample [2]	61
3.3	Generalised rock failure envelope [3]	62
3.4	Alternating stress field generated during fatigue	63
3.5	Typical S-N curve showing the fatigue limit	64
3.6	Failure envelopes for different porosity values [4]	66
3.7	Flow of fluid through a sample of a given permeability	67
3.8	Rock strength change with addition of fluid [3]	68
3.9	Rock strength with relation to Pore Fluid Pressure [5]	68
4.1	Compressive strength samples with strain gauges attached	74

	xii
4.2 Stress - strain curve for sample . . . . .	75
4.3 Perpendicular and parallel crack positioning relative to the applied force . . .	76
4.4 Sample following failure stage . . . . .	77
4.5 Sample before and after indirect tensile strength test . . . . .	78
4.6 Samples placed in vacuum chamber with saturation fluid . . . . .	81
4.7 Experimental setup for hydraulic pressure application . . . . .	81
4.8 Sample mounted within membrane in the chamber . . . . .	82
4.9 Hydraulic pressures applied to the sample . . . . .	82
4.10 Pressures applied through saturation stage of the permeability experiment . .	84
4.11 Saturation B-value with increasing cell pressure . . . . .	84
4.12 Pressures applied through the consolidation stage of the permeability experiment	85
4.13 Pressures applied through the permeability stage of the permeability experiment	86
5.1 Stresses generated on each plane in 3 axis . . . . .	93
5.2 Simplistic diagram of 4 elements (black lines) and 9 nodes (red dots) . . . . .	95
5.3 Symmetry boundary conditions . . . . .	98
5.4 FEA model of the Characterisation tank and test tank (not to scale) . . . . .	101
5.5 Cavitation bubbles generated at the horn surface at high amplitudes with cavitation regions highlighted by the arrow . . . . .	103
5.6 The doppler effect . . . . .	105
5.7 Typical LDV configuration . . . . .	106

5.8	Experimental configuration for the 1D/ 3D LDV . . . . .	108
5.9	Displacement of 20 kHz horn showing the longitudinal mode . . . . .	109
5.10	Typical LDV configuration . . . . .	110
5.11	Amplitude of vibration at horn tip in relation to the amplitude in at transducer power generator . . . . .	111
5.12	Frequency analysis of Pressure measurements from an alternative 20 kHz horn, showing sub-harmonics and harmonic measurements . . . . .	114
5.13	Frequency analysis of voltage recorded from the 20 kHz horn . . . . .	115
5.14	Plot of cross section of the pressure field measured using the Hydrophone (right) and calculated using FEA (left) . . . . .	116
5.15	Comparison of axial scan of the Pressure field radiated from the centre of the horn calculated using FEA and measured using the Hydrophone . . . . .	116
5.16	Pressure measured at a fixed point of 40 mm from the ultraonic source with increasing amplitude of transducer power source . . . . .	117
5.17	Pressure field comparison of the transducer amplitude in the characterisation bath . . . . .	118
5.18	Pressure field generated in the fluid of the test tank . . . . .	119
5.19	Calculated maximum axial stress generated with the sandstone during testing with corresponding maximum axial acoustic pressure generated . . . . .	120
5.20	Stress field generated in the sandstone as a result of the pressure within the test tank . . . . .	120
5.21	Calculated maximum acoustic pressure generated with the test tank for $2.5 \mu$ m and $5 \mu$ m input . . . . .	121
5.22	Cavitation clusters evident within the Cavitation vessel with regions of cavitation activity highlighted by orange arrows . . . . .	121

5.23	Cavitation erosion of aluminum foil . . . . .	122
5.24	NPL Cavimeter . . . . .	123
5.25	Recordings from the Cavimeter . . . . .	125
6.1	Normal distribution of standard deviations around the mean . . . . .	128
6.2	Distribution of normalised tensile strength measurements for the Control Batch 1 samples . . . . .	129
6.3	Fisher distribution of variances, highlighting the 0.05 level of significance in which the data must sit in to be considered valid . . . . .	131
6.4	Comparison of Average Tensile Strengths and 95% confidence levels between samples treated with 5 $\mu\text{m}$ ultrasonic field compared to the control batch . .	133
6.5	Comparison of Average Tensile Strengths and 95% confidence levels between samples treated with 2.5 $\mu\text{m}$ amplitude ultrasonic pressure field and the control batch . . . . .	135
6.6	Comparison of Average Mass Gain and 95% confidence levels between samples treated with with 5 $\mu\text{m}$ amplitude ultrasonic pressure field ultrasonic field and the control batch . . . . .	136
6.7	Comparison of average mass gain and 95% confidence levels between samples treated with 2.5 $\mu\text{m}$ amplitude ultrasonic pressure field and the control batch	137
6.8	Cavitation erosion evident during testing . . . . .	141
7.1	Experimental set-up for an optimum cavitation field . . . . .	147
7.2	Filter from transient cavitation exposure of sandstone samples saturated with the three saturation fluids, after three amplitudes of BIP . . . . .	149
7.3	Control vs Transient Cavitation bath exposure of Plaster samples. Note: control sample is on the left . . . . .	150

# Nomenclature

Symbol	Definition
$p_{ac}$	Acoustic pressure
$H_1$	Alternate hypothesis
$A_d$	Amplitude at distance d
$A_i$	Amplitude initial
$\theta$	Angle of fracture plane
$F$	Applied force
$A$	Area
$\alpha$	Attenuation coefficient of material
$\varepsilon_a$	Axial strain
$P_b$	Back Pressure
$B$	Bulk modulus, or modulus of elasticity
$m_{testing}$	Change in mass following overall testing
$m_e$	Change in mass following ultrasonic exposure
$\delta P_p$	Change in pore pressure
$\Delta l$	Change of length
$V_P$	Compressional wave velocity
$F_c$	Compressive force
$C_0$	Compressive strength
$\sigma_c$	Compressive stress
$P_c$	Confining pressure
$T_c$	Constant Temperature
$T_C$	Critical temperature
$A_{cs}$	Cross-sectional area
$\rho$	Density
$D$	Diameter
$y$	Displacement in y direction
$d$	Distance
$\delta x$	Distance travelled in direction $x$

$m_d$	Dry mass
$\mu_d$	Dynamic Viscosity
$\sigma_{eff}$	Effective stress
$z$	Elevation
$G_e$	Equivalent Shear Modulus
$P$	External Load Vector
$m_d$	Final dry mass
$E_g$	Free gas expansion
$E_o$	Free oil expansion
$E_w$	Free water expansion
$f$	Frequency
$g$	Gravitational Acceleration
$\sigma_H$	Horizontal stress
$G$	Hydrophone Sensitivity
$Z_i$	Impedance of material i
$p_i$	Instantaneous localised pressure
$I$	Intensity
$I$	Intensity of light 1
$I_i$	Intensity of the incident wave
$I_r$	Intensity of the reflected wave
$\gamma_i f$	Interfacial tension
$p_i$	Interior bubble pressure
$I$	Internal Load vector
$\varepsilon_l$	Lateral strain
$L$	Length
$l$	Length in the transverse direction
$\alpha_s$	Level of Significance
$m$	Localised mass
$v_l$	Longitudinal
$M$	Mass Matrix
$m_{absorbed}$	Mass of fluid absorbed
$m_r$	Mass remaining in the sample
$P_{max}$	Maximum pressure or amplitude of the wave
$x_i$	Mean of sample
$W_g$	Net gas withdrawal
$W_o$	Net oil withdrawal
$W_w$	Net water withdrawal
$H_0$	Null hypothesis



$N$	Number
$p_o$	Original pressure
$R$	Outer bubble radius
$x$	Partial position
$r_1$	Path length of beam 1
$k$	Permeability
$\nu$	Poisson's ratio
$C_{pv}$	Pore volume contraction
$\phi$	Porosity
$Pr$	Power
$p$	Pressure
$dV$	Pressure Change
$p(R)$	Pressure in the liquid at the bubble boundary
$\delta P_c$	Pressure Increment
$p_a$	Pressure variation due to the acoustic wave
$\dot{R}$	Rate of change of bubble radius
$\delta L_a$	Rate of Change of Length a
$\mu_m$	Sample mean
$n$	Sample Size
$m_s$	Saturated mass
$T_s$	Saturation Temperature
$M_S$	Shear modulus
$\tau$	Shear stress
$v_s$	Shear wave speed
$h$	Soil cohesion value
$c$	Speed of sound
$M_{ij}$	Stiffness coefficient
$C$	Stiffness tensor
$\epsilon$	Strain
$\sigma$	Stress
$R$	Stress Ratio
$s$	Standard Deviation
$S$	Surface Tension
$F_t$	Tensile force
$TS$	Tensile Strength
$q$	The rate of flow
$r$	Throat dimension
$T$	Time period

$\delta t$	Time taken
$P_v$	Vapour Pressure
$s^2$	Variance
$U$	Velocity Component Amplitude
$\sigma_V$	Vertical stress
$\mu$	Viscosity
$V_p$	Volume of pores
$V_m$	Volume of solid matrix
$V$	Volume of the fluid
$V_v$	Volume of void
$I_w$	Water influx
$r$	Wave Beam Path
$c_o$	Wave Speed
$\lambda$	Wavelength
$E$	Young's modulus

# Chapter 1

## Introduction and Aim of Thesis

### 1.1 Introduction

Statistics show an increasing demand for petroleum with 2017 showing a global growth of oil consumption of 1.3% per annum [6]. Petroleum has become an essential part of the modern world for daily operation from an individual level to the global industry. The earth's petroleum supply is far from endless. By the end of 2015 the world proven oil reserves had reached 1697.6 billion barrels [7]. This finite quantity of remaining oil highlights the fact that we are fast approaching a potential global shortage. This emphasises the need for research into alternative oil recovery methods.

Once currently utilised mechanisms of oil recovery have been incorporated, it is estimated that over 60% of the original oil in place still remains within the reservoir [8]. Enhancing the initial stages of recovery or devising a means of obtaining of this remaining petroleum could further extend the global supply.

Correlation between seismic activity and increased reservoir recovery has been observed, indicates the potential for improved oil yields using acoustic wave technology. One method of simulating an acoustic effect similar to that experienced in a reservoir as a result of seismic activity is by applying an ultrasonic acoustic field. This investigation aims to introduce, explain the association between the seismic wave and ultrasonic wave then explore the possible applications of an ultrasonic field and analyse its effectiveness in oil recovery operations through laboratory based experiments. There is a wide range of promising mechanisms which

may arise as a result of an ultrasonic field on fluid saturated porous media, representative of a saturated oil reservoir, which could aid reservoir recovery. The aim of this thesis is a preliminary study into these mechanisms and their effects on the porous media and saturation fluid at ambient pressures and temperatures to validate the progression of studies at more realistic reservoir simulated conditions.

This chapter outlines the current problems preventing optimum reservoir recovery and touches on the technologies and processes which are relevant to the investigation. Generation of oil within a reservoir is discussed, describing the mechanisms involved in its formation and progression to recovery. There is an introduction to acoustic fields with particular consideration of ultrasonic wave fields. The generation of ultrasonic waves within a reservoir and the methods which have been theorised and observed within the laboratory and on site are outlined. A contrast between these theories and studies is drawn up for the progression of the study.

## 1.2 The Petroleum Reservoir

### 1.2.1 Reservoir Rock

Petroleum is the second most abundant fluid in the outer layers of the earth after water. The word petroleum originates from the Greek words 'petra' which means rock, and 'eleon' meaning oil. The recovery of petroleum from the earth's sub-surface is associated with sedimentary rock which is formed due to the accumulation of rock matter eroded from upland regions. This eroded rock matter, or sediment, is broken down during transportation by gravity to lower areas of land where they settle and accumulate. This region of sediment accumulation is known as a sedimentary basin. In transportation the rock pieces get further broken down and smoothed off. Within the sedimentary basin, these pieces are sorted according to size by the varying strengths of the currents and wave action causing larger heavier rock pieces to fall below the lighter. The increasing mass during this process of sediment accumulation continues over tens or even hundreds of millions of years. As it continues the lower, older layers are slowly loaded by younger ones. This causes much of the water to be gradually squeezed out from between the grains and the sediment becomes harder and eventually forms solid coherent rock in a process called induration. Induration occurs as a result of the earth's thermal energy and overburden pressure. This sediment accumulation occurs at a rate of roughly 0.1 mm a year or 100 m in 1 million years making it an extremely slow and gradual process [9].

### 1.2.2 Petroleum generation

Petroleum is formed as a result of the earth's heat on the remains of microscopic animal life such as algae, plankton and bacteria which are incorporated and preserved within the sedimentary rock as it is formed. The types and amount of petroleum which is generated depends on the nature of the remains of the living organisms, the quantity of organic matter and the extent to which the matter has been heated and pressurised through burial. In order for this organic material to be preserved during early burial it must be protected from oxidation or consumption from other lifeforms. Preservation of these remains of organic matter takes the form of an anoxic, or oxygen deficient environment which prevents the process of decomposition. A common environment which provides these ideal conditions is one enclosed in a fine grained sedimentary mud, most commonly found in large lakes or sea beds. Where this anoxic fine grained mud contains an abundant supply of inorganic material and the burial process by sedimentary build up occurs, the generation of petroleum can begin. The same thermal temperatures and overburden pressures which act on the sediment and cause it to indurate will modify the material properties of the inorganic material eventually creating petroleum, or oil and gas. Not all of the inorganic material which is present in the source rock gets converted into petroleum, about 70 % at best [10]. During the induration process this fine grained sedimentary mud forms shale rock. This shale rock where the petroleum is formed is referred to as source rock.

### 1.2.3 Migration

Migration occurs within the source rock as a result of the high pressure beneath the surface generated by the millions of tonnes of overlying rock and the earth's natural heat in the reservoir. These high pressures and temperatures expand any gases that might be contained within the oil. Movement of the oil and gas from where it is generated can be categorised into two stages; primary and secondary migration.

Where generated, the oil and gas is spread too thinly in the source rock to be exploitable as it is unable to flow quickly enough through the compact source rock to a region where it can be recovered. Migration is a slow process by which the oil and gas percolates through the tight impervious source rock as minute droplets and accumulates. Not all oil or gas that is generated manages to move through the pore spaces or successfully leave the source rock. Expulsion efficiency will depend on the mobility of the generated oil and the characteristics of the surrounding source rock whose pore diameters range from 0.05 to 0.1  $\mu m$  in diameter [11]. This part of the process is known as primary migration.

Secondary migration occurs once the oil and gas have made their way out of the source rock and into the surrounding less restrictive sedimentary rock, possessing a pore diameter from about 0.03 to 2  $\mu m$  [11]. From here, the oil and gas travels through the fine channels and pore spaces of the rock, alongside water trapped during induration and fills the more permeable channels. The ease at which this fluid can flow through is determined by the rock and fluid properties. The high pressure causes the oil and gas to percolate upward through the water due to differing densities. This oil and gas will continue to travel upward until a surface is reached or they become trapped by an impermeable layer of rock which prevents further migration. Where this occurs, the oil and gas will accumulate in a region of porous rock where they are essentially trapped. This region of trapped oil and gas is what is referred to as a reservoir.

#### 1.2.4 Petroleum constituents

Petroleum exists as a mixture of molecules made up of carbon and hydrogen in varying quantities known as hydrocarbons. Oxygen, nitrogen, sulphur and metals may be present in a single crude oil at proportions which dictate the wide range of properties and materials which are observed. Petroleum can be broken down from heavier into lighter molecules due to the temperature and pressure conditions within the reservoir in a process known as cracking. Cracking breaks down hydrocarbons from long chains into simpler molecules as a result of high temperatures or pressures.

Water almost always co-exists

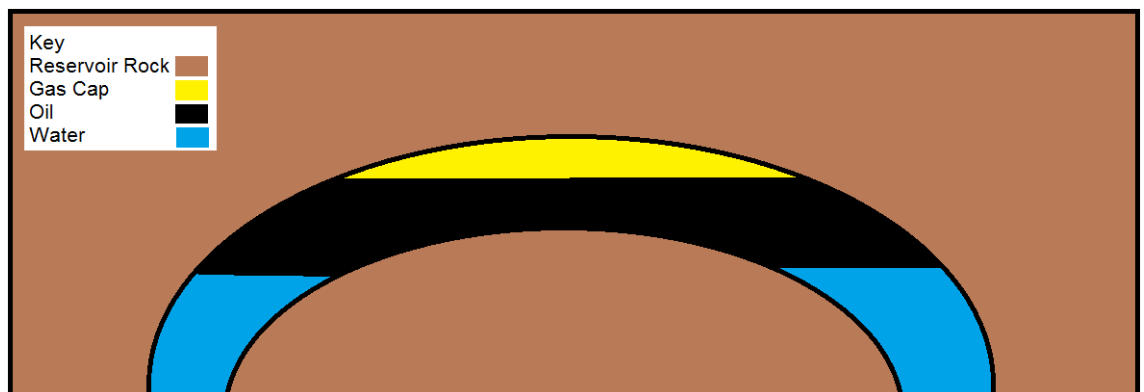


Figure 1.1: Material segregation within a reservoir

### 1.3 Oil and gas recovery

Oil and gas recovery is performed in various stages in order to obtain the maximum amount of petroleum which is available from a reservoir. Primary, secondary and potentially tertiary recovery processes are performed, depending on the type of reservoir and economic viability.

#### 1.3.1 Primary recovery

Primary reservoir recovery involves using the naturally existing high reservoir pressures to drive the petroleum to the surface where it can be collected [10]. During this primary recovery, the way in which the various fluids and gases behave in response to this pressure differential drives the oil to the surface. It is important to understand the interactions which are occurring. There are three driving methods which can occur within a reservoir; compaction drive, gas cap expansion drive or water drive methods.

The conservation of mass equation dictates that the reservoir must sit in a state of material balance. The material balance equation has been devised by a number of researchers for initially saturated volatile and black oil reservoirs [12–15] in terms of free gas expansion  $E_g$ , free oil expansion  $E_o$ , free water expansion  $E_w$ , water influx  $I_w$ , pore volume contraction  $C_{pv}$ , net gas withdrawal  $W_g$ , net oil withdrawal  $W_o$  and net water withdrawal  $W_w$  as shown in Equation 1.1.

$$E_g + E_o + E_w + I_w + C_{pv} = W_g + W_o + W_w \quad (1.1)$$

The free gas, oil and water expansions of a reservoir are directly related to the original volume of each product and the expansion properties of each product. As the reservoir depletes and the volume of each product falls, the remaining product expands to occupy the previously occupied volume.

Pore volume contraction is related to the pore volume of the reservoir and the rock formation expansion properties. These expansion properties are inversely related to the compressibility of the reservoir.

The water influx water drawn into the reservoir from an underlying nearby aquifer which replaces the produced fluids. Water influx into a reservoir almost always takes place at some

rate during reservoir production to some degree. Whether water is also produced depends on the location of the reservoir recovery point to the oil water or gas water contact.

The net gas, oil and water withdrawal dictate the cumulative gas, oil and water produced, less any product which is re-injected to enhance recovery.

Reservoir recovery will be dominated by one or a combination of these mechanisms in order to obtain a combination of gas, oil and water. The material balance equation (1.1) shows that an increase of free gas, oil, water expansion, pore volume contraction or water influx will result in an increased gas, oil or water recovery.

### **Compaction drive**

The least common reservoir drive method is compaction drive, a predominant mechanism of a reservoir which is fully sealed or closed off to surrounding rock. During compaction drive recovery, the pores within the reservoir collapse and the pore fluids expand as the pressure falls. A reservoir most likely to exhibit this mechanism is one with elevated pore volume or rock compressibility, up to 50 times greater than normal. The compressibility of a rock is a function of reservoir pressure.

### **Gas cap drive**

A reservoir containing free gas is likely to exhibit gas cap drive. During gas cap expansion drive the falling pressure during recovery causes any gas dissolved within the body of oil to percolate upward to accumulate in a pool known as the gas cap. This gas cap will progressively expand as the pressure falls during recovery, lowering the gas solubility of the saturation fluids, causing the gas to leave. This pushes the gas-oil contact downward and forces the oil through the reservoir into the well. This process tends to occur if the reservoir is limited in extent and there is not therefore a good supply of oil. Where these conditions exist, the gas cap can enhance oil recovery considerably.



## **Water drive**

A water drive reservoir is characterised by an unsealed reservoir connected to a body of free water such as aquifers. In a water drive the water layer which sits below the oil column moves up from beneath as oil is depleted, pushing the oil water contact upward. Since this upward push will result in low force, it will only be effective if the reservoir is regionally extensive. The pressure of the reservoir is heavily dependent on the rate of intake of water to the volumetric rate of fluid withdrawn from the reservoir. If the reservoir producing rate is too high for the influx of water then the process will stop. As the oil and gas are recovered the pressure in the reservoir falls until it is insufficient to drive any further oil and gas to the surface. At this point primary recovery ceases and another stage of recovery must be employed.

### **1.3.2 Secondary Recovery**

As primary recovery methods naturally subside, secondary recovery can be implemented to further increase the yield. The most practical way to further increase the recovery yield is by modifying the material balance of the reservoir by increasing the free gas, free oil, free water, pore volume or water influx as shown in Equation 1.1. Secondary recovery methods have been defined as "the injection of (fluids) after the reservoir has reached a state of substantially complete depletion of its initial content of energy available for (fluid) expulsion or where the production rates have approached the limits of profitable operation" [16].

It has been estimated that between 75 - 90% of the overall oil available in a reservoir still remains after primary recovery [17,18]. At this point an alternative driving source known as the secondary recovery mechanism can be incorporated. Secondary recovery relies on the supply of external energy into the reservoir to maintain the pressure driving the oil and gas to the surface. This pressure can be maintained by injecting water beneath the oil column or pumping additional gas in to provide extra drive to force the oil to the surface. This re-injection essentially mimics the natural drive mechanisms present in primary recovery. Alternatively the permeability, or ease of flow of fluid through the rock can be increased by fracturing the reservoir in a process known as fracking. It can be performed by injecting a high pressurised liquid into the reservoir to create fractures in the rock. The appropriate driving mechanism will be applied depending on the specific reservoir suitability. The completion of secondary recovery is primarily dictated by economic criteria.

### 1.3.3 Tertiary Recovery

After primary and secondary recovery methods have been implemented, residual oil remains in the form of isolated droplets trapped in the pores of reservoir rock or as films around rock grains. It has been estimated that about 60 % of the original oil in place remains in a reservoir after primary and secondary recovery has been performed [19]. An effective further recovery process will mobilise these dispersed oil droplets and form an oil cluster that can move toward a region where it can be recovered. This needs to be accomplished both on a microscopic scale at pore level and on the macro scale to affect the largest possible volume of the reservoir.

Some unconventional processes include the pumping of detergents or steam into the reservoir. The detergent changes the interaction between the oil and the reservoir surface essentially loosening the oil held back in the pores. These detergents can be costly, more than the value of the oil which will be recovered; therefore the costs must be weighed up before performing. Steam injection can be used to aid the recovery of more viscous oils, which are difficult to shift from their position. Steam changes the interactions between the oil and the pores and enhances the recovery. Carbon dioxide can also be pumped down into the reservoir which will act as an additional gas cap drive.

Tertiary methods of recovery tend to create unfavourable side effects within the reservoir such as clogging from the residual by-products created as a result of the processes or infrastructure corrosion. Permeability of the rocks can decrease due to by products produced such as scales and precipitants [20]. Substantial set up costs along with the production down time associated with implementing these tertiary technologies often make tertiary recovery methods economically non-viable. Environmental issues are also brought into consideration, particularly where the storage of carbon dioxide is introduced [8]. Optimising recovery of the entire oil reservoir would increase efficiency of the oil recovery process in general. A larger quantity of oil would be recovered resulting in a more attractive cost in to cost out ratio.

## 1.4 An ideal reservoir

We know from the material balance equation that increasing the free gas, free oil, free water, pore volume or water influx will yield a greater amount of gas, oil and water, creating a more efficient reservoir. Further, expulsion efficiency of a reservoir will depend on the mobility of the generated oil and the characteristics of the surrounding rock. In order to achieve a better method of recovery, additional understanding of the processes and mechanisms occurring

naturally within a reservoir in a more localised scale is essential.

### 1.4.1 Reservoir Rock

In order for a reservoir to be effective for oil recovery it should hold several properties:

- High permeability
- High porosity
- Sufficient size to generate enough oil

These properties correspond to an high pore volume, water influx or oil, gas and water yield.

The ease of fluid or gas flow throughout the rock is measured as permeability, a characteristic of the rock itself. A high permeability material will allow a more rapid flow of fluid or gas. In addition to flow through pores in the rock, permeation can occur through inter-granular space or cracks in the reservoir. The unit of permeability ( $q$ ) with SI units  $m^2$  is calculated using Darcy's law. Darcy's law describes the rate of flow of fluid per unit area ( $A$ ) in a length squared ( $l^2$ ) as a result of a pressure gradient applied to the porous media. The rate is a physical property of the rock (Equation 1.2) showing a dependence on fluid density ( $\rho$ ), pressure ( $p$ ), gravitational acceleration ( $g$ ), elevation ( $z$ ), and dynamic viscosity ( $\mu_d$ ). It should be noted that this is an idealistic representation of a reservoir. In nature there are many variables which can arise such as a naturally existing clay or mineral deposit within a reservoir, decreasing the permeability and modifying the pore fluid interactions.

$$\frac{q}{A} = -\frac{l^2}{\mu_d} grad \cdot (p - \rho \cdot g \cdot z) \quad (1.2)$$

The porosity of the reservoir is the proportion of the rock which is free of solid rock material. It is related to the grain size of the sediment which was involved in the generation of the rock. Larger grains will result in a larger porosity as shown in Figure 1.2 which gives more space or channels for the fluid to flow within the rock. Additionally, the degree of sorting of the grains of sand by the tides prior to induration will influence the porosity of the rock. Sorting occurs as a result of varying density grains and surrounding transporting fluid with sufficiently high velocity currents or flows to carry grains. The transporting fluid can move the smaller grains and leave the larger heavier grains behind. Where wave or wind energy is

concerned such as beach sands the sorting tends to be high as opposed to in slow moving streams. A poorly sorted accumulation of grains will contain grains of various sizes where smaller grains will fill the spaces in amongst the larger grains, leaving less space. Rounding of the grains also impacts the porosity, with a more rounded series of grains providing less pore space. Rounding occurs as a result of the abrasive nature of the transportation process of the grains.

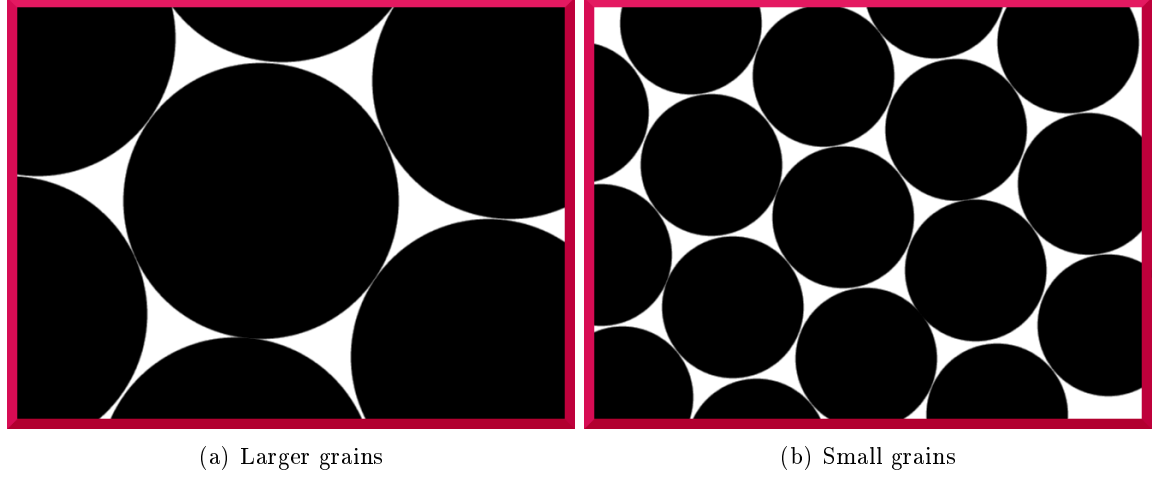


Figure 1.2: Comparison between grain sizes for porosity

The presence of pores within a reservoir provides the pathway for fluid flow and the quantity is described by the porosity ( $\phi$ ). The nature of the pores within the reservoir is a function of permeability ( $k$ ) and pore throat dimension ( $r$ ) as shown in Equation 1.3.

$$k \propto r\phi^2 \quad (1.3)$$

#### 1.4.2 Reservoir Fluid

The fluid properties can affect the permeability characteristics of the reservoir. In order for the fluid in the reservoir to be easily recoverable it must possess the appropriate properties within its environmental conditions. Since water, oil and often gas exist alongside each other within the reservoir, there is a wide range of reactions and forces interacting. As oil migrates the pore spaces are not left empty as another fluid moves in to take its place, either gas or water. The way in which these fluids move in the reservoir is determined by the interacting forces [21], governing the production rates and the overall yield.

In a saturated reservoir the oil, water and gases are intermixed and dispersed. At low oil

saturations the oil exists as a series of minute isolated droplets. If the droplets are too small and dispersed over too large an area they are more difficult to recover than clusters as they require additional energy to overcome the forces holding them in place [22,23] and become immobile within the reservoir [23,24]. These oil droplets The mechanisms which prevent the oil from moving through the reservoir can be categorised under capillary and gravitation forces.

Another cause of low reservoir mobility is a result of the petroleum constituents. Asphaltene is a molecular substance found in petroleum which causes problems during recovery when it precipitates due to decreasing pressure associated with primary recovery or when oil mixes with an injected solvent during tertiary reservoir recovery [25] or during drilling, acid stimulation or hydraulic fracturing. It can exist in suspension floating within the oil phase or deposited onto the rock surface and can cause problems with reservoir recovery by plugging the well bore tubing and valve, or coat the surfaces of the equipment [26]. In suspensions within the reservoir, it imparts a high viscosity to the oil hindering oil recovery and when deposited can block pores from fluid flow or alter the rock wettability from water wet to oil wet. This precipitation can prove problematic to oil recovery.

### Capillary Forces

In a reservoir, capillary forces are the inter-molecular forces between the saturation fluids, gases and the adjacent rock surface. The capillary forces can be separated into three main interactions; wettability, interfacial tension and surface tension. They are brought about due to cohesive and adhesive forces. Molecules in a liquid state experience strong intermolecular attractive forces. When these forces are between like molecules, they are referred to as cohesive forces. For example, water molecules in a droplet are held together by cohesion. When the attractive forces are between unlike molecules such as the interaction between a water molecule and the side of a glass tube they are said to be adhesive forces.

Wettability of a solid describes the tendency of one fluid to spread onto or adhere onto its surface in the presence of other immiscible fluids. A reservoir rock can be either fluid neutral, water-wet or oil-wet. A droplet of oil suspended in water in contact with a rock surface will behave differently depending on if the rock is water or oil wet. If water wet, a film of water adheres to the surface of the pore wall, effectively reducing the diameter of the pores, shown in Figure 1.3(a). If oil-wet, the oil adheres to the surface of the pore wall, and is more difficult to move, as shown in Figure 1.3(b). A larger pressure gradient will be necessary to overcome oilwet rock so a reduction of this effect would be advantageous to oil recovery. Wettability can

be determined by grain roughness and shape or mineral composition and surface chemistry.

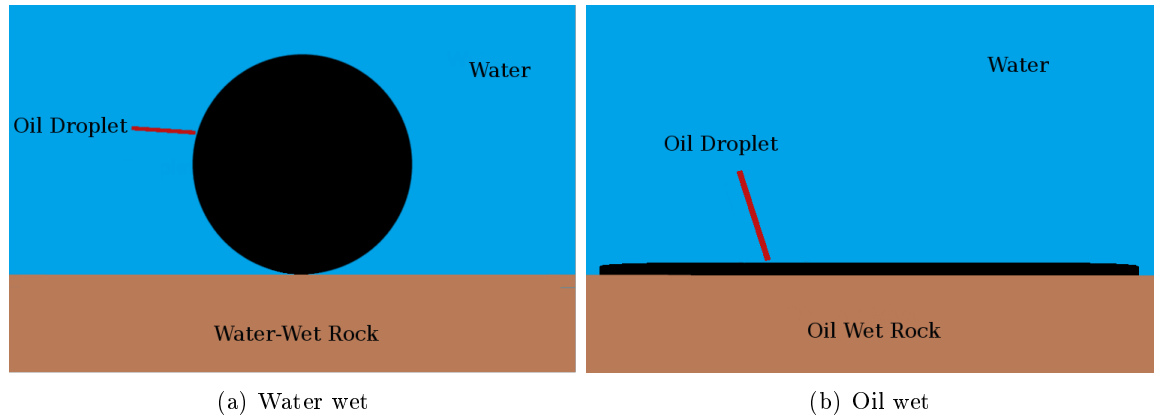


Figure 1.3: Response of oil and water wet rock to an oil droplet

Surface tension exists as a result of an imbalance of molecular forces. In a body of fluid exposed to a gas, each molecule within the bulk of the fluid has the same magnitude of force pulling it to every side, shown in Figure 1.4(a). Considering a molecule at the surface of this body of fluid the dominant forces acting on it are from the fluid below and either side, Figure 1.4(b). This causes the exposed molecules to be attracted more so toward the fluid molecules below as there is no opposing molecular draw from above, creating a packed layer of molecules. This surface layer of molecules acts as a thin film, providing the tensile strength on the fluid. This is a property determined by the pressure and temperature of the fluid and is important where oil or water and gas are interacting.

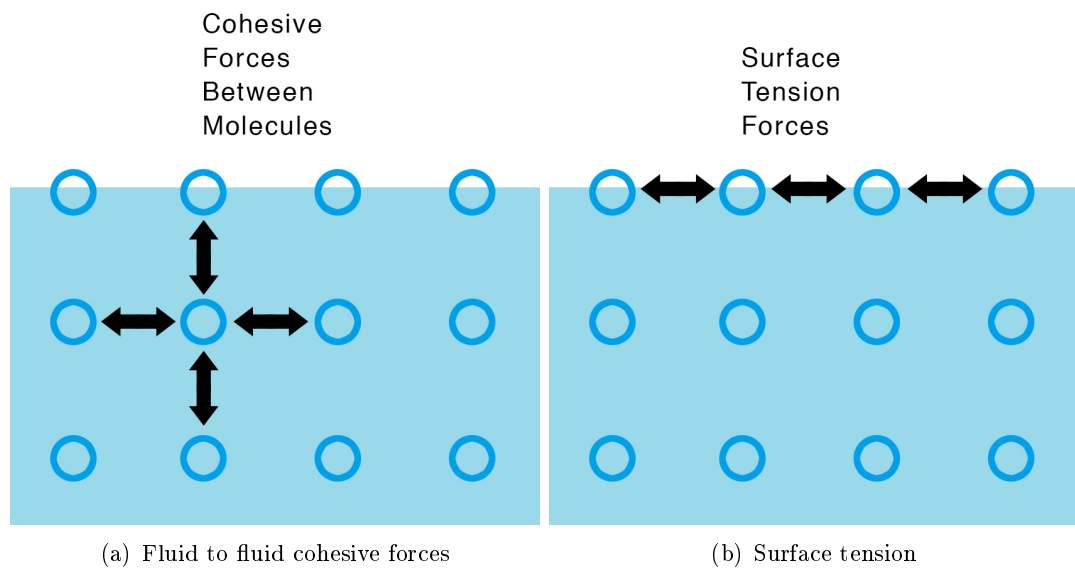


Figure 1.4: Surface tension at a fluid interface

Inter-facial tension forces are similar to surface tension forces in that they exist from an

imbalance of forces at an interface of two separate phases. They differ in that the interface is between two immiscible liquid phases. Fluids are said to be immiscible when they cannot mix together. The imbalanced molecules on the interface experience not only the cohesive forces from the body of the fluid below, but also forces from the second fluid. This results in a region of inter-facial tension. Inter-facial tension at a fluid-fluid interface is a reflection of the excess energy associated with under-saturated intermolecular interactions at the interface. This excess energy tends to drive interfaces to adopt geometries that minimise the inter-facial area which can modify, restrict or even block the space available in the pores for each fluid. Some enhanced oil recovery processes are designed to decrease the inter-facial tension between the fluids such as with the injection of detergents.

### Gravitation forces

Density also governs the ease of recovery of oil, with the denser oils often being abandoned, being deemed uneconomic to recover. The density of the oil is determined by the organic material from which it was made and the conditions it experienced throughout its generation.

Gravitational forces act on the different densities of the phases between the pore fluids and gases causing separation within the pores. An upward pressure is created by the buoyancy of the oil relative to the water saturated rock around it. The lower the density of the oil in relation to the surrounding water, the more buoyant it will be. If the buoyancy forces acting on the oil droplet cannot overcome the capillary forces holding it in place, the oil droplet will not migrate. If more oil is added, by coalescence of droplets for example, it may develop enough buoyancy to move again. A table of typical specific densities for various oil categories can be seen in Table 1.1. The specific density is the ratio of the density of the material relative to water. Typically most oil will lie within the defined 'Heavy' range.

Oil type	Specific Density
Light Oil	<780
Heavy Oil	780 - 934
Unrecoverable Oil	965+

Table 1.1: Oil densities

Referring to Darcy's law for permeability in Equation 1.2, the rate of flow is influenced directly by the fluids dynamic viscosity. A fluids' dynamic viscosity is a property which quantifies its resistance to flow. An example of a low and high viscosity fluid would be water and honey

respectively. The viscosity of petroleum is determined by the types of inorganic material from which it was made and the environmental conditions it has been exposed to throughout its generation and storage. An oil of high viscosity would require a higher quantity of energy to be mobilised. The dynamic viscosity of a fluid is a function of the pressure, temperature and specific gravity which is the density of the petroleum compared to water.

## 1.5 Basis for research

### 1.5.1 Waves and Reservoirs

Interest in vibroseismic reservoir stimulation spawned from the early 1950s where increased oil and water recovery was observed as a result of cultural noise and earthquakes. A seismic wave is a low frequency acoustic wave which travels through the earth's layers. Due to the low frequency nature of these waves, less energy is lost as they travel and have been shown to penetrate depths of up to 90 km into the earth's surface.

Natural rises in the water level of water bearing reservoirs known as aquifers have been observed in Florida due to seismic waves generated by earthquakes and bypassing trains, with the influence lasting up to 5 days [27]. It has been proposed that pore pressure may undergo variations under seismic wave exposure. In a field test of pore pressure a rise of factor 1.5 was observed at a depth of 2.2 m in response to seismic waves generated by a surface vibrator. This surface vibrator produced a maximum force of 400 kN at a frequency of 30 Hz [28]. In another instance pore pressure in a sedimentary layer was shown to increase by an order of magnitude at a depth of 3 - 6 m due to a nearby earthquake [29].

With regard to the effects of seismic activity on oil and gas reservoirs, there are various cases of observed response, but with no clear authoritative trend. Oil reservoirs have been shown to respond to seismic vibrations. Following an earthquake in 1938, increased oil production of up to 45 % was detected in a well in Northern Caucasus [30]. Variation of oil recovery was recognised in an oil field in California due to an earthquake in 1952 [31]. It was shown that some oil wells exhibited an increase in oil recovery while others showed no change. In the case of two neighbouring wells one showed an increase in recovery while the other showed a decrease. It was claimed that an increase in reservoir recovery rates as a result of low frequency vibrations on the surface was generated by additional localised pressure gradients in the oil layer. These were said to reduce interfacial tension and promote fluid flow. This in turn was claimed to improve the permeability, redistribute the gas, oil and water phases and



influence the relative permeabilities [32].

Research confirms that the mechanisms associated with earthquakes and man made seismic stimulations are very complex. Variations in oil or water production could be a consequence of not only seismic vibrations, but also rock fracturing and many other effects associated with earthquakes. These complex responses coupled with the lack of reliable observations of the seismic effect on oil and gas reservoirs [20] necessitates further investigation into the processes involved, however it does show that acoustic waves have a significant effect on oil reservoir recovery.

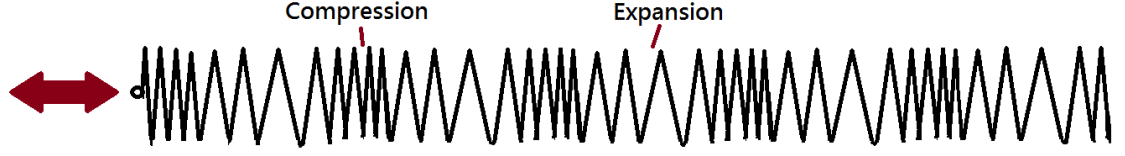
## 1.6 The Acoustic Wave

To investigate the optimal tertiary methods of oil extraction using ultrasonic technology, a base review of acoustics must be made including its various applications in many fields of science. Acoustics is the interdisciplinary science that deals with the production, control, transmission, reception and the effects of waves in gases, liquids and solids. The term "Acoustics" is derived from the Greek Akoustos, meaning "hearing".

Acoustic waves have been a subject of study since the 6th century BC when the ancient Greek philosopher Pythagoras investigated why musical notes sounded different to one another. By subdividing a string into segments he formulated a seven note scale based on these intervals. He found an answer in terms of numerical ratios representing the harmonic overtone series on a string, known as a scale [33]. Joseph Sauveur observed that "in string instruments and bells besides the principal sound, one hears the octave the fifth, the third etc." During extensive acoustic studies and after discovering the presence of nodal points within a vibrating string, Sauver came to the conclusion that for a vibrating string to continue vibrating, the overtones must always be integer multiples of the fundamental frequency, i.e. they must be harmonic [34].

When a disturbance or fluctuation from equilibrium occurs in an elastic medium such as air, water or rock, a wave is generated. The energy which was involved in producing the disturbance is transferred onto the surrounding media depending on the angle of disturbance and the surrounding medium. A wave can be transverse or longitudinal. A longitudinal wave results from a disturbance in the direction of the wave travel, shown in Figure 1.5(a). Longitudinal waves can travel in gases, liquids and solids. In contrast to a longitudinal wave, the disturbance for a transverse wave occurs perpendicularly to the direction of travel, as in

Figure 1.5(b). Transverse waves can only effectively propagate within a solid material and are relatively weak in comparison to longitudinal waves.



(a) Longitudinal wave



(b) Transverse wave

Figure 1.5: Disturbance orientation and resulting wave progression for a longitudinal and transverse wave

An acoustic wave is a type of longitudinal wave generated as a result of a disturbance such as a moving surface. This moving surface transfers its energy onto the surrounding particles. This is exhibited in Figure 1.6 showing a sinusoidal wave causing a fluctuation of the pressure from the resting atmospheric pressure to high pressure then low pressure states. The lower diagram shows the corresponding response of the molecules due to this pressure fluctuation. During the compressive stage the particles are forced together and a partial void is left where the original particles originally were, causing an area of negative pressure, or tension. As a result of this sinusoidal wave application, particles within the wave field will undergo a cycle of compressive states due to the positive pressure with respect to the atmospheric pressure and tensile states as a result of the negative pressure with relation to atmospheric pressure.

Acoustic waves vary in time and space. Considering the spatial progression of a wave in one dimension, temporal separation can be calculated using Equation 1.4 where  $\delta x$  is a distance travelled,  $\delta t$  is the time taken to travel the distance and  $c_o$  is the speed at which the wave is travelling. The speed of a wave travel in a material depends on the material properties of the medium in which it is travelling, specifically the bulk modulus, or modulus of elasticity  $B$  and the density,  $\rho$ . The speed of wave travel can be calculated using Equation 1.5.

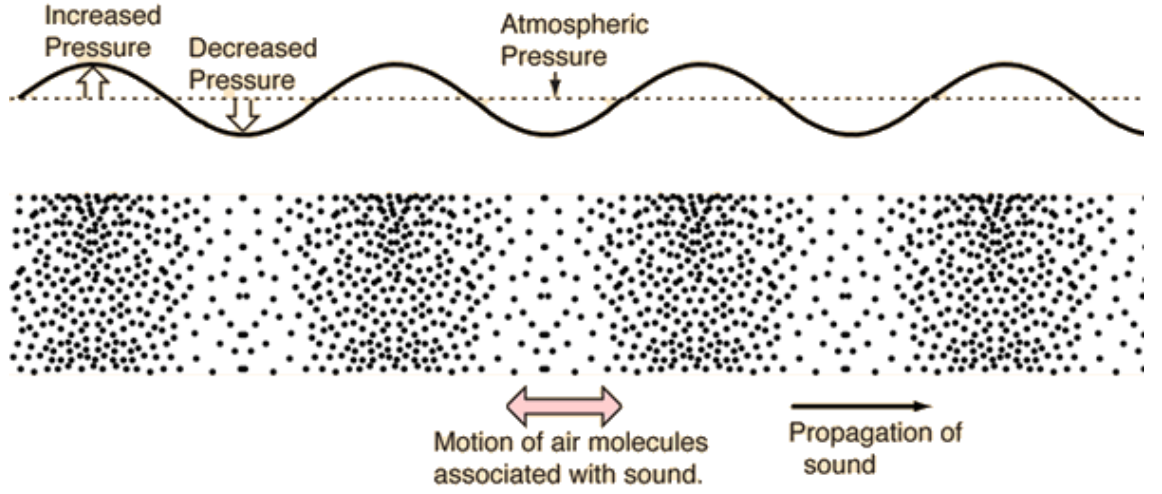


Figure 1.6: Response of matter to a sinusoidal acoustic wave

$$\delta x = \delta t \cdot c_o \quad (1.4)$$

$$c_o = \sqrt{\frac{B}{\rho}} \quad (1.5)$$

As an acoustic wave propagates, it affects the localised density which in turn affects pressure and particle velocity in the medium. An increase in local density will cause an increase in localised mass  $m$  within an area  $A$ , meaning a higher localised pressure,  $p_i$ , Equation 1.6. A particle can travel faster in a denser medium as the closer molecules can pass on the energy at a faster rate. The instantaneous localised pressure  $p_i$  is a sum of the original pressure  $p_o$  and the pressure variation due to the acoustic wave  $p_a$  travelling through. This can be calculated using Equation 1.6.

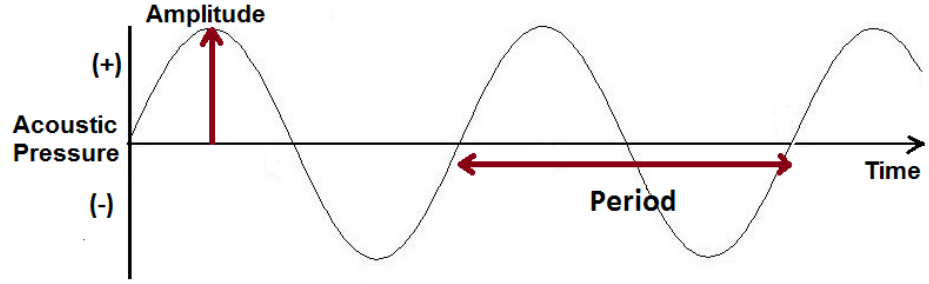
$$p_i = p_o + p_a \quad (1.6)$$

Acoustic pressure and density are related by the equations of state which can be seen in Equation 1.7, which shows that with a compressive wave the pressure will be positive, and with a tensile wave the pressure will be negative.

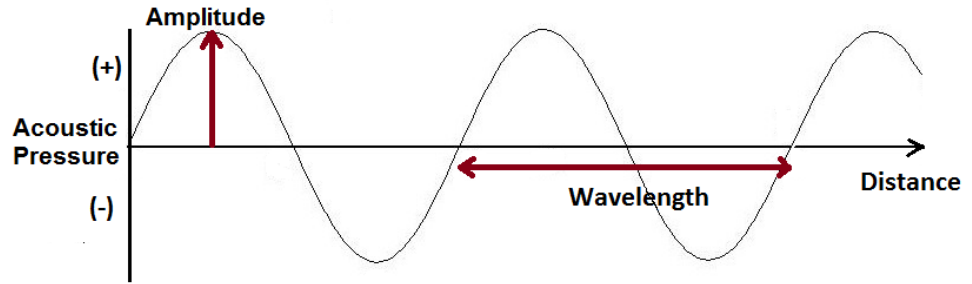
$$p_a = \rho_a c_o^2 \quad (1.7)$$

### 1.6.1 Wave properties

Various parameters can be used to characterise an acoustic wave. The maximum pressure or amplitude ( $P_a$ ) of the wave is shown in Figure 1.7 which indicates the amount of fluctuation of force of the wave per unit area in units of  $\frac{N}{m^2}$ , or Pascals (Pa).



(a) Wave progression with time



(b) Wave progression with distance

Figure 1.7: Wave propagation in terms of time and distance

The period ( $T$ ) of a wave is the time it takes for one cycle of the wave to pass a fixed point, and is related to the frequency by Equation 1.8. The speed of sound ( $c$ ) propagation in a material is related to the frequency and wavelength by Equation 1.9. The wavelength ( $\lambda$ ), as shown in Figure 1.9 is the distance travelled by the wave in one cycle. The frequency ( $f$ ) of the wave represents the number of pressure cycles per second in Hertz, or (Hz).

$$T = \frac{1}{f} \quad (1.8)$$

$$c = f\lambda \quad (1.9)$$

The impedance of the material,  $Z$  describes the ratio between the acoustic pressure amplitude in a medium to the resulting acoustic volume flow rate through a surface perpendicular to the direction of the acoustic wave. It is the measure of opposition or resistance of the medium to acoustic flow. It is determined by the materials density and wave velocity,  $c_o$ , and is calculated using Equation 1.10. The impedance describes the relation between the acoustic pressure and the particle velocity using Equation 1.11.

$$Z = \rho c \quad (1.10)$$

$$p_a = c_o Z \quad (1.11)$$

The intensity of a wave is the measure of the rate of work performed on a material, in units of Watts per square metre,  $W/m^2$ . The power,  $Pr$ , or rate at which energy is transferred and the cross-sectional area which is affected by the acoustic wave,  $A_{cs}$ , can be used to calculate the intensity,  $I$ , using Equation 1.12.

$$I = \frac{Pr}{A_{cs}} \quad (1.12)$$

With each cycle of a wave, a portion of the energy is absorbed and dissipated within the medium. Essentially, the wave is weakened as it propagates. Attenuation occurs as a result of absorption where the energy is converted into heat and scattering of the wave occurs as it encounters interfaces and reflected. The attenuation of a wave will depend on the attenuation coefficient of the material involved,  $\alpha$ . The amplitude of the incident wave,  $A_i$ , decreases with the distance travelled,  $d$ . The amplitude of pressure at a point,  $A_d$ , can be calculated using Equation 1.13.

$$A_i = A_d \cdot e^{-\alpha \cdot d} \quad (1.13)$$

When an acoustic wave reaches a boundary of a material of different properties, an exchange in energy will occur. When an acoustic wave travelling in material 1 which has an acoustic impedance,  $Z_1$ , meets material 2 with acoustic impedance,  $Z_2$ , part of the wave will be reflected and part will be transmitted across the boundary, shown in Figure 1.8. The exact

behaviour of this reflection and transmission will depend on the impedance of the materials either side of the boundary. The fraction of the intensity of the reflected wave,  $I_r$ , to the intensity of incident wave,  $I_i$ , can be calculated using Equation 1.14.

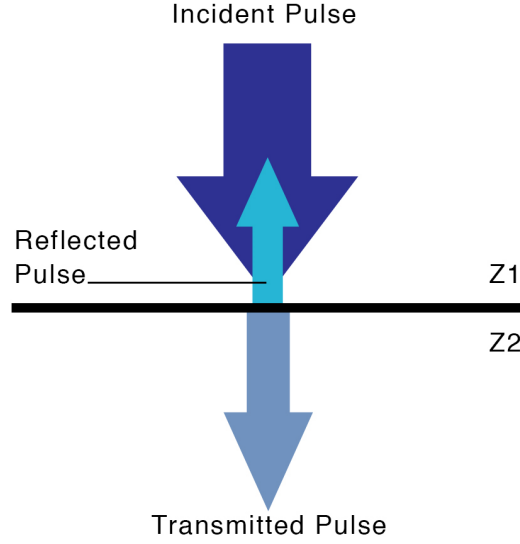


Figure 1.8: Wave travelling from one medium into another

$$\frac{I_r}{I_i} = \left( \frac{Z_2 - Z_1}{Z_2 + Z_1} \right)^2 \quad (1.14)$$

### 1.6.2 Wave Linearity

#### Linear waves

A linear system is one in which the input is directly proportional to the output. The generated wave is a direct linear relation to the driving source. The resulting disturbance oscillates with a frequency and wavelength in a linear or constantly relatable manner. It is approximately described using a linear equation, where in each term of the equation the dependent variable and its derivatives are at the most first degree and is relatively simple to solve. A wave equation for a one dimensional propagation with an undamped linear wave within an isotropic medium can be described using Equation 1.15. In this equation, the direction of travel is  $x$  and the displacement perpendicular to the direction of travel is  $y$ . Use of Linear equations can be solved using a much more simplistic method than a non-linear equation due to the limited number of unknowns and variables.

$$\frac{1}{c^2} \frac{d^2 y}{dt^2} = \frac{d^2 y}{dx^2} \quad (1.15)$$

### Non-linear Wave Effects

A non-linear system is one where the output is not directly proportional to the input. This can occur with acoustic waves at sufficiently high amplitudes within the medium of travel. As the acoustic wave propagates through a compressible material, the pressure causes an increase in the local density of the medium. Equation 1.5 shows that an increase in density is related to an increase in wave speed, so the particles in these regions of high density will travel much faster, particularly in the high pressure extreme of the sinusoidal wave. This change in speed will gradually result in a steeper waveform, becoming distorted and changing shape from a sinusoid to a sawtooth wave as shown in Figure 1.9. This change of wave shape indicates that the wave no longer consists of only one frequency, but several frequency components. This effect occurs in linear waves also, however the linear behaviour prevails. This is why non linearity only becomes apparent at large amplitudes or close to the acoustic source.

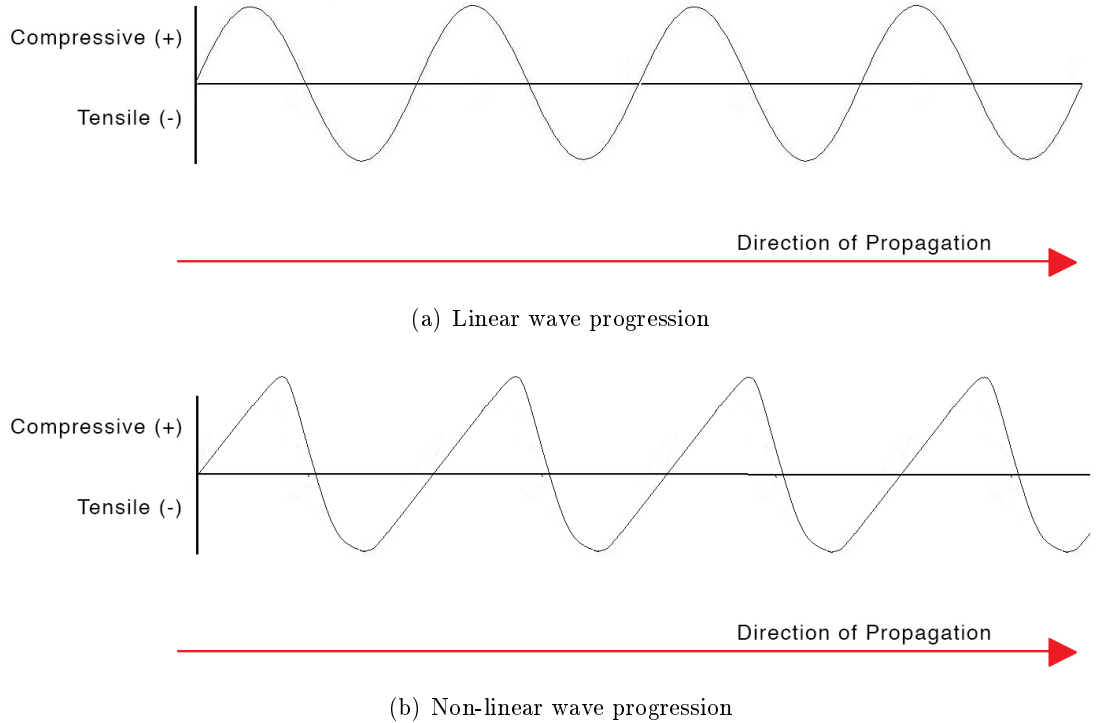


Figure 1.9: Comparing the progression of a linear and non-linear wave

### 1.6.3 Ultrasonic Waves

An ultrasonic wave is one which has a frequency above the upper threshold of human hearing, on average 20 000 cycles per second, or 20 kHz. Besides being used in nature as a means of communication between bats and frogs, ultrasound used for a wide range of technological applications ranging from welding to bone cutting.

Ultrasonic devices are often employed within technology as they have the advantage of being able to be applied in a non-invasive manner. An examples of this include a prenatal ultrasound scan, allowing visualisation of a foetus within the womb or ultrasonic non-destructive testing, allowing any air bubbles or fractures within a material to be detected. During the recent years there has been an increase in the application of ultrasonic technology as the understanding of its uses broadens.

### 1.6.4 Seismic Waves

A seismic waves is a type of sound wave, where the medium of travel is the earth. Measurements of seismic waves on the earth's surface led to the discovery of the earth's core and the eventual mapping of the layers of the earth. In a similar way which a prism refracts light at each face through which is passes, seismic waves bend, reflect and change speed at boundaries between the different materials.

There are four main layers to the earth which are categorised as the crust, mantle, outer core and inner core working from the surface inward. The crust is relatively thin and rocky, the mantle has the properties of a solute but can flow slowly and the cores are made of nickel and iron.

An earthquake is defined as any event which generates a seismic wave and can be caused by a range of events including the rupture of geological faults within the earth's crust, volcanic activity or landslides. Relative motion between the tectonic plates which make up the earth's crust generate 'tectonic earthquakes.' This interaction between tectonic plates during this type of earthquake can be compared to two solid rocks coming in contact with dissimilar directions of motion. The pressures generated on each rock as a result of the motion of the other will generate a sound and friction, as is generated during an earthquake.

Three types of seismic waves are generated during an earthquake; primary (P) waves, secondary (S) waves and surface waves. P and S waves travel within the earth's core and



are collectively known as 'body waves'. In contrast, surface waves travel only along the surface crust of earth.

P waves are known as compressional waves and travel fastest, at a speed of 1.5 - 8 km/s in the earth's crust shaking the ground in the direction which they are propagating. S waves are shear wave and travel roughly 1.7 times slower than P waves. They shake the surface perpendicular to the direction in which they are travelling. They are unable to travel through liquids as liquid media do not have enough shear strength to support wave propagation. Earthquake like seismic waves can also be caused by underground explosions or erupting volcanoes. The speed of P waves and S waves increases as they travel deeper into the mantle and the media of travel is denser. The waves travel through the Earth in curved paths, but they change direction suddenly when they pass through the boundary between substances in different states.

An earthquake itself can be split into two parts, the fault rupture itself which lasts between 10-30 seconds and the travel of the resulting seismic wave into the surrounding earth which has been recorded to be present for weeks following earthquake. It is difficult to state the exact duration of the seismic wave of an earthquake as this depends on how long the earthquake lasted and how the wave travels within the surrounding rock which depends on the internal reflections and presence of any resonances within the rock. Reflections and resonances would extend the duration of the seismic wave [35].

The amplitude of a seismic wave can be expressed in terms of the local magnitude or Richter magnitude, the surface wave magnitude, body wave magnitude and the moment magnitude. The body wave magnitude is that travelling through the earth's rock so is the most relevant to the application. The Richter magnitude scale is a logarithmic scale of amplitudes of waves recorded by seismographs. The surface wave measures the Rayleigh surface wave magnitude and is the national standard earthquake amplitude classification in the Peoples Republic of China. The body wave magnitude determines the amplitude of the initial P-wave. The moment magnitude or seismic moment is the standard earthquake reporting format of magnitude used by the United States Geological Survey. It measures the seismic moment of the earthquake, or shear modulus of the rock near the fault multiplied by the average slip on the fault and size of area that slipped.

#### **1.6.5 Generation of Ultrasonic waves from Seismic waves**

Ultrasonic waves have an extremely high attenuation, making them unsuitable as a directly applied technique for influencing reservoir behaviour from the earth's surface.

Seismic waves have a relatively low frequency, up to 10 Hz. Ultrasonic waves have a frequency of over 20 000 Hz. Seismic waves in fluid saturated earth materials have shown to disperse and attenuate in a broad range of frequencies, including ultrasonic frequencies. The presence of fluids in the pore space of rocks causes attenuation and dispersion by a mechanism broadly known as wave induced fluid flow (WIFF). As a wave passes through the fluid saturated rock a pressure gradient is caused generated within the fluid phase and the resulting movement of the fluid relative to the solid (known as the fluid flow) is accompanied with internal friction until the pore pressure is equilibrated. The theory involved in this dispersion process is extensive and falls out with the scope of work for this research.

Attenuation refers to the exponential decay of wave amplitude with distance; dispersion is a variation of propagation velocity with frequency. Attenuation and dispersion can be caused by a variety of physical phenomena that can be divided broadly into elastic processes, where the total energy of the wave-field is conserved scattering attenuation, geometric dispersion, and inelastic dissipation, where wave energy is converted into heat. Of particular interest to exploration geophysics is inelastic attenuation [36].

The use of ultrasonic waves generated as a result of seismic wave dispersion in saturated porous rock is therefore considered within the investigation. Investigations have demonstrated the presence of waves at ultrasonic frequencies as a result of seismic waves travelling within porous media. An advantage of using these generated ultrasonic waves is the non-preferential path of the wave, which can reach regions of the reservoir which would otherwise be isolated.

As already introduced, seismic activity has shown modifications to reservoir recovery. It is postulated that this is due to the minute pore sizes (0.05 to 2  $\mu m$ ) it is proposed that waves of similar size which is causing an effect at this level and causing these modifications. Presuming the wave speed within sandstone of 1500  $m/s$  [37] this corresponds to wave of a frequency range of 9600 to 240 MHz. The generation of ultrasonic frequencies as a seismic wave travels through porous rock has been observed experimentally [36, 38, 39] resulting in investigation into the mechanisms of generation. This has been shown mathematically through various methods for seismic waves in porous rock, and seismic waves in the fluid within the porous rock. The state of saturation has a large influence on the frequency of the generated wave, where frequencies 50-150 MHz were measured in Navajo Sandstone when dry, falling to 0.2-0.8 MHz when saturated [40].

'Long-wave-short-wave resonance' (LSWR) has drives the non-linear dispersion of seismic waves into higher frequencies at the grain boundaries and defects within elastic porous media [41]. LSWR is described using the 'Cosserat Double Continuum' which describes a double continuum of wave travel through granular media. A new variable, spin velocity of grains is

the foundation to the theory [42]. Grain rotation occurs within shear bands of the granular material, and depending on the velocity and phase of these micro-rotations of the long wave (low frequency) coupling into the short wave (high frequency) occurs [43–45]. These high frequencies generated within a reservoir are independent of one another and consist of a wide range of frequencies and velocities depending on the number and distribution of the cracks and the properties of the saturation fluid and rock matrix [40, 46–50]. LSWR has been mathematically derived to support experimental observations [44].

As previously mentioned, the generation of ultrasound within porous rock as a result of seismic wave interaction is a complex topic worthy of its own branch of investigation and lies outwith the scope of this project. It is the prospect of ultrasound being generated within a saturated reservoir which is key to this research.

## 1.7 Previous Laboratory Research

There has been vast laboratory research into the mechanisms suggested to enhance the recovery of oil as a result of ultrasonic wave exposure. The modes of application and resulting mechanism are the focus of investigation to gain insight into if and how these mechanism can be manipulated to further enhance oil recovery.

Modification of the rock permeability as a result of low frequency ultrasonic wave exposure has been observed through laboratory experiments. Oil percolation through a sample under a 20 kHz ultrasonic wave-field showed an increased flow when compared to percolation rates in its absence [51]. Similarly, an exposure of 26.5 kHz yielded an increase of water permeability of porous samples [52]. Samples prepared to a state of residual oil content (similar to that found in a reservoir once primary and secondary recovery) were pressurised and exposed to a 50 kHz cavitation bath exhibited a change in relative permeability of the samples to oil and water [19]. Relative permeability effects were claimed to be a result of changed of wettability by dislodging naturally existing deposits on the surface of the pore wall [53]. A change in wettability was mathematically derived where thermal energy facilitated a transition of a rock sample from oil wet to water wet [54]. Rock fracture between trapped or restricted pores and free flow will increase the permeability of the reservoir by increasing the pathways through the material [53]. Vibrations travelling along the pore channels cause deformations along the wall and peristaltic transport can be induced as a result. This may destroy the surface films across the pore boundaries reducing capillary forces, as shown with use of a 20 kHz ultrasonic source [55]. A decrease in clusters of a viscous molecular component of reservoir oil

as a result of ultrasonic irradiation of 20 kHz was demonstrated [56]. Displacement of fluids within core samples has been shown due to the exposure of ultrasonic wave fields. In a study of the displacement of oil with water in loose sand, an increase in displacement was observed under the exposure of 50-80 kHz, under a 6 hour exposure [57]. Applied to oil saturated porous rock, the displacement of oil by water was observed after an exposure of 6-9 hours of 1-1.5 MHz application, with an increase in displacement with decreasing oil viscosity [46]. The displacement of mineral oil and kerosene with a brine solution under ultrasound and in its absence was observed under ultrasonic frequencies of 20-40 kHz. Ultrasound application resulted in either an improvement or deterioration of production depending on the applied conditions and test subject [21].

There are several non-linear mechanisms observed through laboratory tests which are claimed to cause enhancement to oil recovery from porous rock. The motion of isolated or immobile oil droplets has been studied at length with various conclusions being drawn. Non-linear effects arise from a high intensity, high frequency field within the pores [58]. These effects include in-pore turbulence, acoustic streaming and cavitation [20,59]. In pore turbulence and acoustic streaming cause the coalescence of oil drops due to the interaction between the droplets within the pores promoting oil mobility. Cavitation bubbles generated within the pores as a result of the ultrasonic field can generate extremely high pressures and temperatures causing disruption of the water or oil film formed on the pore walls. Ultrasonic waves have wavelengths comparable to the average oil droplet size. As a result the waves cause suspended droplets within the pores to oscillate and induce movement due to the differing densities between the pore fluid and oil droplets [22]. It has been shown that gas bubbles within the fluid may adhere to the surface of oil droplets. These gas bubbles carry the oil droplets in response to the oscillatory field [22]. The attractive forces which act between oscillating droplets of one fluid in another fluid are known as Bjerknes forces. It has been claimed that it is these forces which induce the coalescence of nearby oil droplets, so a continuous stream of oil can be induced from dispersed oil droplets with wave excitation [58,60]. The destruction of the surface film at pore boundaries has been observed in both weak and intense wave fields. .

### 1.7.1 Reservoir Testing

Down hole stimulation techniques involve the application of lower frequencies over a prolonged period of time. With a 5-50 kHz application over several hours an increase of permeability was observed which lasted over 95 days [60]. Frequencies below 2 kHz applied to a reservoir showed an effect ending soon after sonication ceased in a reservoir in Eastern Gilbertown [61]. Despite the fact that ultrasound can modify reservoir recovery, there has been little use

of this technology and the low penetration depth of use due to the high attenuations will prove an overly invasive means of application. An example of direct application of down-hole acoustic stimulation is that of the use of Hydro-Impact tool installed 30ft above the shallowest producing layer. This tool generates shock waves, each lasting less than 1/100th of a second at ten second intervals. The acoustic wave travelling 1.5 miles per second and affected wells up to 1/4 of a mile away from source. Claimed increase recovery over substantially larger areas of a reservoir at lower cost than any other stimulation technology.

## 1.8 Summary

The generation of a reservoir and petroleum oil has been outlined, with the processes involved in how it is obtained through natural primary and secondary mechanisms. The features of an ideal reservoir and reservoir fluid are displayed, highlighting the mechanisms which prevent recovery.

There is a vast amount of evidence indicating that acoustic waves generated by seismic activity change the way in which oil saturated porous rock behaves. There is a lack of agreed upon reason for this for two reasons. Firstly, there is little consistency with the actual effect these seismic waves are having on saturated porous rock where some recoveries are enhanced and others decreased. Secondly, the naturally occurring events which cause this seismic activity are uncontrollable and there is normally little viable information on the wave field generated. This has spawned speculation into what is causing these changes.

Studies have shown ultrasonic frequencies of up to 150 MHz being measured when seismic wave passes through saturated porous rock, with further support from theoretical investigation. There has been a significant branch of research into the behaviour of fluid within capillaries under exposure to an ultrasonic wave field. Changes of behaviour between the fluid and rock were observed as well as a decrease in fluid viscosity.

If correlation can be found between the way ultrasonic waves change the fluid within the rock and the enhanced reservoir recovery observed as a result of seismic waves then it may support that the ultrasonic fields generated within the reservoir as a result of wave dispersion may be a driving mechanisms behind the change of reservoir recovery observed following seismic activity. Once the mechanism is pinpointed it could be used to modify current reservoir recovery mechanism to enhance reservoir recovery. Testing for this investigation is performed at ambient temperature and pressure. This is clearly significantly different

from the conditions from within a reservoir. The most commonly postulated mechanisms are focused on throughout the investigation. The outcome of this investigation aims to provide a solid basis for further research into a more realistic reservoir set of conditions to determine what effect these have on the generation.

## Chapter 2

# Ultrasonic Generated Mechanisms

In this chapter, the processes involved in the modification of saturation fluid within porous rock resulting from an ultrasonic wave field are introduced. The mechanisms are investigated at atmospheric pressure for this investigation to determine if they viable prior to recommending them for further research into realistic reservoir feasibility. The first mechanism considers the interaction between the ultrasonic wave and the rock matrix, where localised regions of stress are generated causing a weakness in the rock. These regions of stress are a result of the interaction between the acoustic wave and complex rock structure. The second mechanism considers cavitation effects resulting from the interactions between the acoustic wave and the pore fluid. This cavitation can modify behaviour of the fluid within at the pores and enhance or generate fractures of the rock matrix.

We have seen in the material balance equation that an increase in yield from a reservoir depends on the quantities of fluids within the reservoir and the pore volume of the reservoir. Weakening of the rock increases the changes of fracture which increases the pore volume and may release and trapped reservoir fluid. Changing the behaviour of the pore fluid within the reservoir may enhance the rates of recovery of the oil and gas.

## 2.1 Stress Generated Fragmentation

When a stress waves travels within a complex structure containing discontinuities such as grain boundaries and pore interfaces in sandstone, high stress regions can be generated. As the stress wave travels through the sandstone it is reflected and refracted at discontinuities,

decreasing rock strength by dynamic stress concentrations, energy channelling and stress wave superposition [62, 63]. There has been a considerable quantity of theoretical analysis of incident plane waves with rock fractures within geology. Analysis has shown that these internal interactions heavily depend on the rock composition and structure [64, 65].

Investigations into the effect of ultrasonic waves interacting with rock led research into the field of medicine, to a procedure known as lithotripsy. Lithotripsy is a non-invasive medical procedure which fragments porous calculi by focusing ultrasonic waves at kidney stones within the body. This fracture is a result of complex ultrasonic shock wave interactions within the kidney stone structure. These focused shock waves cause the kidney stone to break down to a size which can be naturally passed out through the renal system. Literature claims that this rock fragmentation is a result of internal stresses are generated within the rock as a result of complex acoustic wave interactions within the kidney stone. Internal focussing of the waves within the rock due to the complex stone geometry and material properties as the wave travels through the grain structure may also cause regions of high tensile and shear stress resulting in fracture.

Direct fragmentation of porous rock due to an ultrasonic wave field will be investigated with an attempt to replicate the complex interactions between the acoustic wave and the porous rock which result in fracture. The effect of the ultrasonic wave field on the kidney stone is investigated in order to gain better insight into the interactions between the ultrasonic field, the porous material and the surrounding medium to determine if the same principles of stress generation to fracture to be applied with the sinusoidal acoustic pressure field. With a better understanding of these interactions, an attempt to manipulate the processes involved is considered with a view to finding the most effective mechanism of fracture. The identified mechanisms will be applied to a more representative reservoir rock to further evaluate the possibility of use in petroleum recovery mechanisms.

### 2.1.1 Background

Extra-corporeal shock wave lithotripsy (ESWL) is a widely used, non-invasive medical procedure which focuses ultrasonic shock waves on kidney stones. Over a period of 45-60 minutes, up to 3000 shock waves are applied to the stone, depending on its size and composition [66]. The acoustic waves cause the kidney stones to fragment to a size which can be naturally passed via the urinary tract. The first widely distributed clinical lithotripsy machine (known as a lithotripter) was the Dornier HM3, introduced in the USA in February 1984 [67]. Since then, lithotripsy has taken preference over kidney stone surgery, having the



strong benefits of it being performed under local or no anaesthetic on an out-patient basis. This saves both money and time of the surgeon and is given preference over the preceding standard treatment of surgery by most patients.

### Shock Wave

In contrast to a sinusoidal wave field which has a linear response with equal compressive and tensile phase amplitudes, a lithotripter shock wave is characterised by its high amplitude, relatively long wave period and low pulse rate. While there are many different types of lithotripters, the nature of the wave remains the same. A typical shock wave can be seen in Figure 2.1. The wave pulse consists of a sharp rise in positive pressure which lasts approximately  $5\mu s$  followed by a sharp  $1\mu s$  fall to a negative pressure. This negative pressure gradually levels out back to a neutral state over about  $3\mu s$ . This overall pulse lasts under  $10\mu s$  with positive pressures in the range of 40 MPa and negative pressure in the range of -10 MPa being obtained [68].

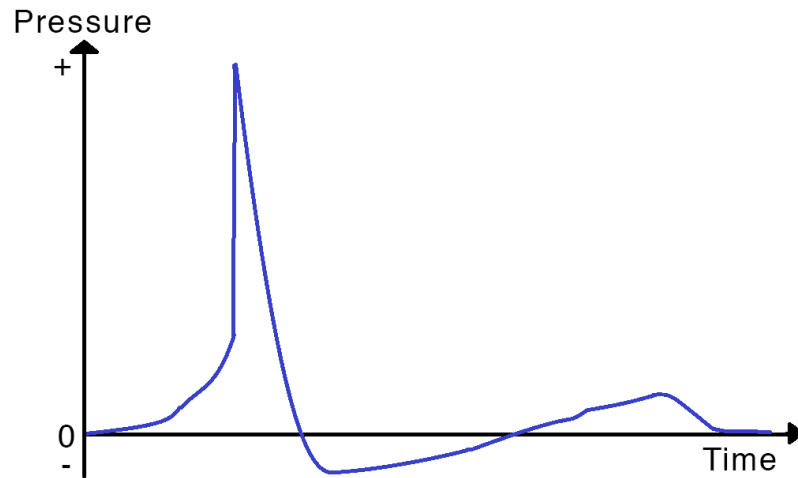


Figure 2.1: Typical shock wave pressure field created with time

It is generally accepted that the Mohr-Coulomb criterion is the most satisfactory explanation for the fracture of brittle materials such as kidney stones. This works on the assumption that fracture occurs by the rapid extension of sub microscopic pre-existing flaws randomly distributed throughout the material. The Griffith theory of fracture describes the behaviour of these pre-existing flaws or micro-cracks within the porous structure throughout failure [69].

Micro-cracks can be generated and expanded when the localised stresses exceeds the ultimate stress of the material, dictated by the material composition. These micro-cracks eventually

grow and combine to create a macro-crack [68, 70, 71] which can result in structure failure. These generated stresses can be compressive, tensile or shear, depending on the mode of application, as shown in Figure 2.2. Several mechanisms are said to generate the direct stresses associated with the shock wave interacting in and around the kidney stone, however the exact method of fragmentation remains a topic of discussion amongst researchers [72].

Laboratory based experiments are often performed using kidney stone mimic samples in a water bath to simulate kidney stones within the body. This method of experimentation has the advantage in that it reduces the large degree of variability associated with in vivo work such as body temperature, differences in renal calculi composition and movement as a result of breathing.

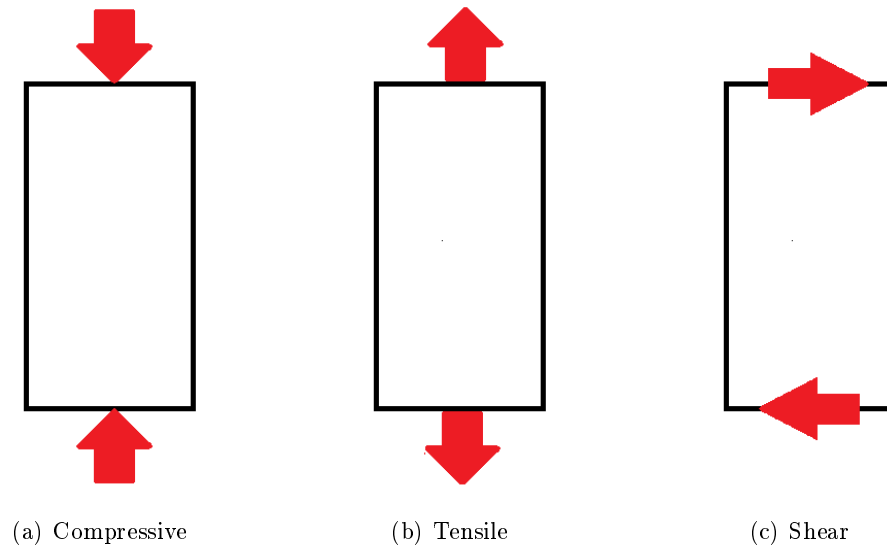


Figure 2.2: Compressive, tensile and shear stress generation as a result of the angle of force application

There has been considerable investigation in the most appropriate focal width for optimum fragmentation in kidney stone fragmentation [71, 73]. As a result there is a wide range of lithotripters available on the market with varying beam widths, each designed to complement the process which the designer deems most influential on fragmentation. The Dornier HM3 which was the most widely used lithotripter for many years has a focal diameter of 10-12 mm [68] whereas the newer electromagnetic lithotripters have a focal diameter of 4-6 mm [74]. Focal diameters as small as 2.8 mm are implements with the Storz Modulith lithotripters [68]. Varying the focal width has been shown as a way to control the wave interacts with the kidney stone and as a result the way in which the stresses are generated. The main mechanisms which are thought to arise due to these the lithotripter shock wave interacting with the kidney include spallation fragmentation, circumferencial squeezing and cavitation.

The generation of shear stress as a result of the shear and compressive waves travelling through the stone have been stated as the most dominant mechanism by researchers [68, 70]. Super-focusing occurs due to a particular stone geometry and material properties which can lead to the generation of regions of high tensile and shear stress causing failure [68].

Spallation occurs where the compressive part of the shock wave enters and travels through the kidney stone, as presented in Figure 2.3. As the wave reaches the back surface it is reflected as a tensile wave. This reflected tensile wave interacts with the relatively long duration tensile tail end of the same oncoming compressive wave resulting in a localised area of large tensile stress closer to the back of the stone. It is this tensile stress which is suggested to bring about fragmentation in a lithotripter with a more narrow beam where the majority of the energy passes through the stone.

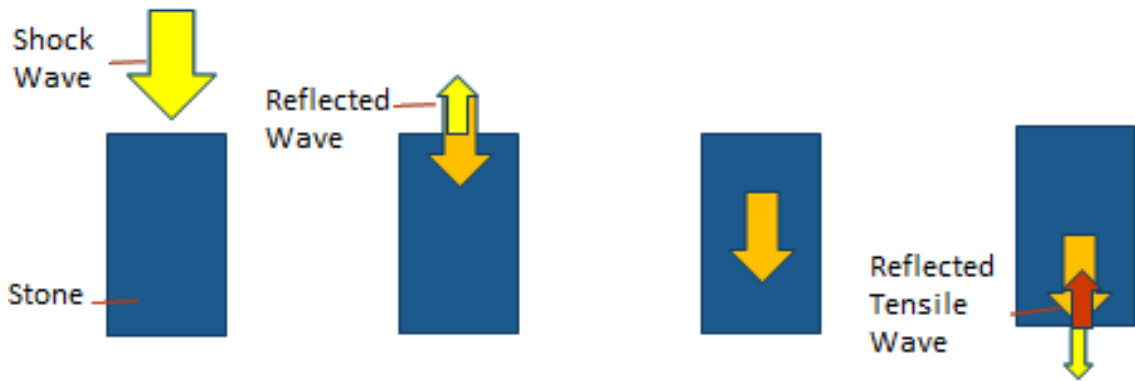


Figure 2.3: Process of spallation

Circumferential squeezing of the kidney stone occurs due to the difference in speed of a wave as it travels through different materials. A representation of this mechanism is shown in Figure 2.4, the wave travels much faster through the kidney stone than in the surrounding fluid. This causes a circumferential squeezing effect or hoop stress to be generated on the side of the sample [75]. This circumferential squeezing creates a region of tensile stress in the front and back faces of the sample. It is this stress which is thought to cause fragmentation as a result of maximum tensile stress at the proximal and distal ends of the stone and a fragmentation plane parallel to the path of acoustic wave travel.

In a study which suppressed the wave from travelling parallel along the side of the stone by use of a baffle, fragmentation was prevented from occurring within mimic kidney stones [71]. This effect is most prominent in a weakly or broadly focused wave where the portion of the wave travelling surrounding the stone interacting with the wave travelling within the stone generates sufficient stress for fracture to occur [76]. Interaction between the acoustic waves and the sandstone samples are investigated to determine if these same complex stress patterns

can be generated, resulting in a decrease in sample strength.

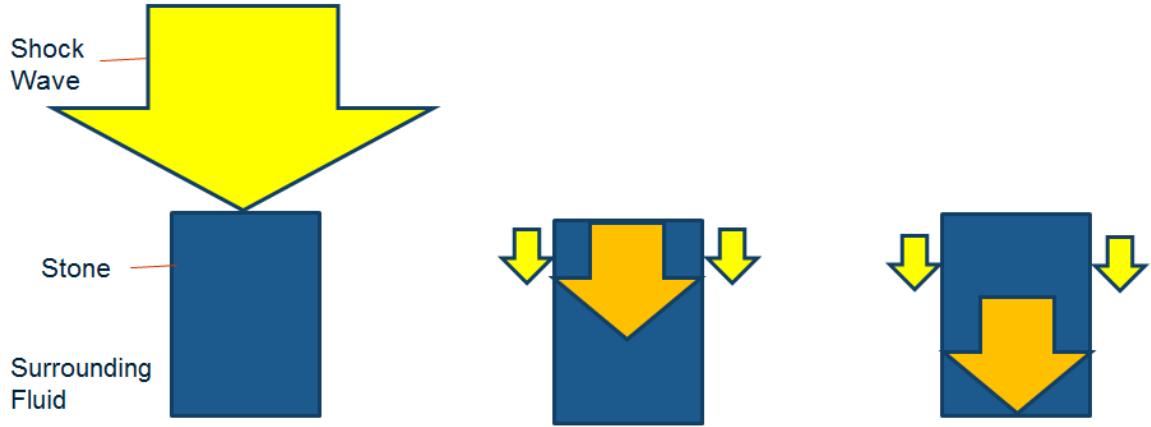


Figure 2.4: Process of circumferential Squeezing

## 2.2 Cavitation

Cavitation is a process which has been postulated a possible influence on the behaviour of petroleum in reservoir rock as a result of seismic activity. In addition, cavitation is a proposed mechanism involved in lithotripsy fragmentation. Cavitation occurs within liquid exposed to ultrasonic wave oscillations, which causes the local pressure to alternate between positive (compressive) and negative (tensile) pressure states.

The ultrasonic acoustic source places the liquid under a cyclic state of compression then tension. Considering the liquid as a group of molecules, the compressive part of the wave will cause the molecules to cluster together temporarily, pushing the molecules ahead in a domino effect. Once the compressive part of the wave passes, the molecules which were previously under compression are left in a state of tension as they try to find their original molecular equilibrium position.

If the negative tensile state is of sufficient amplitude to overcome the tensile strength of the fluid under its specific set of mechanical and atmospheric conditions then a cavity or bubble can be formed [1].

Cavitation can be categorised into two types; stable and transient. Comparison of the two forms of cavitation is depicted in Figure 2.5. A stable cavitation bubble will grow and oscillate in steady state within the ultrasonic field, giving rise to acoustic streaming in the surrounding

fluid (Figure 2.5(a)). Transient cavitation bubbles grow cyclically until the bubble life ends in collapse releasing energy in the form of micro-jets of extremely high localized pressures and temperatures [77], estimated at  $10000K$  and  $1000MPa$  [78], (Figure 2.5(b)). It is these localised energy surges created from transient cavitation bubble collapse which are thought to generate sufficient stress to fragment the kidney stones [79–82].

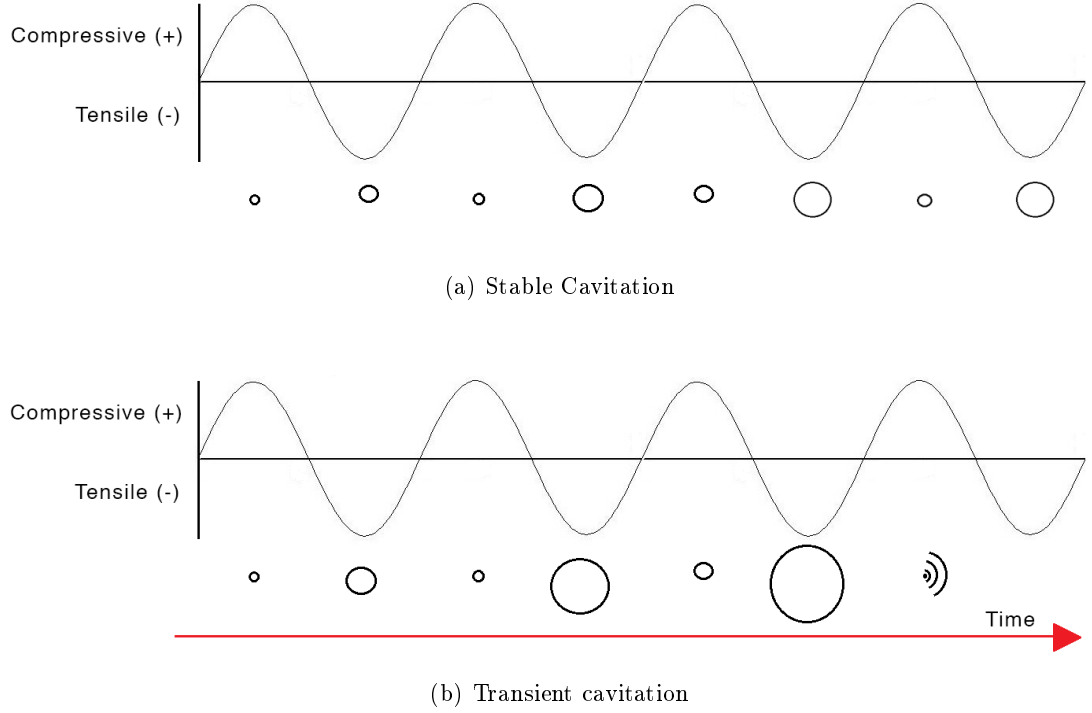


Figure 2.5: Comparison of the generation and behaviour of stable and transient cavitation

Cavitation has been used to fracture porous rock, a lab based lithotripsy simulation tests. It has been shown that when kidney stones are submerged in a viscous fluid which suppresses cavitation effects, that no fragmentation is occurs [82]. Similarly, this can be seen with failed attempts of gallstone fragmentation in the gall bladder. The high viscosity of the bile fluid surrounding the gallstone suppresses cavitation activity. As a result gall stones are not fragmented as easily as kidney stones. The low viscosity of urine allows for fast saturation of cracked stone and allows fragmentation by cavitation in the cracks [75,81].

### 2.2.1 Cavitation Generation

Cavitation is an extremely complex process with a wide range of parameters which must be within a certain range for it to occur. There are three main stages for a cavitation bubble; generation, life and collapse.

Cavitation bubble generation is a process consisting of a breakdown of the fluid and creation of a void, the introduction of vapour into this void and finally vapour saturation. Bubble life is the duration of oscillation within the fluid. Bubble collapse is how the bubble ceases oscillation. The behaviour of the fluid and void in each of these stages can vary dramatically depending on the parameters of the applied ultrasound, cavitation fluid properties and proximity to a surface.

Bubble generation occurs in three main stages.

- Breakdown or void creation
- Filling of void with vapour
- Saturation with vapour

### **Cavitation Threshold**

For bubble generation to occur, the fluid must first be ruptured. The value of negative pressure under which the tensile strength of the liquid is exceeded and cavitation process can occurs is known as the cavitation threshold. This threshold value has been a subject of extensive investigation. Determining the cavitation threshold is difficult due to the number of influencing conditions and parameters which can influence the tensile strength of the liquid. For example, a change of temperature causes a change in strength of the fluid, change in solubility of gas in the fluid, change in fluid viscosity and therefore a change to the negative pressure necessary to cause cavitation.

The cavitation threshold has been estimated for a variety of fluids in a range of environmental conditions by a large number of researchers. A reason for the lack of definitive value is, in part, due to the wide range of dependent parameters which have been used for the experimental analysis of this threshold value. Another reason is the lack of clarity in identifying cavitation activity. At low acoustic frequencies cavitation effects are dramatic and visible however the effects may be unnoticed at higher frequencies, although observable on a microscopic scale [83].

Considering the thermodynamic properties of a fluid, we can observe the relationship between pressure, temperature and volume. Figure 2.6(a), shows the phase diagram for a pure liquid. A triple point occurs where, for a specific temperature and pressure, three phases of water state can exist in thermodynamic equilibrium. From this point, the line extends along a curve

known as the liquid-vapour line, or bimodal line, which separates the conditions of pressure and volume of liquid and vapour states. Along this bimodal line, the vapour and liquid states represent two limiting forms of a single amorphous state, one of which can be obtained from the other by isothermal volumetric change.

Figure 2.6(b) shows the pressure and volume relationship of a typical fluid, comprising of a mixture of gas and dissolved vapour. To the right of the saturated vapour line and above the critical point, the liquid exists in a state of superheat. In this state, the liquid is essentially pressurised hot water. Stability within this state exists due to the overpressure which raises the boiling point. A liquid in any state lying on the saturation lines can contain a mixture of the two states while in equilibrium. Increasing the pressure or volume can cause the transition from the mix of fluid and liquid to gaseous state.

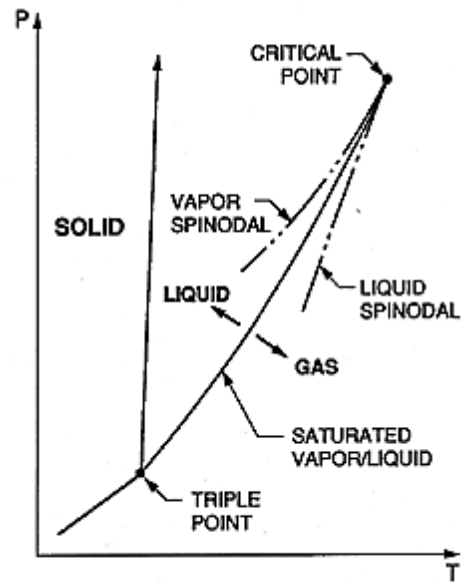
Crossing the curve into a different state is a reversible action under static conditions such as the evaporation or condensation of a fluid as it moves from fluid to gas or vice versa, by increasing or decreasing the pressure  $p$  above the vapour pressure  $P_v$  at a constant temperature  $T_c$ . Cavitation can be generated in a liquid by lowering the pressure at constant temperature. It is similar to boiling which uses an increase in temperature in excess of the fluids saturation temperature  $T_s$  at a constant pressure as the mechanism. This increase above the saturation temperature changes the state from liquid to gas. The magnitude of pressure in excess of the vapour pressure can be calculated using Equation 2.1.

$$dP = P_v - p \quad (2.1)$$

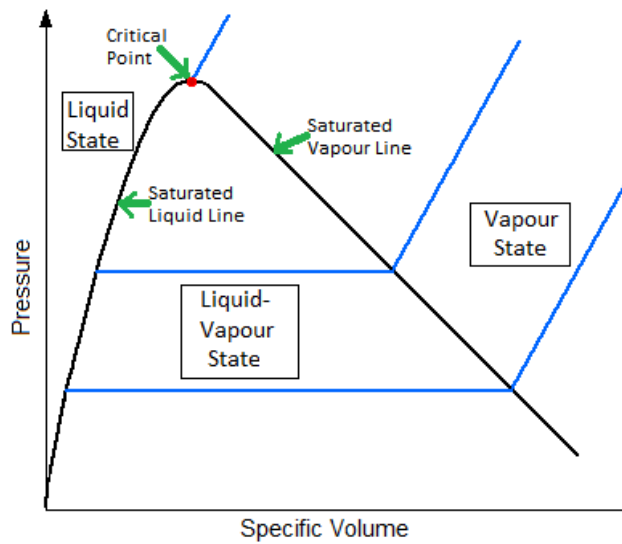
### Nucleation Sites

The reduction of pressure below the saturated vapour pressure quantifies the crossing over of the cavitation threshold. If no nucleation sites are present, this may lead to the continuation of the state down the theoretical isotherm to a metastable state.

A matter with pressure and temperature values of the isotherm sits in an excited state, where the liquid and vapour co-exist on the theoretical isotherm line relating the temperature and pressure. Surface tension of the matter pulls the liquid in preference to one state. If one phase is brought temporarily into the other, it is observed for a finite space of time as being in the 'metastable state.' Liquid in a metastable state to vapour is a cavitation bubble.



(a) Pressure and Temperature state relationship of a fluid



(b) Pressure and Volume state relationship of a fluid

Figure 2.6: Phase diagram of an ideal fluid [1]



There are two main nucleation types that determine the form of cavitation which is generated; homogeneous or heterogeneous. Homogeneous nucleation occurs within the bulk of the pure fluid and is purely a result of change of liquid state creating microscopic voids. Homogeneous nucleation tends to generate a cavitation field of stable cavitation. Heterogeneous nucleation is the most common type and generally occurs at a weakness within a weakness in the fluid at a boundary from fluid to a solid such as a container wall or particle of dust within the fluid. Another weakness can be a micro-bubble of contaminant gas present in crevices within the solid boundary or within suspended particles or within the liquid.

In a pure liquid, surface tension is present due to the intermolecular forces that tend to hold the molecules together. The pressure of a liquid  $p$ , radius of a bubble  $R$ , interior bubble pressure  $p_i$ , and surface tension between the gas and fluid,  $S$  are related by Equation 2.2. If the temperature of the liquid is uniform and the bubble contains only vapour then the interior pressure at which cavitation will occur will be the saturated vapour pressure  $P_v$ .

$$p_i - p = \frac{2S}{R} \quad (2.2)$$

The liquid pressure (outside bubble) will have to be less than the saturated vapour pressure in order to produce equilibrium conditions. If the pressure in the surrounding medium is maintained at a constant value just slightly below  $P_v - 2S/R$  the bubble will grow, the radius  $R$  will increase, the excess pressure causing growth will increase and rupture will occur. The maximum bubble size can be calculated using Equation 2.3 where  $R_C$  is the critical radius, the tensile strength of the liquid  $TS$ .

$$TS = \frac{2S}{R_C} \quad (2.3)$$

As opposed to homogeneous nucleation which manifests as microscopic voids which grow when the pressure is reduced below the fluids' tensile strength, heterogeneous nucleation occurs as void generation at the interface between a fluid and another surface. Heterogeneous nucleation typically results in a transient cavitation field. The contact angle at an interface between the liquid and vapour or solid  $\theta$  has a high influence on the tensile strength required to generate a void  $\Delta p_{cht}$  as with heterogeneous nucleation. This value can be calculated using Equation 2.4 which relates to the exterior bubble radius  $R$  and surface tension  $S$ . An example of nucleation sites with contact angles are shown in Figure 2.7 where case (A) exhibits a non-water wet surface, case (B) exhibits a water-wet surface and case (C) shows nucleation at a cavity, such

as with pores or crevices.

$$\Delta p_{cht} = \frac{2S \sin \theta}{R} \quad (2.4)$$

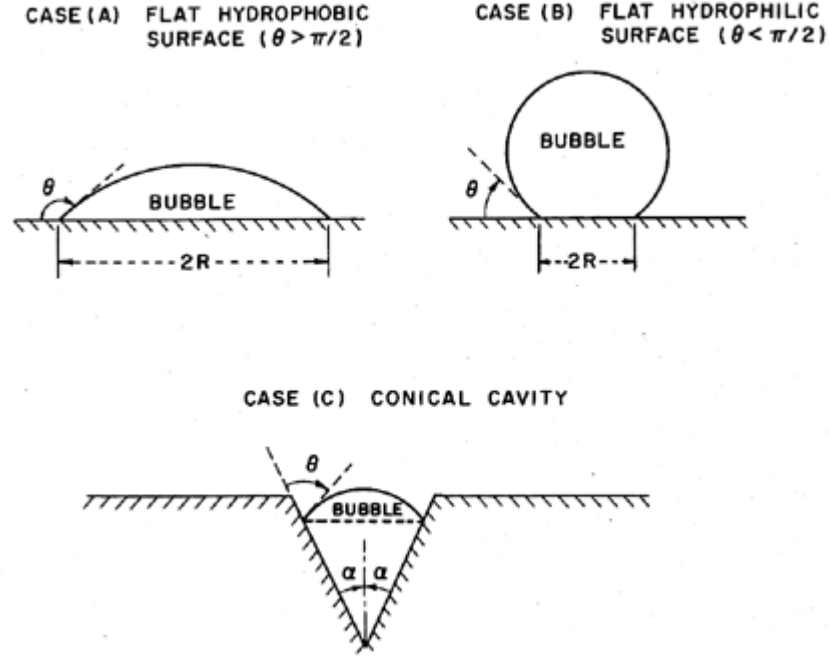


Figure 2.7: Contact angle associated with Heterogeneous Cavitation, taken from [1]

### Tensile Strength

For the acoustic waveform to cause a void in the fluid, the incident wave must be of sufficient amplitude to create a negative acoustic pressure within the fluid which will surpass the fluids molecular strength. Essentially, the localised pressure falls below the saturation vapour pressure. The quantification of this value has been investigated by many researchers to find a universal acoustic pressure threshold for water. There is a wide range of negative pressure values stated as the minimum negative threshold for water, below which no cavitation will occur. Galloway found the threshold to vary from -0.1 MPa for an air-saturated liquid to -10 MPa for distilled degassed water. On the other hand Frenkel based his investigation on the pressure required to overcome the molecular forces of the water and found a value of 3-30 GPa [84]. Due to the wide range of conditions used for experimental configurations, a wide range of threshold values are found in literature [85].

A high pressure environment such as within a reservoir will require a larger pressure differential

to overcome the tensile strength of the water and generate cavitation. It must also be considered that a maximum acoustic pressure amplitude threshold exists above which the pressure is too high and the compressive stage of the acoustic wave will suppress cavitation bubble growth during the compressive phase. Once the initial stage of cavitation has been instigated and there is a void in the fluid, the conditions must be appropriate for cavitation to survive or the void will close up. The acoustic source is important in the development of tensile stress within the body of fluid and therefore can dictate whether cavitation is generated.

The amplitude of pressure of an acoustic wave from ambient  $p_{ac}$  is related to the generated amplitude at position  $x$  and the speed of sound  $c$  by Equation 2.5. For a single frequency sinusoidal wave and a constant speed of sound, the general solution to this equation is given by Equation 2.6, where  $\omega$  is the angular frequency of the wave and  $k$  is the wave number.

$$\frac{\delta p_{ac}}{\delta x^2} - \frac{1}{c^2} \frac{\delta^2 p_{ac}}{\delta t^2} = 0 \quad (2.5)$$

$$p_{ac} = p_o \sin(\omega t \pm kx) \quad (2.6)$$

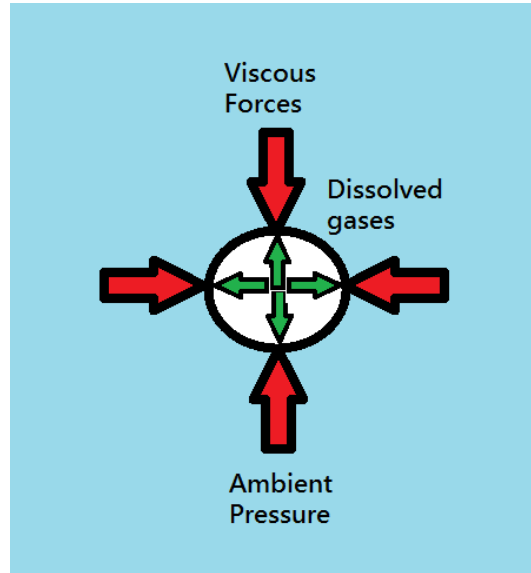


Figure 2.8: Forces experienced by a cavitation bubble within a sinusoidal acoustic field

As illustrated in Figure 2.5 a cavitation bubble grows in size within the tensile state of the cyclic wave, provided the localised fluid strength is exceeded. The time which the fluid is in a state of tensile strength is critical in determining the behaviour of the bubble.

If this tensile stage of bubble growth is sufficiently long in duration to allows expansion and

a state of equilibrium to be achieved between the internal and external forces acting on the bubble, the bubble wall will have gained stability to withstand compressive force brought about in the compressive half cycle of the acoustic wave.

The frequency of the acoustic wave dictates the length of time which the bubble lies within the tensile half-cycle of the wave. Increasing the frequency of the acoustic source decreases the time in the tensile phase in which the bubble can grow. A threshold frequency will exist above which no cavitation can occur [86]. Additionally, a minimum threshold frequency also exists, below which the bubble is not given sufficient time to grow to a stable size within the tensile half cycle so is suppressed in the compressive state of equal duration so the frequency range is critical.

Considering currently utilised cavitation equipment, cavitation cleaning baths are a good example to base successful cavitation tests on as their key function is to create a cavitation field. Cavitation effects are maximised to remove debris from the surface of medical instruments a solid. Frequencies of under 100 kHz are generally used with the appropriate cleaning solvent or even tap water at ambient conditions and have shown substantial cavitation results [87]. Evidence of success with this frequency allows a baseline frequency value to refer to when considering the acoustic set up.

### **Cavitation Fluid**

The properties of the fluid medium in which the acoustic wave is travelling can significantly affect cavitation bubble generation, life and collapse. Impurities such as dust provide a weakness in the fluid and act as heterogeneous bubble nucleation sites. Crevices or imperfections in walls or surfaces also act as preferable nucleation sites to the bulk of a fluid. A higher quantity of impurities within a fluid would increase the likelihood of cavitation generation.

During bubble expansion in the tensile half cycle of a sinusoidal wave, bubble size increases and a resulting influx of vapour and dissolved gases from the surrounding liquid into the bubble. A higher quantity of dissolved gas in the surrounding fluid increases the likelihood and rate of cavitation due to higher rates of diffusion into the bubble during the tensile phase [73].

In addition to its influence on bubble formation, vapour or gas content within a bubble can determine the way in which a cavitation bubble ruptures. Any gas within a bubble will act as a buffer to the explosion, cushioning the effects of collapse. As a result, vaporous

cavitation bubbles are significantly more erosive than gaseous cavitation bubbles. Degassed liquid tends to generate more violent yet less abundant cavitation bubble collapse and an increased repeatability due to content consistency.

### Viscosity

As mentioned previously, liquids viscosity is a measure of its resistance to deformation by tensile or shear stress and acts as a resistant force to the cavitation process.

The viscosity alters the boundary conditions of the bubble, influencing the balance of the pressure inside and outside of the bubble. Equation 2.7 show the relationship between the pressure inside the bubble  $p_i$ , the pressure in the liquid at the bubble boundary  $p(R)$ , the surface tension of the fluid  $S$  and the viscosity  $\mu$ , and its affect on the rate of change of bubble radius  $\dot{R}$  [88]. Increasing the viscosity will make it more difficult for the bubble to grow as the tensile pressure will have to overcome the viscous forces acting upon the bubble [89].

$$p(R) = p_i - \frac{2S}{R} - \frac{3\mu}{R}\dot{R} \quad (2.7)$$

The surface tension of a liquid is a property directly relating to the fluids tensile strength, as seen in Section 2.2.1 and Equation 2.7. It describes the behaviour at the interface of a fluid and a gas. The molecules on the interface with the gas within a cavitation bubble are attracted toward the molecules in the body of the fluid by cohesion. This creates a strong tensile interface and acts to resist bubble growth [89]. An increase of viscosity, such as with petroleum in reservoirs would increase the pressure differential necessary to generate cavitation.

### Environmental conditions

Referring to the pressure volume phase diagram in Figure 2.6(a), it can be seen that by increasing the ambient pressure of the a fluid, the pressure differential which much be achieved by the acoustic source in order to cause cavitation is increased.

High ambient pressures suppress nucleation sites and force any undissolved gasses to remain within the fluid. The acoustic source must be able to overcome both the ambient pressure

and to the tensile strength of the liquid for cavitation to occur.

Likewise, the temperature directly relates to the formation of vapour from liquid. At lower temperatures there will be a lower gas content within the fluid, therefore cavitation will be scarcer but more powerful on collapse as the presence of gases within a cavitation bubble buffer the impact of the bubble collapse. In addition to the gas content, an elevated temperature will increase the surface tension of the water and diffusion rates of the gasses dissolved, while decreasing the solubility of the gases within the fluid and decreasing the viscosity.

### 2.2.2 Cavitation effects in Reservoir applications

Both stable and transient cavitation generate mechanisms with the potential for application in enhancing reservoir recovery. The effects which come about during a stable cavitation bubble lifetime, and on transient cavitation collapse are investigated. As illustrated in Figure 2.5(a), stable cavitation bubbles gradually grow with each wave cycle and continue to oscillate about a state of equilibrium while the environmental conditions remain appropriate for cavitation to occur. Stable cavitation bubbles have a longer bubble lifetime when compared to transient cavitation bubbles.

Stable bubble oscillations, while less spectacular, gives rise to various non-linear acoustic effects including in-pore turbulence and acoustic streaming. It is these effects which may aid modification of the interaction properties of the fluids and rock matrix, enhancing oil mobility. Bjerknes forces are generated due to attractive forces between nearby oscillating bubbles. These attractive forces may cause localised motion within the fluid [17], [90]. Additionally the cavitation bubbles fill with gas which is present in the oil which can adhere to the wall as a film of gas and expel any trapped oil [91].

For transient cavitation, application of reservoir recovery enhancement focuses on the destructive effects that are associated with bubble collapse, particularly erosion and modification of fluid properties. As shown in Figure 2.5(b), transient cavitation bubbles generally have a much shorter lifetime, ending in catastrophic collapse. The high compressibility of the bubble means the potential energy obtained from the acoustic wave during bubble expansion and kinetic energy is concentrated when the bubbles collapses, generating extreme conditions of up to  $10000K$  and  $1000MPa$ . These localised energy surges can cause modification of the interaction between and properties of the fluids and the rock. The heat and pressure generated at bubble collapse can decrease the viscosity of oil, alter cohesive and adhesive bonding and modify the wettability of rock surface. These changes may bring about a reduction of the

resistance of the fluid to flow. Bubble collapse can also cause the removal of blockages within the capillaries [20] and destroy surface films which have formed across pore boundaries [21]. In addition, this bubble collapse can cause the formation and growth of micro-cracks in the rock.

While the atmosphere of test is at atmospheric pressure, the parameters which govern cavitation bubble generation remain the same. Compensation of the applied acoustic field parameter could be appropriate to generate cavitation bubbles within a reservoir of aquifer.

## 2.3 Ultrasonic Setup

A transducer is a device which converts energy from one form into another. A common example of this is a loudspeaker, converting electrical energy to acoustic energy. Piezoelectric transducers are one of the most commonly used ultrasonic transducers, which utilise the piezoelectric effect to generate mechanical motion from an applied current. A piezoelectric material generates an electrical current when squeezed. The reverse also occurs where an electrical current can generate a motion, or a vibration back and forth. This vibration generates a wave which can generate a sound or acoustic wave. Transducers range in size and shape depending on the required wave field. Two types of waveform will be discussed with this study; a planar ultrasonic transducer and a focused ultrasonic transducer. A comparison between the shape of the two different type of transducers and resulting acoustic wave field can be seen in Figure 2.9

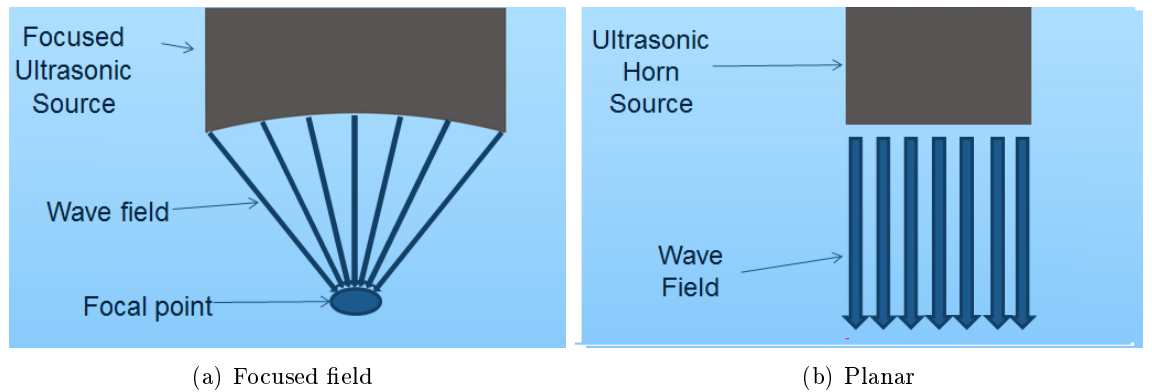


Figure 2.9: Comparison between Focused and Planar ultrasonic transducer face and resulting wave field

A planar ultrasonic transducer can be referred to as a piston transducer as the sound field resembles a cylindrical mass in front of the transducer. A planar ultrasonic transducer often has a coupling device attached known as a horn, which can be used to manipulate the

amplitude and dimensions of the waveform. For example, a tapered horn could be used to increase the amplitude of the generated wave. Shapes of four types of ultrasonic horn are shown in Figure 2.10. The straight horn provides no increase in amplitude of ultrasonic field. The exponential, catenoidal and step gain give an increasing gain of amplitude, signified by their decrease in diameter at the end of the horn.

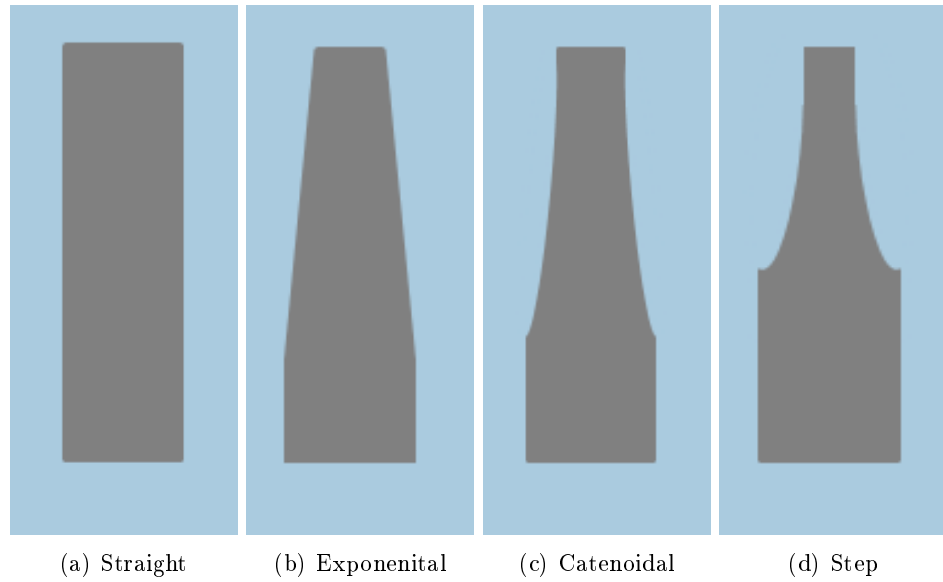


Figure 2.10: Ultrasonic horn types

Focused acoustic waves fields can be generated as a result of numerous individual wave generating sources angled in a way which focuses the wave in a small area. This can result in the generation of extremely high pressures and intensities. High intensity focused ultrasonic (HIFU) waves are often used in the medical field for the destruction of tissue such as tumours with the advantage of being non-invasive.

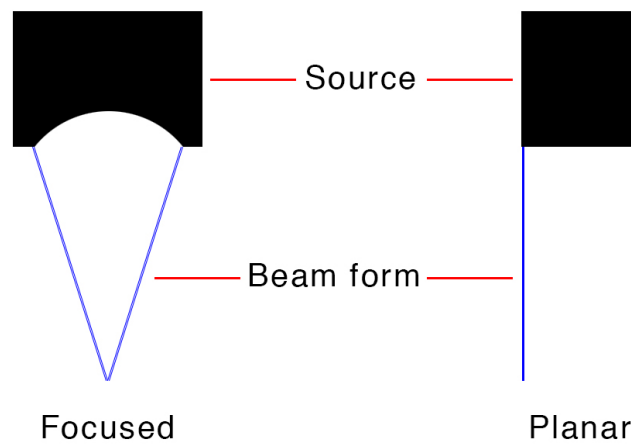


Figure 2.11: Comparison between focused and planar transducer



The wave field used for this investigation was generated by a 20 kHz Sonic Systems 20kHz ultrasonic controller. The ultrasonic controller converts the mains power supply at a frequency of 50/60 Hz and converts it to the driving frequency of the transducer. The transducer was used to drive a 20 kHz ultrasonic horn which generated the ultrasonic wave field. This particular horn and transducer were tuned to function at 20 kHz, as shown in Figure 2.12. An ultrasonic horn (sometimes known as a sonotrode, ultrasonic probe or acoustic waveguide) is a tool used to modify the amplitude of the field generated by the transducer. This configuration is typical of all power ultrasonic set-ups and is used in contact with materials for ultrasonic welding, cutting, soldering or in contact with fluid to aid in chemical processes within such as sonochemistry or homogenization.

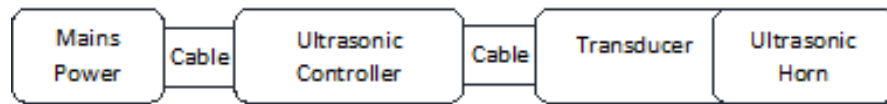


Figure 2.12: General transducer, ultrasonic transducer and horn configuration

## 2.4 Summary

Enhanced permeability of a reservoir and increase fluid flow is proposed as a result of the acoustic wave field interacting with saturated porous rock. The investigation focuses on two key areas. The first concentrates on internal stresses generated within the samples as a result of the acoustic pressure field interactions with the complex rock structure generating fatigue stress and localised areas of high stress. The second looks at cavitation generating micro-erosion to enhance cracks and pores within the samples and cause a decrease in strength and modification of the interaction between the rock surface and pore fluid. The method of application will be further discussed. Additional modifications between the fluid and rock structure as a result of cavitation effects are also considered through the investigation.

The importance of fluid state for the understanding of cavitation and bubble behaviour has been highlighted. Saturation fluid used for the predominant experiments was tap water at room temperature. Water present within a reservoir is abundant in gas and irregularities which would be expected to produce transient cavitation within the pores under ultrasonic exposure. The fluid used for the surrounding medium in test tank is degassed tap water. Degassing was performed for two reasons. The first was to provide repeatable cavitation results within the chamber. Tap water could vary in gas content depending on the day and time of year, whereas consistency of degassing method will ensure most of the gas has been removed from the fluid. The second reason was to reduce the transient cavitation activity

in the bulk of the fluid during testing. While we want to observe the effects of cavitation erosion, the coupling of the acoustic wave to the samples and surrounding area is the aim. At the sample face and within the pores, cavitation would be expected to be more likely to occur due to pore faces acting as crevices, or nucleation sites. Any impurities introduced into the tank water as a result of the adjacent sandstone sample would also act as an impurity.

## Chapter 3

# Material Properties

This chapter describes the properties of rock strength and provides a description and justification of use of the material used in experiments. The sandstone samples are used to represent the reservoir rock with its naturally existing, randomly dispersed pores and cracks. The properties of reservoir rock will be compared to the sandstone samples used for the investigation to confirm they are a suitable representation. The behaviour of the materials used is also important for understanding the mechanisms generated during testing and what the investigation aims to achieve. The properties of fluid and how the presence of fluid changes the behaviour of the solid is described.

### 3.1 Acoustic and Mechanical properties

The mechanical properties of a material describe its behaviour when exposed to an external force. Mechanical properties of interest for the investigation of fracture under the exposure of acoustic waves include the elastic modulus, Poisson's ratio and density. The acoustic properties of a material describe how a mechanical wave will travel within it, such as the longitudinal wave velocity, shear wave velocity and impedance. The speed of a wave travelling through a solid can be calculated in terms of the mechanical properties.

Mechanical failure of a rock generally means the fracture or permanent deformation as a result of an application of force. In the simplest of terms, when a load or force ( $F$ ) is applied over an area ( $A$ ) the energy transfer causes the generation of a stress within the material. This stress causes a deformity within the material known as a strain. The type and magnitude

of strain which develops depends on the type of force which is applied and the nature of the material. Most rocks obey the laws of linear elasticity, showing the relationship between the stress applied and the corresponding strain generation, for small strains.

### 3.1.1 Material Properties

A materials mechanical properties dictate how it will respond to an external force. The compressive and tensile strength, Elastic modulus and Poisson's ratio are briefly described. A material's compressive strength describes its capacity to withstand an axially compressive force ( $F_c$ ). The compressive force generates a compressive stress ( $\sigma_c$ ) within the material over an area ( $A$ ) as seen in Equation 3.1 until it reaches its ultimate stress limit where it fragments. This stress at which failure occurs is known as the maximum compressive stress of the material.

$$\sigma_c = \frac{F_c}{A} \quad (3.1)$$

How a material responds to an applied stress is important for understanding behaviour under certain conditions. The compressive strength of rock can be related to its porosity. There have been many studies to find the direct relationship between the uni-axial compressive strength and the porosity for various types of rock, all of which show a decrease of strength with increasing porosity. A relationship established using the Griffith criterion gives the Compressive strength ( $C_0$ ) in relation to the porosity ( $\phi$ ) as shown in Equation 3.2.

$$C_o = \frac{800}{\phi + 4} \quad (3.2)$$

The maximum stress that a material can experience before failure in tension is referred to as its tensile strength. In a material where a tensile force ( $F_t$ ) over an area ( $A$ ) is applied, a stress ( $\sigma_t$ ) is generated with a magnitude calculated using Equation 3.3.

$$\sigma_t = \frac{F_t}{A} \quad (3.3)$$

According to the Griffith criterion which describes fracture in one plane, the tensile strength

of a brittle material is theoretically 1/8 of the compressive strength of the material [92]. A brittle material is defined as one which will rupture quickly before any plastic deformation occurs. This is unlike ductile material which has a large quantity of time between the elastic limit and rupture where the material elongates.

The elastic modulus expresses the ratio of stress to strain. The description of the elastic modulus depends on the type of stress applied. Young's modulus ( $E$ ) applies to uni-axial compressive stress, Bulk modulus to hydrostatic pressure and Shear modulus to shear stress. The Young's modulus of a material describes its elasticity or stiffness in compression or tension. It is a measure of the ratio of stress generated within a material as a result of an applied strain ( $\varepsilon$ ). Strain is the ratio of the change in length ( $\delta l$ ) to original length ( $l_o$ ) and the resulting stress is generated as a result of the applied force per unit area. The relationship between stress and strain defines the Young's modulus, shown in Equation 3.4.

$$E = \frac{\sigma}{\varepsilon} = \frac{F \cdot l_o}{\delta l \cdot A} \quad (3.4)$$

The relationship applies for the shear modulus ( $M_S$ ) in terms of shear stress  $\tau_{xy}$  (where the subscript  $xy$  denotes the stress is on the  $x$  axis in the  $y$  direction) and shear strain  $\epsilon_{xy}$  shown in Equation 3.5. Here,  $\delta x$  describes the change in transverse displacement in the  $x$  axis,  $\frac{\delta x}{l}$  is the transverse spatial extension of the material (in the  $x$  axis) and  $l$  is the original length in the transverse direction.

$$M_S = \frac{\tau_{xy}}{\epsilon_{xy}} = \frac{F \cdot l}{\delta x \cdot A} \quad (3.5)$$

The bulk modulus  $B$  defines a material's resistance to change of volume under uniform compression. It applies to a fluid under hydrostatic pressure and is calculated using Equation 3.6 where  $V$  is the original volume of the fluid,  $dV$  is the volume change and  $dP$  is the change of pressure.

$$B = -V \frac{dP}{dV} \quad (3.6)$$

Poisson's ratio describes the relationship between the lateral and axial strain of a material in the linear elastic region, it is the negative ratio of transverse to axial strain. When applying lateral strain ( $\varepsilon_l$ ) to a material, an axial strain ( $\varepsilon_a$ ) will almost always accompany. Strain from

an increase in length yields a positive value whereas a decrease in length generates a negative strain value. The ratio of the lateral strain to axial strain, or the decrease in thickness of a bar when stretched a certain amount is the Poisson's ratio  $\nu$ , shown in Equation 3.7. The ratio is a dimensionless value ranging from -1 to 0.5 for a stable, isotropic, linear elastic material. Most materials hold a Poisson's ratio of between 0 where no transverse strain results from an axial strain, such as with cork, and 0.5, for a perfectly incompressible material such as rubber. Auxetic materials exhibit a negative Poisson's ratio, where a positive transverse strain will result from a positive axial strain, an effect occurring due to uniquely oriented molecular bonds within the material.

$$\nu = -\frac{\varepsilon_l}{\varepsilon_a} \quad (3.7)$$

Poisson's ratio can be used to relate horizontal stress ( $\sigma_H$ ) generated on a body to the application of vertical stress ( $\sigma_V$ ) using Equation 3.8.

$$\sigma_H = \frac{\sigma_V \nu}{(1 - \nu)} \quad (3.8)$$

Regarding the acoustical properties of the material, the Poisson's ratio is related to the ratio of shear wave speed  $v_s$  to longitudinal wave speed  $v_l$  in a material using the Equation 3.9.

$$\frac{v_s}{v_l} = \sqrt{\frac{1 - 2\nu}{2(1 - \nu)}} \quad (3.9)$$

### 3.1.2 Acoustic Properties

The velocity and pressure components of a sound wave are related to each other in terms of density and 'springiness' of the propagating medium. A low density medium with low 'springiness' will have a higher amplitude in its velocity component for a given amplitude compared with a medium which is denser with a higher level of 'springiness'. This relationship describes the impedance ( $Z$ ) of a medium, and can be thought of as the resistance of the wave propagation, much like a resistor in an electrical circuit. The impedance is described in Equation 3.10. The springiness function is the Modulus of elasticity of the material, and the volume velocity component is a function of the density. Using Young's Modulus of elasticity, impedance can be calculated using Equation 3.11.

$$Z = \text{Constant} = \frac{\text{Pressure Component Amplitude}(p)}{\text{Velocity Component Amplitude}(U)} \quad (3.10)$$

$$Z = \sqrt{\rho E} \quad (3.11)$$

The acoustic properties of a material are described by the longitudinal wave speed ( $v_l$ ), shear wave speed ( $v_s$ ) and impedance of the material. These are related to the mechanical properties in Equations 3.12, 3.13 and 3.14. The longitudinal wave speed only will apply to fluids as they provide no resistance to shearing and therefore cannot support a shear wave. A fluid can be defined as a material that will deform permanently and continuously under the application of a shearing stress.

$$v_l = \sqrt{\frac{E}{\rho}} \quad (3.12)$$

$$v_s = \sqrt{\frac{M_S}{\rho}} \quad (3.13)$$

$$Z = \sqrt{\frac{V_s}{\rho}} \quad (3.14)$$

Using the relationship between the Young's modulus and the velocity of a wave travelling through an acoustic medium, the impedance can be stated in terms of wave velocity using Equation 3.15.

$$Z = \sqrt{\rho E} = \sqrt{\rho^2 \frac{E}{\rho}} = \rho v \quad (3.15)$$

### 3.1.3 Material Failure

A standard approach to material failure is to predict that failure will occur by a particular mechanism, and using that mechanism, derive the combination of principal stresses that will

cause failure. These mechanisms are known as Theories of failure and can include maximum shear stress, maximum normal stress, maximum normal strain and maximum shear energy. Two theories which apply to brittle material which have been experimentally validated include the Griffith's crack propagation theory and Mohr's theory. These two theories are based on different concepts yet are mathematically related.

For analysis of rock failure, several assumptions are made regarding the rock properties and applied stress. These include:

- The rock material is isotropic and homogeneous
- The applied stress is uniformly applied
- Textural characteristics such as grain size and sorting have no influence
- Temperature and strain rate can be ignored

### **Griffith Criterion**

Griffith first proposed a fundamental concept of brittle failure in 1920s, which has since been accepted as the best explanation of brittle failure, the Griffith Criterion. The Griffith Criterion describes the behaviour of cracks in a rock under a state of stress. Rocks in their nature have numerous micro-cracks or pores, with different orientation. He claimed that it is the high tensile stresses at the tips of microscopic cracks in all materials which causes brittle failure. He discovered that where both the principle stresses are compressive, the stress at the tip of a properly oriented crack can be tensile [93]. These small micro-cracks propagate and coalesce into a macro-crack or fracture under the application of force.

Under conditions of uni-axial compression, the applied stresses build up the stresses in the region where the micro-cracks lie and a stress concentration occurs. Where a material is confined by the application of lateral forces, as shown in Figure 3.1(b), the compressive strength necessary for failure will be much higher because lateral force provides resistance to micro-crack development in the lateral axis. This means that the propagation of micro-cracks to macro-crack will require greater axial force.



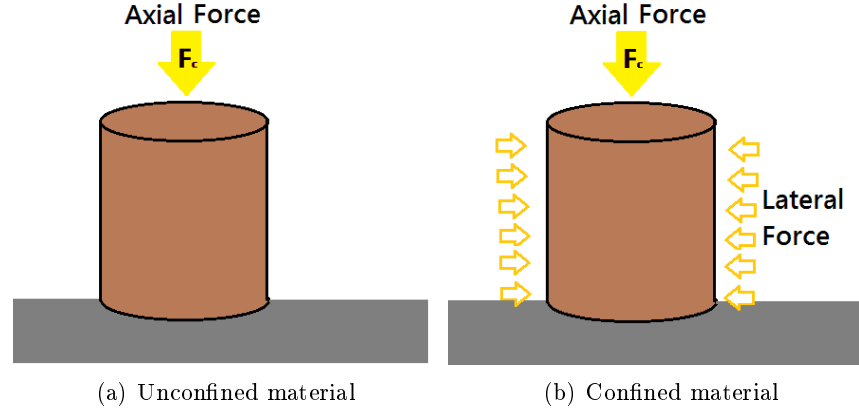


Figure 3.1: Forces applied during confined and unconfined testing

### Mohr - Coulomb Failure

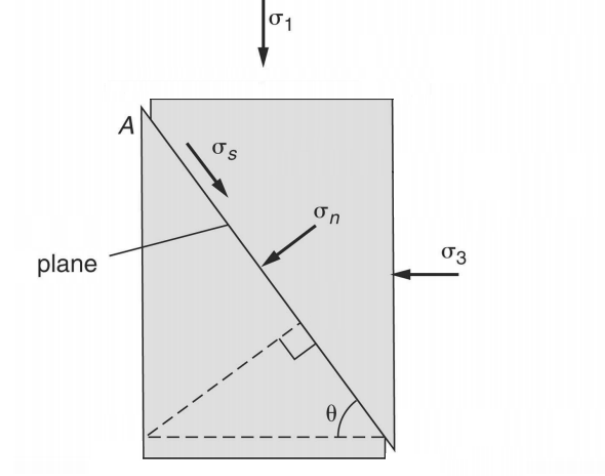
Further to Griffith's description of crack propagation, the Mohr-Coulomb criterion of brittle fracture provides a basis for a model of rock failure along a plane. Failure occurs once the localised stress exceeds the rock strength. This can be described by the Mohr - Coulomb criterion and dictates the behaviour of a rock when exposed to combinations of shear and normal stresses. The criterion is specific to each material and is calculated by a series of experiments on samples which will identify a threshold boundary region in the relationship between the shear stress (component coplanar to the plane of applied force) and normal stress (component parallel to the applied force) beyond which fracture of the rock is predicted. Axial stress  $\sigma_1$  is applied to the test sample with a confining lateral load generating a lateral stress  $\sigma_3$ , where  $\sigma_1 > \sigma_3$ . This combination of axial and confining stress generates a shear stress  $\sigma_s$  and normal stress  $\sigma_n$  within the sample, as shown in Figure 3.2.  $\sigma_1$  and  $\sigma_3$  are referred to as the maximum and minimum principal stresses respectively.

The normal and shear stresses upon a plane of a body can be seen in Figure 3.2(a) shows the normal stress  $\sigma_n$  and shear stress  $\tau$  generated as a result of the application of the maximum  $\sigma_1$  and minimum stress  $\sigma_3$  on the material.

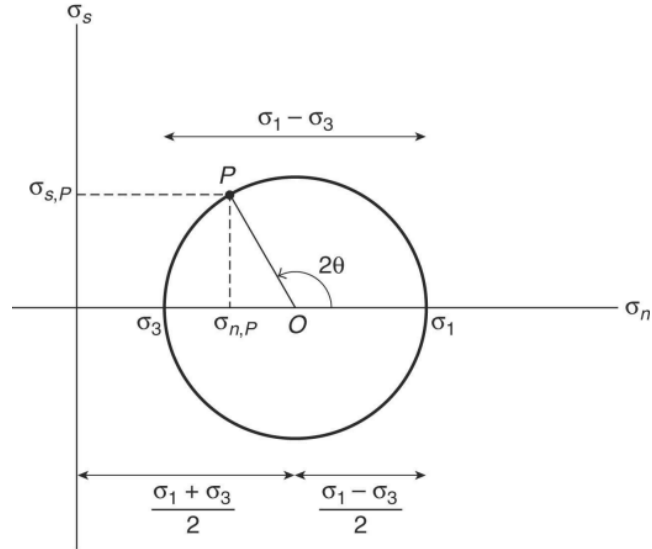
The normal and shear stress generated as a result of this experimental set-up can be calculated using Equations 3.16 and 3.17 with the use of fracture plane angle  $\theta$  which is the angle between the fracture plane and the plane of the minimum principal stress  $\sigma_3$ . These values will allow the plotting of the relationship of shear to normal stress in a diagram known as a Mohr's circle, seen in Figure 3.2(b).

$$\sigma_n = \frac{1}{2}(\sigma_1 + \sigma_3) + \frac{1}{2}(\sigma_1 - \sigma_3)\cos 2\theta \quad (3.16)$$

$$\sigma_s = \frac{1}{2}(\sigma_1 - \sigma_3)\sin 2\theta \quad (3.17)$$



(a) Normal and Shear Stress generated in a sample



(b) Mohr's circle plotted as shear stress against normal stress

Figure 3.2: Shear and Normal stresses generated in a sample [2]

Repeating this experiment for samples with a variety of confining pressures will provide multiple Mohr's circles outlining a boundary region outwith which the shear and normal

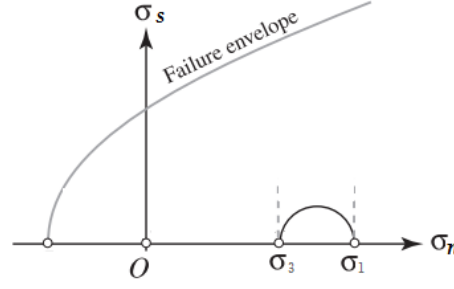


Figure 3.3: Generalised rock failure envelope [3]

stress relationship will result in material failure. Failure occurs across a plane where the shear stress and normal stress are related by a function which is characteristic for the material, Equation 3.18 where  $h$  is the soil cohesion. The shear failure envelope is represented by this relationship. An example envelope can be seen in Figure 3.3. The cohesion is produced by the fusion of materials or cementing of grains.

$$\sigma_s = f(\sigma_n) = \sigma_n \tan(\theta) + h \quad (3.18)$$

### Fatigue Failure

Fatigue failure occurs in a material as a result of a cyclic stress application causing crack initiation and propagation. In brittle failure, this occurs with minimal plastic deformation, where crack propagation occurs rapidly without an increase in applied stress.

Cyclic stresses are characterised by a maximum ( $\sigma_{max}$ ), minimum ( $\sigma_{min}$ ) and mean stress ( $\sigma_m$ ) of the stress characteristic as shown in Figure 3.4 as the range of stress ( $\sigma_r$ ), stress amplitude ( $\sigma_a$ ) and stress ratio ( $R$ ), shown in Equations 3.19 to 3.22. Stresses are commonly plotted as S (stress) against N (Number of cycles to failure) for samples. A number of samples are tested and the S-N plotted providing a Fatigue Limit characteristic. for the particular material under test, under which the the material is expected to remain intact. An example of a typical curve can is shown in Figure 3.5.

There are three stages of fatigue failure:

- Crack initiation at areas of stress concentration

- Cumulative crack propagation
- Rapid crack propagation once the crack has reached critical size

Sites of crack initiation could take the form of pores or irregularities within the sample. With the onset of fracture at these regions, an initial slow propagation along the grains of the sample where localised shear stress has time to propagate steadily. As the crack progresses, rapid propagation perpendicular to the applied stress occurs. The crack reaches a critical dimension and rapid propagation occurs.

The total number of cycles to failure ( $N_f$ ) is the sum of cycles at the first and second stages ( $N_i + N_p$ ). For a high cycle fatigue, of low loads,  $N_i$  is relatively high and the predominant damage occurs during the gradual crack propagation stage. Increasing the stress level causes  $N_p$  to dominate where the rapid crack propagation is the key driving stage.

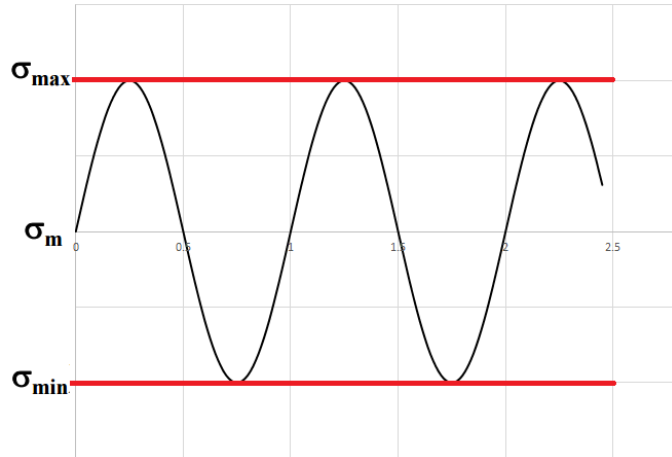


Figure 3.4: Alternating stress field generated during fatigue

$$\sigma_m = \frac{(\sigma_{max} + \sigma_{min})}{2} \quad (3.19)$$

$$\sigma_r = (\sigma_{max} - \sigma_{min}) \quad (3.20)$$

$$\sigma_a = \frac{\sigma_r}{2} \quad (3.21)$$

$$\sigma_m = \frac{\sigma_{min}}{\sigma_{max}} \quad (3.22)$$

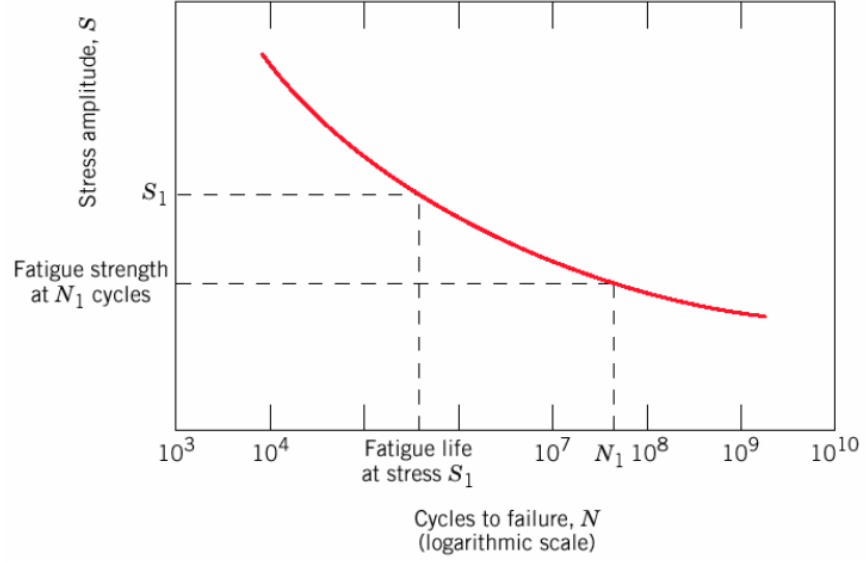


Figure 3.5: Typical S-N curve showing the fatigue limit

Failure will occur below the maximum strength loading condition as a result of accumulative damage.

Fatigue failure can occur significantly below the tensile or yield stress of the material under a static load. It is proposed that the cyclic pressure field resulting from the alternating acoustic pressure field that will cause a change in strength of the sandstone samples.

## 3.2 Physical Properties

The physical properties of a material describe the state of the matter composition. For porous rock typical of rock found in an oil reservoir the main physical material properties to be considered include porosity and permeability.

### 3.2.1 Porosity

The porosity ( $\phi$ ) is a measure of the ratio of the volume of void ( $V_v$ ) to volume of solid matrix ( $V_m$ ) within a material, and can be calculated using Equation 3.23. With natural material there is often two types of porosity to consider, connected and isolated porosity. As the name implies, connected porosity refers to the porosity which can be obtained by free flow through the pore channels. Isolated porosity refers to the pores which are trapped at all sides from a

pore network or pathway. These pores may contain fluid, but without a network for the fluid to move through, it is unobtainable [94]. The measure of connected porosity of a material will exclude these isolated pores spaces. The porosity of the sample has a high influence on the material strength, as pores provide weaknesses for micro-crack propagation. An example of typical changes in generalised failure envelopes as porosity can be seen in Figure 3.6.

$$\phi = \frac{V_v}{V_m} \quad (3.23)$$

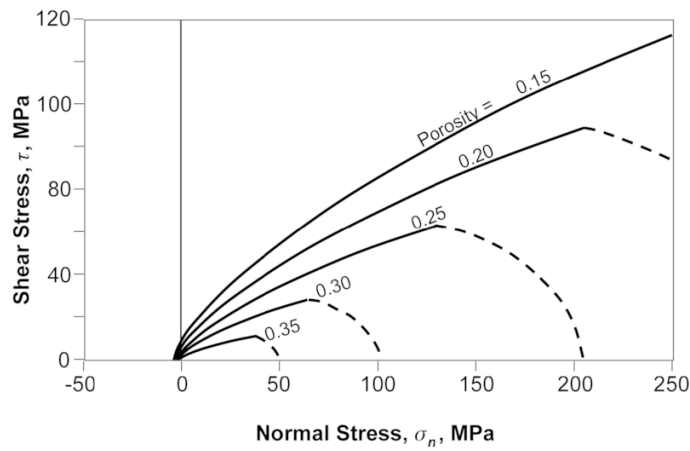


Figure 3.6: Failure envelopes for different porosity values [4]

### 3.2.2 Permeability

The permeability of a rock measures the ease by which fluids can pass through it. A higher permeability rock is one where fluid can flow through the material with greater ease. The permeability of the rock can be related to the connected porosity as these pores provide a means of travel through the rock. The fluid can also travel via grain boundaries and cracks in the material.

Permeability ( $k$ ) measures of the rate at which water can flow through a medium. Darcy's law describes the rate of flow of a fluid through a porous medium due to a pressure differential  $dP = P_2 - P_1$ , shown in Figure 3.7. The rate of flow ( $Q$ ) is the volume of fluid of viscosity ( $\mu$ ) which is discharged from the column of cross-sectional area ( $A_{cs}$ ) and length ( $L$ ) per unit time.

The permeability of the medium is directly related to the rate of fluid flow along a specific length of material  $dL$  and can be calculated using Equation 3.24. The value is negative as the flow is from a region of high pressure to one of lower pressure.

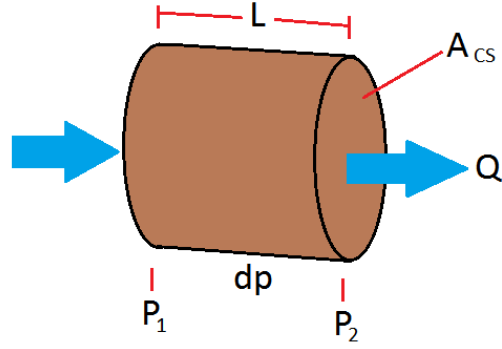


Figure 3.7: Flow of fluid through a sample of a given permeability

$$Q = -\frac{k \cdot A_{cs}}{\mu} \frac{P_2 - P_1}{dL} \quad (3.24)$$

### 3.3 Fluid Properties

The presence of fluid within a sample will decrease the strength of the material. This can be seen graphically in Figure 3.8. The properties of the fluid influence the pore pressure generated under force. An increase of pore fluid could translate the Mohr's Circle toward a region where it makes contact with the envelope and rock failure will occur, Figure 3.9.

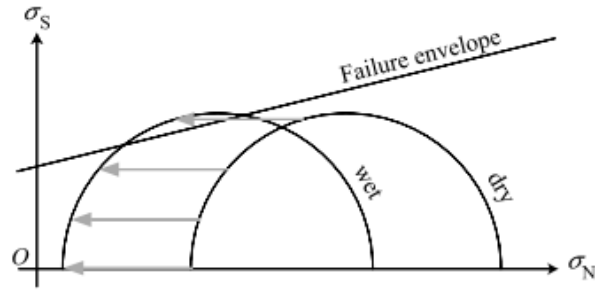


Figure 3.8: Rock strength change with addition of fluid [3]

The properties of a saturation fluid will affect how the fluid flows within rock, alter the rock's mechanical properties through fluid pressure and chemical reactions with mineral's. The fluids density, viscosity, surface tension and inter-facial tension properties are important because they will determine how the fluid behaves within the fluid pores and under the effect of ultrasonics.

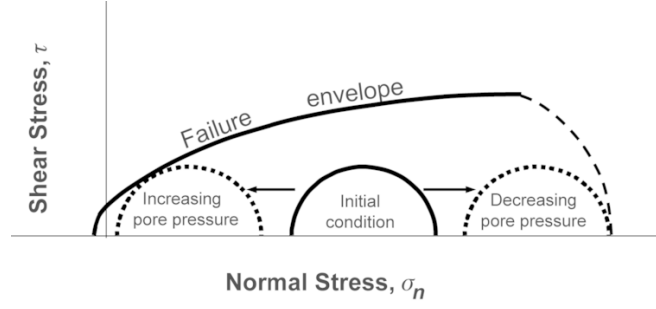


Figure 3.9: Rock strength with relation to Pore Fluid Pressure [5]

### 3.3.1 Fluid Density and Buoyancy

A fluid's density is the amount of fluid material within a volume with units of  $\frac{kg}{m^3}$ . Fluid density depends on the fluid temperature and pressure, where a decrease in density is observed for an increase in temperature or a decrease in pressure. When fluids of different densities  $\rho_1$  and  $\rho_2$  are stationary and alongside one another without any external influencing forces such as in an oil reservoir, the relative density  $\rho_R$ , calculated using Equation 3.25 will affect the way in which they behave. A relative density above a value of 1 for Equation 3.25 will result in the material of density  $\rho_1$  floating on the material of density  $\rho_2$ . For a value below 1, the opposite will occur

$$\rho_R = \frac{\rho_1}{\rho_2} \quad (3.25)$$

The density of any fluid within pores will influence the density of the overall material. The density  $\rho$  determines the speed of wave travel  $c$  with relation to a general coefficient of stiffness  $C$  using the Equation 3.26. The coefficient of stiffness selected dictates the speed of wave you are calculating: Young's modulus, Bulk modulus or Shear modulus can be used to calculate longitudinal wave speed, bulk wave speed in water or shear wave speed respectively.

$$c = \sqrt{\frac{C}{\rho}} \quad (3.26)$$

### 3.3.2 Surface Tension and Inter-facial Tension

The surface tension  $\gamma_s$  of a fluid occurs at the interface of differing phases, such as a fluid and a gas. It is a result of an imbalance of molecular forces which generates a tensile force along the



interface. It is measured as the force per unit length  $N/m$  but is often stated in *dynes/cm*, where  $1\text{dyne/cm} = 0.0001N/m$ . Surface tension decreases under increasing temperature conditions. As the temperature of a liquid increases, the movement of the molecules disrupts the imbalanced forces on the surface of the water, weakening the barrier between the water and gas.

Similar to surface tension, inter-facial tension  $\gamma_{if}$  is the work required to make a unit of interface at a fluid surface but only where the surface is in contact with another immiscible fluid. It is the elastic tendency of liquids to make them use the least surface area possible. It is a function of pressure, temperature and composition of each fluid phase. Between immiscible phases it is always positive in value and tends to decrease with the area of the interface. This excess energy is numerically equal to the force  $F$  per unit length  $L$ , which is numerically equal to the interfacial tension, Equation 3.27. This fluid film which attaches to the pore walls will effectively decrease the pore size restricting flow, perhaps blocking it altogether.

$$\gamma_{if} = \frac{F}{L} \quad (3.27)$$

As with surface tension, the increase in temperature of a liquid to  $T$  causes molecular movement which disrupts the imbalanced forces on the surface of the liquids and weakens the barrier. Eötvös devised a relationship between surface tension and temperature as seen in Equation 3.28 where  $M_V$  is the molar volume of that substance,  $T_C$  is the critical temperature,  $k$  is a constant valid for most substances (typically  $2.1 \times 10^{-7} \frac{J}{Kmol^{\frac{2}{3}}}$ ). For water,  $M_V = 18$  ml/mol and  $T_C = 374^\circ C$ . The Eötvös assumed that the surface tension is a linear function of the temperature which is approximately fulfilled for most known liquids.

$$\gamma_s M_V^{\frac{2}{3}} = k(T_C T) \quad (3.28)$$

### 3.3.3 Reservoir Rock and Sandstone Samples

Reservoir rock ranges in its mechanical and physical properties depending on the conditions in which it was generated. A comparison was made between the material properties of typical reservoir rocks found in literature and the material properties of the sandstone rocks chosen for experimentation.

**Reservoir Rock**

A wide range of material properties have been listed as typical reservoir rock properties, Table 3.4. This range of properties is extensive, so one form of reservoir rock was chosen. The most common forms of sedimentary reservoir rock are sandstone, limestone and dolomite [95]. The range of natural properties of these types of rock are listed in Table 3.1, 3.2 and 3.3 [96]. Of the range of appropriate materials, sandstone was selected due to its high availability.

Property	Symbol(unit)	
Density	$\rho(g/cm^3)$	2 - 2.65
Young's Modulus	E (GPa)	0.1 - 30
Poisson's Ratio	( $\nu$ )	0 - 0.45
Unconfined Compressive Strength	$\sigma_c(MPa)$	1 - 250

Table 3.1: Material properties of Sandstone

Property	Symbol(unit)	
Density	$\rho(g/cm^3)$	2.4 - 3.2
Young's Modulus	E (GPa)	10 - 100
Poisson's Ratio	( $\nu$ )	0 - 0.5
Unconfined Compressive Strength	$\sigma_c(MPa)$	40 - 350

Table 3.2: Material properties of Dolomite

Property	Symbol(unit)	
Density	$\rho(g/cm^3)$	1.4 - 2.9
Young's Modulus	E (GPa)	2 - 100
Poisson's Ratio	( $\nu$ )	0 - 0.3
Unconfined Compressive Strength	$\sigma_c(MPa)$	5 - 250

Table 3.3: Material properties of Limestone

Property	Symbol(unit)	Minimum	Maximum
Density	$\rho(g/cm^3)$	1.4	3.2
Young Modulus	E (GPa)	0.1	100
Poissons Ratio	( $\nu$ )	0	0.5
Unconfined Compressive Strength	$\sigma_c(MPa)$	1	350

Table 3.4: Material properties of Reservoir Rock

### 3.4 Summary

A materials properties dictate how it will behave under an external load. The properties of the materials used for testing are described in this chapter. This will give a good basis for understanding how the acoustic waves interact with the samples during testing and will be helpful for understanding results. Rock fracture is described to give a better visualisation of the proposed processes involved in increasing permeability. The importance of both the rock matrix and reservoir saturation fluid properties give a good basis for explanation in further chapters.

Sandstone was used in testing as its porous structure is representative of reservoir rock and should be susceptible to similar types of failure. The suitability of sandstone for material testing was confirmed due to material property analysis via literature research.

## Chapter 4

# Sample Testing

This Chapter describes the testing which was performed during the investigation. Characterisation of the mechanical properties was performed on sandstone samples which had not been exposed to an ultrasonic wave field to obtain more accurate values of Young's Modulus, density and Poisson's ratio of the samples than the wide range of properties which were listed within literature. This allowed for a more realistic representation of the samples with finite element analysis (FEA) and provided a control set of results for comparison with samples which have undergone ultrasonic treatment. FEA was used as a non-invasive method of calculating the effect the acoustic field was having on the samples. Two batches of tests were performed. The first aimed to characterise the sandstone samples for more accurate finite element analysis. The second batch was performed on samples treated with an ultrasonic field and compared to control results. These were carried out to understand what influence the ultrasonic field had on the samples. Characterisation tests can be categorised into two categories; mechanical property and physical property.

### 4.1 Sample Characterisation

#### 4.1.1 Compressive Strength Test

An unconfined uni-axial compressive strength test was performed on sandstone samples using the ASTM Standard test method for compressive strength and elastic modulus of intact rock core specimens D7012-10 [97]. ASTM recommends a diameter to length  $D:L$  ratio of 2:2.5

for the maximum compressive strength test. Samples of  $38 \text{ mm} \pm 0.85\%$  length diameter rock cores were cut to  $76.5 \text{ mm} \pm 0.23\%$  in length (2.1 ratio) and machined flat at the ends to maintain the core shape. They were then cleaned and oven dried at  $65^\circ\text{C}$  for 48 hours to remove moisture. This temperature was chosen to avoid thermal change of properties of the sample which can occur at elevated temperatures [98]. An increase of temperature of the sample causes expansion of the grains and propagation of micro cracks. After drying the samples were considered to be at a controlled baseline of saturation for the tests. HBM  $120\Omega$  3/120 XY11 strain gauges with gauge factor 1.98 were attached to the samples using the recommended epoxy adhesive. A strain gauge is a sensor which consists of a foil pattern on a flexible insulating backing. When a strain is generated in a sample, it causes a change in resistance within the metallic foil (with known material characteristics) from which the change of length can be calculated. The change in length is measured in both the vertical and horizontal planes and is used to calculate the strain. Knowing the rate of applied force ( $\frac{dF_c}{dt}$ ), allows calculation of the stress-strain relationship. Each gauge gives an axial or transverse strain reading depending on gauge orientation. Four gauges were applied at mid-height around each sample's circumference at equal spacing as shown in Figure 4.1. Four gauges were applied to increase reliability of the results and compensate for faulty gauges. A Zwick Roell 250kN servo hydraulic testing machine was used to apply a compressive load at a cross-head speed of  $0.5 \text{ mm/min}$  until sample failure occurred.

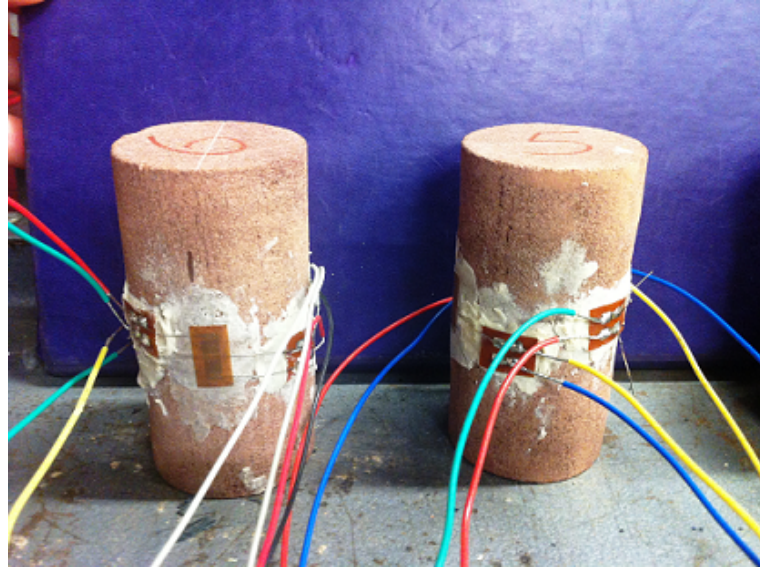


Figure 4.1: Compressive strength samples with strain gauges attached

We have seen in Chapter 3 that a compressive force generates compressive stress on a cross sectional area. The resulting deformation, measured as a relative displacement between particles in the material as it deforms under the applied load, is captured by the strain gauges. This deformation can indicate a lot about the way the sample is behaving. We know that the axial strain  $\varepsilon_a$  is a measure of the change in axial length,  $\delta L_a$  compared to the

original axial length of the sample  $L_a$  while under the compressive load using Equation 4.1. A typical stress strain response of the sandstone samples can be seen in Figure 4.2. There are three main stages associated with the compressive failure of this brittle material from initial loading to material failure. Understanding how fracturing occurs can provide insight into the way in which the material is responding to the applied force.

$$\varepsilon_a = \frac{\delta L_a}{L_a} \quad (4.1)$$

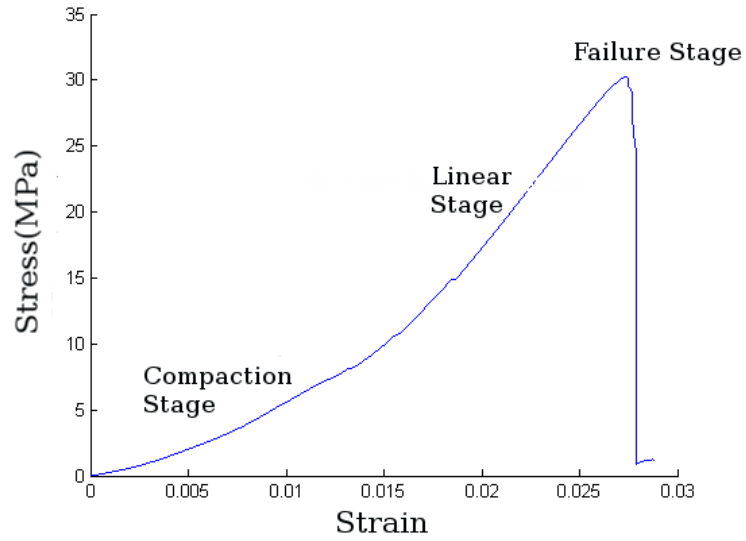


Figure 4.2: Stress - strain curve for sample

The beginning of this graph show the compaction stage, identified by the gradual increased in gradient. During this stage, pre pre-existing micro-cracks begin to close, where the orientation of these closing micro-cracks or pores determines how they are affected by the stress. Pores and cracks within the rock act as regions of weakness, and the rock matrix directly supporting these pores are more susceptible to failure than rock matrix in a solid region. Micro-cracks and pores sitting at an angle almost perpendicular to the applied load are forced closed with the initial generation of stress due to the relative lack of surrounding supportive material for the stress to distribute itself within this orientation and resist failure this applied force, as depicted in Figure 4.3.

The linear elastic stage follows, where the strain is proportional to the generated stress. During this stage, fracture propagation occurs in a stable manner where cracks propagate independently of each other and are distributed throughout the specimen. Provided the applied force continues, the failure stage follows. With increasing stress, micro-cracks no longer propagate independently from one another but dependently, with a higher clusters of

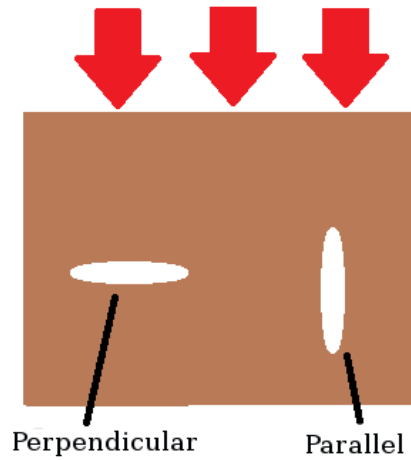


Figure 4.3: Perpendicular and parallel crack positioning relative to the applied force

micro-crack propagation developing in the zones of highest stress. Dependent propagation begins to occur, where micro-cracks coalesce to form macro-cracks causing a redistribution of stress. This redistributed stress causes alternative micro-cracks to generate and the cycle repeats until failure occurs. In these zones micro-cracks fork out and coalesce to form macro-cracks and eventually a rock fracture (Figure 4.4). The material reaches its ultimate stress limit and failure occurs. The maximum stress which the sample can endure is used to calculate its ultimate compressive strength.

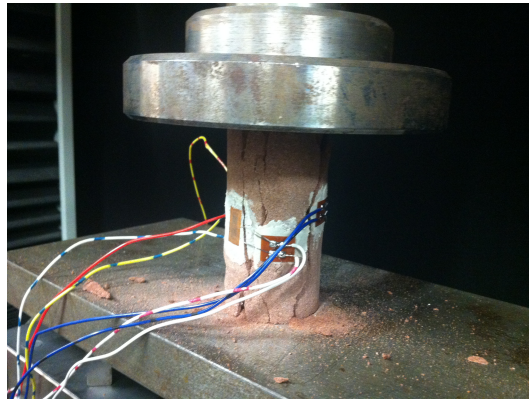


Figure 4.4: Sample following failure stage

#### 4.1.2 Tensile Strength Test

An alternative method of measuring the direct tensile strength test of a sample, known as the 'Indirect Tensile Strength test' or the 'Brazilian Tensile Strength Test' was developed by Berrenbaun and Brodie in 1959 [99] and has been widely popular due to its strong practical appeal over the standard uni-axial tensile strength test. The main disadvantage

of the conventional uni-axial tensile strength test is the difficulty of performing to acceptable standard for brittle materials [100] due to complications with gripping the sample without compromising its structural integrity. It provides diametral compression to a disc of material and works on the assumption that the samples are isotropic and homogeneous [101]. While sandstone samples are not categorised as isotropic and homogeneous, the indirect tensile strength test is widely used for the testing of porous rock and has been shown to successfully determine the tensile strength of anisotropic rocks [102]. It has also been shown to give tensile strength results similar to the standard uni-axial tensile test [103]. Its applicability is further supported by being a suggested method for tensile strength testing by the International Society for Rock Mechanics (ISRM) [104].

The indirect tensile strength test was performed on samples in accordance with ASTM D3769-08 [105]. The ASTM standards recommended diameter to length ( $D:L$ ) dimension ratio is 2:1 for determining the indirect tensile strength testing. The 38 mm diameter samples were cut to a length of 18.4 mm giving a dimensional ratio of 1.93:1, in keeping with the prescribed diameter to length ratio. These samples were then washed to remove residue and oven dried at  $65^{\circ}\text{C}$  for 48 hours before testing to ensure a consistent moisture content. Samples were then allowed to cool. A compressive load was applied to the sample using a Zwick Roell 250 kN servo hydraulic testing machine at a rate of 0.6 mm/min until fracture occurred, as seen in Figure 4.5. The maximum force endured by the sample  $F_t$  allows calculation of the tensile strength  $TS$  using Equation 4.2 where  $D$  is the sample diameter and  $L$  is the length.

The compressional force is applied at the surface of the thin annular disc generating a tensile stress normal to the diameter. This tensile stress is approximately constant over a region about the centre of the sample. The tensile strength is calculated based on the assumption that failure occurs at the point of maximum stress, at the centre of the disc and that the radial compressive stress has no influence on the failure.

$$TS = \frac{2F_t}{\pi \cdot L \cdot D} \quad (4.2)$$

### 4.1.3 Young's Modulus

The Young's modulus  $E$  of a material is calculated from the gradient of the stress-strain curve of the unconfined compressive strength test at the linear part of the curve. It can be calculated using Equation 4.3 where  $A_{cs}$  is the area of the sample face in contact with the applied force  $L$  is the original length and  $\delta L$  is the change in length of the sample. The



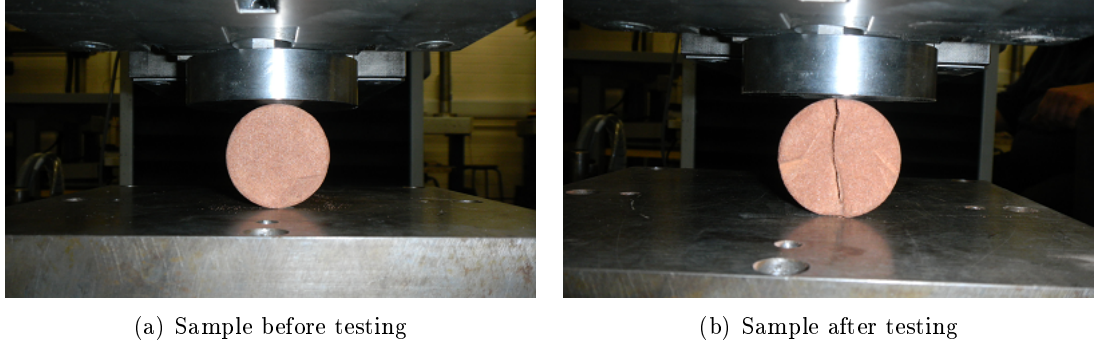


Figure 4.5: Sample before and after indirect tensile strength test

Young's modulus indicates how easy it is to deform a material and reflects how stiff or flexible it is. It is indirectly related to the material strength [100].

$$E = \frac{\sigma}{\epsilon} = \frac{F_c \cdot L}{A_{cs} \cdot \delta L} \quad (4.3)$$

#### 4.1.4 Poisson's Ratio

During the linear elastic stage of the stress-strain curve, the Poisson's ratio is the ratio of the transverse to axial strain generated in the sample as a result of the generated stress. These values are recorded in the axial and lateral directions by the strain gauges [97]. The strains are calculated using Equation 4.4 where  $\epsilon_t$  is the transverse strain (generated around the circumference of the sample) and  $\epsilon_a$  is the axial strain (generated along the sample). Further from the calculation of the axial strain in Equation 4.1, the transverse strain can be calculated by the change in transverse length  $\delta L_t$  over the original length  $L_t$  using Equation 4.5.

$$\nu = -\frac{\epsilon_t}{\epsilon_a} \quad (4.4)$$

$$\epsilon_t = \frac{\delta L_t}{L_t} \quad (4.5)$$

## 4.2 Physical Property Testing

Physical properties of the samples were calculated for the controlled samples which had not been exposed to ultrasonic treatment. The sample density, porosity and permeability was calculated for the sandstone samples.

### Density and Porosity

The samples were oven dried at  $65^{\circ}C$  for 48 hours to find the mass of the dry sample measured  $m_d$  and used to calculate the sample using Equation 4.6. The porosity of the sample was calculated by taking the dry sample and saturating with a fluid of known density,  $\rho_f$  to replace the space in the pores with the fluid. Once saturated, the samples were again weighed and the saturated mass  $m_s$  recorded on a digital scale to 2 decimal places. Each sample was taken from the saturation vessel, wiped of residual fluid and an average of three measurements was taken. Using these measurements, the volume of the pore spaces  $V_p$  can be calculated using Equation 4.7. From this and the volume of the sample material  $V_m$  the porosity  $\phi$  (%) can be calculated using Equation 4.8.

$$\rho = \frac{m_d}{\pi r^2 L} \quad (4.6)$$

$$V_p = \frac{m_s - m_d}{\rho_f} \quad (4.7)$$

$$\phi = \frac{V_p}{(V_m - V_p)} \cdot 100 \quad (4.8)$$

For the porosity of the sample to be determined, it must first be fully saturated. The initial saturation method that was performed was the Wicking method. This involves placing samples directly in the saturation fluid and allowing the fluid to seep in through the pores and displaces air. To determine the appropriate Wicking saturation time, the mass of a sample was periodically recorded over 28 days and it was shown that after the second day the change was negligible. This method gave average sandstone porosity of around 10% which is below expected values of between 11.4 - 25.7% from this type of sandstone, research [106–108]. For this reason, alternative methods of saturation were investigated for characterising the porosity

of the samples.

Vacuum saturation was chosen as the alternative method of saturation for porosity measurements. It was used for its relative simplicity and effectiveness at obtaining full saturation [109]. This method involved placing samples into a sealed chamber with the saturation fluid at the bottom and applying a vacuum to the chamber, (Figure 4.6). During exposure to the vacuum, the sample drew the saturation fluid upward until the sample was fully saturated. Average porosities of 20.7% were obtained with this process which is a more realistic porosity value of this type of sandstone. Vacuum saturation was chosen as the saturation method for porosity measurements.



Figure 4.6: Samples placed in vacuum chamber with saturation fluid

#### 4.2.1 Permeability

Permeability testing was performed using a VJTech tri-axial cell, automatic pressure controllers and a data logger, in accordance with British Standard BS1377-6: Method 6. The test utilises hydraulic pressure to calculate the permeability of the sample. The liquid used to apply this pressure is de-aerated, de-ionised water. Any gas within the liquid would make the fluid more compressible and give inaccurate permeability readings. The sample is encased in an impermeable membrane to separate the pores from the surrounding fluid, to which a uniform hydraulic pressure was applied. Once the sample is fully saturated, the pressure on the outer surface of the sample is increased. The set-up can be seen in Figure 4.7.

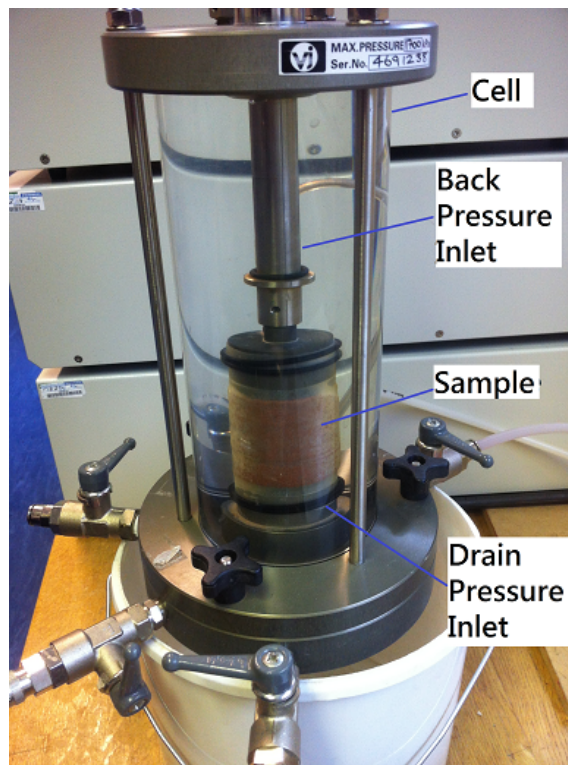


Figure 4.7: Experimental setup for hydraulic pressure application

The specimens were oven dried prior to treatment and placed in a flexible waterproof membrane which is encased in the tri-axial cell as shown in Figure 4.8. Three separate hydraulic pumps were attached to the system. One pump provided hydraulic pressure to the external surface of the sample, referred to as the confining cell pressure. A second pump provided pressure to the fluid flowing through the top of the sample referred to as the back pressure. The third pump provided pressure to the bottom of the sample referred to as the drain pressure, shown in Figure 4.9. A transducer at the base of the sample measures the pore pressure within the sample by measuring the response to the applied pressure gradient. The permeability test is a three stage experiment including a saturation stage, consolidation stage then lastly a permeability stage.

### Saturation Stage

The main aim of the saturation stage is to ensure that the sample is appropriately filled with the saturation fluid. If under-saturated the pores will contain trapped air. Any trapped air within the sample would reduce the effective pore space and increase the compressibility of the fluid giving incorrect permeability measurements. Pressure is applied gradually in steps of  $50kPa$  to prevent damage to the samples. Choosing a higher step could cause micro-cracks to be forced closed or propagate, depending on orientation. The pore pressure coefficient  $B$  is

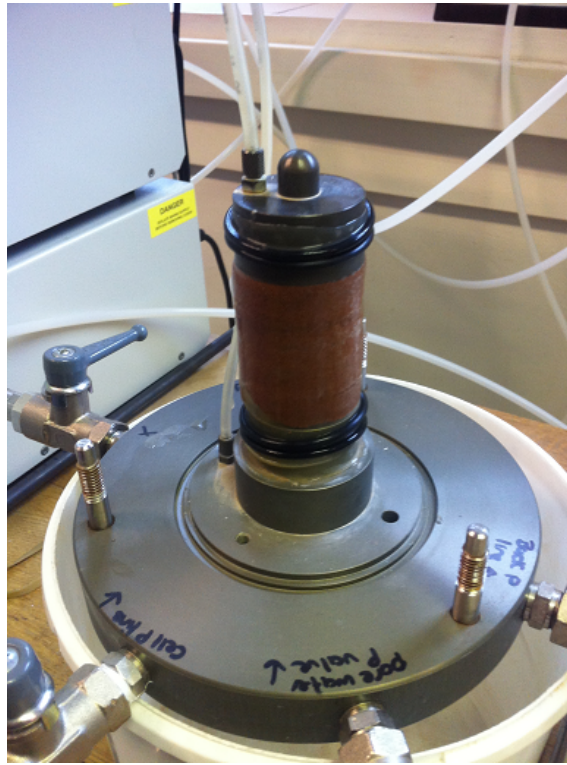
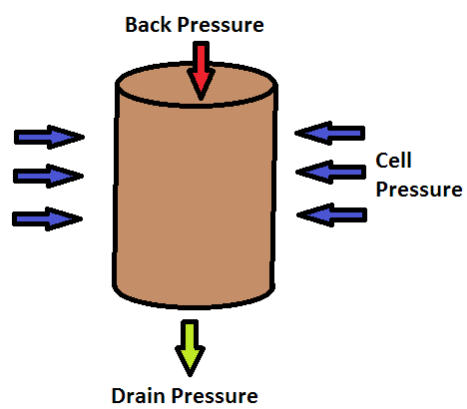
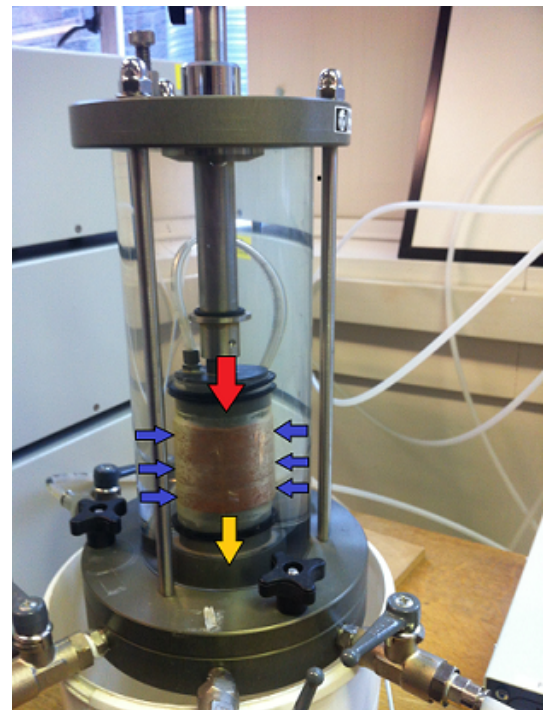


Figure 4.8: Sample mounted within membrane in the chamber



(a) Confining pressure phase



(b) Back pressure phase

Figure 4.9: Hydraulic pressures applied to the sample

calculated at each step of the saturation stage. Each step consists of two phases, the B check phase and the back pressure stage.

The B check stage involves increasing the confining pressure  $P_c$  in increments of  $\delta P_c$ , Figure 4.10. The resulting change in pore pressure due to the increased cell (or confining) pressure  $\delta P_p$  is observed until an equilibrium state is reached and a direct change in cell pressure is measured at the back pressure sensor. From this the pore pressure coefficient for this step is calculated using Equation 4.9.

$$B = \frac{\delta P_p}{\delta P_c} \quad (4.9)$$

The back pressure phase is performed to increase the pressure within the pores. A back pressure  $P_b$  is applied to the cell at a value of  $P_c - \delta P$ , where  $\delta P$  is the pressure differential, and the change in volume is recorded. A pressure differential is maintained between the confining pressure and back pressure to ensure that the membrane keeps in contact with the fluid. When the recorded pore pressure is equal to the applied back pressure the next step can be performed.

This two stage process is repeated until a B-value of 0.96 or above is obtained, indicating that the sample is at least 96% saturated which is deemed acceptable for the following stages to be performed. At this point a pore pressure increase occurs as a result of application of back pressure. A typical set of B-value and corresponding cell pressure steps can be seen in Figure 4.11.

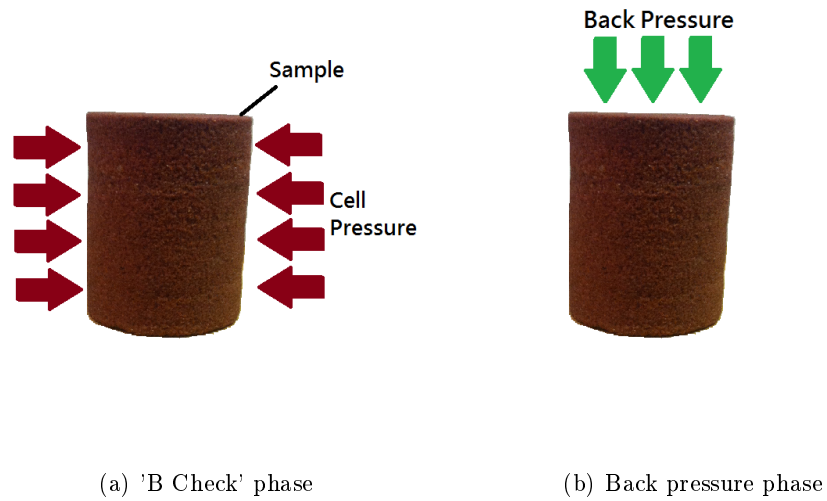


Figure 4.10: Pressures applied through saturation stage of the permeability experiment

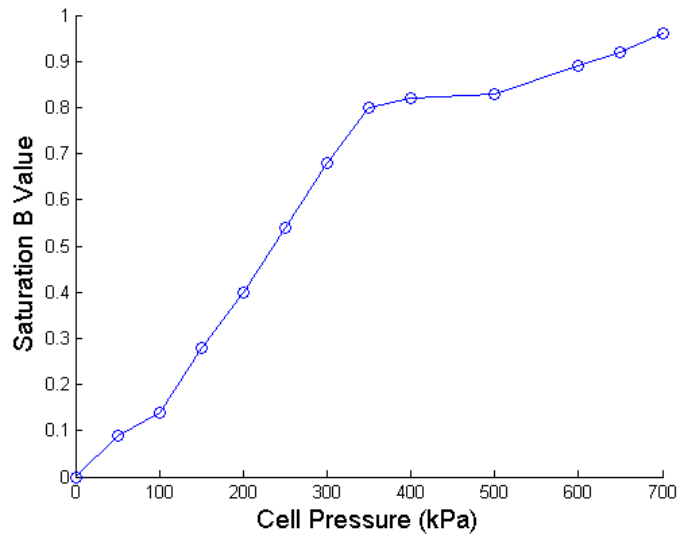


Figure 4.11: Saturation B-value with increasing cell pressure

### Consolidation Stage

The consolidation stage is performed to compress the sample volume. It consists of three or more steps, each consisting of two parts; an undrained phase and a drained phase, Figure 4.12. In the undrained phase the cell pressure is increased so it exceeds the back pressure by the desired effective stress  $\sigma_{eff}$ . This effective stress generates excess pore pressure which eventually reaches an equilibrium. This excess pore pressure generates a stress at the pore walls. In the drained phase the back pressure is allowed to dissipate until the pore pressure is equal to the back pressure. This is achieved by opening the drainage and allowing the excess fluid to leave the sample. The result is a sample with pore fluid at equilibrium pressure throughout and there is no pressure gradient or flow of liquid within the sample.

These steps are repeated until the desired cell pressure for the permeability stage has been reached. The effective stress is increasing gradually at each stage so as not to cause damage to the sample.

### Permeability Stage

Following the saturation and consolidation stages, the fluid within the sample is in an equilibrium pressure state. As a result, when it comes to the permeability stage, any uneven pressure applied to the sample will cause a flow of fluid through the sample. A pressure differential is applied between the back pressure  $P_2$  and drain pressure  $P_1$ , as shown in Figure

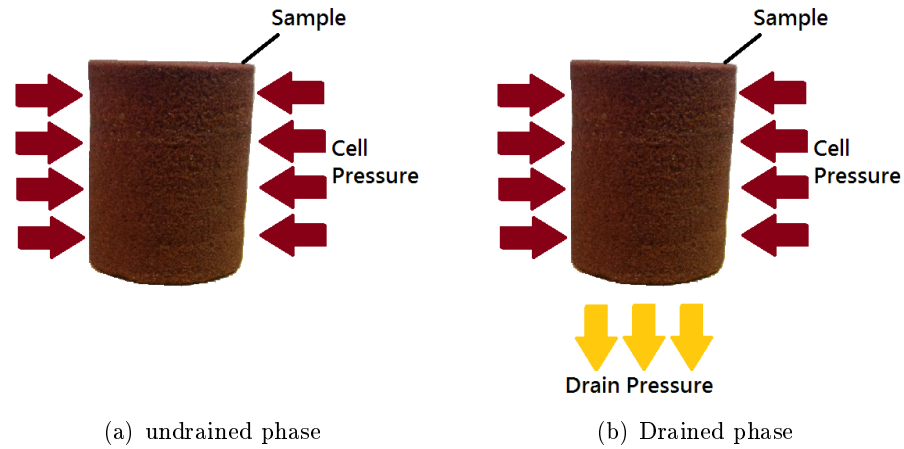


Figure 4.12: Pressures applied through the consolidation stage of the permeability experiment

4.13. Once a steady state of flow is achieved in and out of the sample, the rate of volume flow  $q$  can be recorded. This rate of volume is dependent on the specific pressure differential. This is repeated for three more values of pressure differential and the corresponding rates of fluid flow are plotted against the pressure differential. The gradient of this diagram is the permeability  $k$  of the sample and can be calculated using Equation 4.10. Here,  $L$  is the length of the sample,  $A$  is the cross sectional area,  $R_t$  is the temperature correction factor for the viscosity of the water (value of 1 for  $20^\circ\text{C}$ ) and  $p_c$  is the correction pressure caused by the pressure loss in the system for the specific rate of flow.

$$q = \frac{1.63 \cdot k \cdot L}{A(p_1 - p_2) - p_c} \cdot R_t \cdot 10^{-4} \quad (4.10)$$

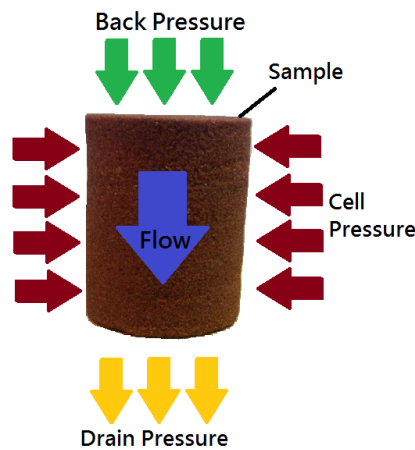


Figure 4.13: Pressures applied through the permeability stage of the permeability experiment



### 4.3 Measured Sample Parameters

Ten samples were exposed to the parameter measuring compressive strength test and indirect tensile strength test. The testing methods of the samples have been described with regard to the recommended Standards. Adaptations of the standardised tests were described along with an justification of test modifications.

The experiments provided material properties of the Locharbriggs sandstone, as seen in Table 4.1. These were used as control values to compare with treated samples, and for inclusion into Finite Element Analysis models.

Parameter		Value
Density	( $kg/m^3$ )	2062
Tensile Strength	( $MPa$ )	3.13
Compressive Strength	( $MPa$ )	29.18
Young's Modulus	( $GPa$ )	2.28
Poisson's ratio		0.45
Porosity	(%)	21.25
Permeability	( $m/s$ )	$4.4 \times 10^{-9}$

Table 4.1: Material properties calculated from compression test for the Locharbriggs sandstone in accordance with ASTM standard

### 4.4 Summary

Rock characterisation tests are described in this chapter. The material properties of the samples were measured to confirm that the specific rock type chosen was suitable as a reservoir rock representative and for use in finite element analysis in following chapters These measurements are presented in Table 4.1. Comparing this rock with the typical reservoir rock properties described in Chapter 3 (Table 3.4) confirms that the sandstone used is an appropriate representation of reservoir rock.

A description of the measurements of the tensile strength of the samples which had been exposed to an ultrasonic field and comparing with control was presented. These measurements are used for comparison between treated and untreated samples to observe any weaknesses resulting in the samples following field exposure. This would indicate that an increase in sample porosity could be possible ultrasonic exposure, since a weakened state would be more susceptible to fracture. This in turn may be used to free any trapped gas, oil or water trapped

within the reservoir, increasing the overall yield.

All samples were cut to the dimensions appropriate for tensile strength testing for tensile strength measurements following ultrasound exposure. These samples were partially saturated with tap water for 21 days and 35 days using the wicking method. As described previously, the use of tap water allows dissolved vapour, as would be representative of fluid within a reservoir to be studied. Using a range of saturation durations allows a varying degree of saturation to be observed, where the 21 day saturated samples would expect to have more trapped air than the 35 day saturated sample.

## Chapter 5

# Finite element analysis and Model Validation

### 5.1 Finite Element Analysis

FEA is a numerical method for problem solving which is often used within the fields of engineering and mathematical physics. It proves a useful tool for dealing with complicated geometries, loading and material properties where other analytical solution are not easily obtained and has the benefit of being non-invasive and relatively simple. It has progressed drastically from its first problem solving method of stress and strain calculation to a wide range of problems including fluid mechanics, electrostatics, heat conduction, vibration and a wide range of material property behaviours. There are a wide range of computer packages which have become available, specific to the particular type of study required. PZFlex was used for dynamic analysis of the acoustic wave travelling within the characterisation bath.

FEA involves taking the physical complex model, idealising it and simplifying it into a mathematical model. The model is then discretised into elements and analysed. The displacements at points on these elements are used to calculate the stresses and strains in terms of this displacement. The equilibrium conditions or boundary conditions are then applied to the elements where appropriate to describe the physical problem.

In order to gain confidence in the design of the FEA model it is good practice to represent the model in the most simplistic of forms and build on complexity as model validity is confirmed.

Simple linear equations are not valid on a large scale or with complex physical geometry, however they can be considered to be valid for a small region of the model such as with an element. With an element, simple equations can be solved with acceptable accuracy using valid numerical approximations. The structure can then be rebuilt, transferring the solution to the surrounding elements resulting in a solution for the entire physical geometry.

An explicit dynamic equation depends on the continual state of equilibrium which the system will strive to adopt. The dynamic equilibrium equation can be applied to any mechanical system. The equation for dynamic equilibrium can be seen in Equation 5.1 where  $P$  is an external force,  $I$  is the internal load vector,  $M$  is the mass matrix and  $\ddot{u}$  is the acceleration.

$$M\ddot{u} = P - I \quad (5.1)$$

Explicit dynamics is the mathematical technique which integrates the equations of motion throughout time. The integration method behind PZFlex analysis is known as the Euler or 'Central Difference' algorithm. Applying a lumped mass matrix  $M$  to the system, PZFlex can calculate the nodal acceleration at any given time using Equation 5.2.

$$\ddot{u}|_{(t)} = M^{-1} \cdot (P - I)|_{(t)} \quad (5.2)$$

Explicit analysis is used as opposed to implicit analysis as it is more appropriate for compact 2D and 3D models spanning tens of wavelengths, typical of ultrasonic applications. Implicit analysis requires the generation of complex matrices which couple the entire structure while calculating the solution. This is a relatively simple process for simple problems however increases in computational resources as the model complexity increases. Explicit analysis does not require these complex matrices so where possible, is preferential.

In this study, the acoustic pressure generated in the fluid and resulting generated stress in the solid material are under investigation. Two tanks are modelled; the characterisation tank and the test tank. The characterisation tank configuration was modelled and the FEA analysis conditions modified to replicate physical pressure measurements from the tank. Once these conditions of the FEA characterisation tank were verified, the same conditions were applied to the test tank for calculation of the field generated during sample testing.

### 5.1.1 FEA Assumptions

The key to generating an effective FEA model is in using the appropriate model simplifications and approximations regarding boundary conditions and material properties. Model simplification were made using a variety of assumptions when approximating the material and geometry. These include:

- The material behaves as if perfect and defect free
- The material behaves as if isotropic
- The material behaves as if a linear elastic
- The geometry can be represented as a 2D cross section

## 5.2 The Model

FEA is only as precise as the data which is entered into the model, so it is important to choose the correct conditions to apply during analysis. The geometry is generated to replicate the physical configuration. Once this has been modelled, the appropriate conditions must be applied to the geometry. The material properties are applied to the appropriate section or part. The part is then discretised before the boundary conditions are applied. The material properties allow the description of how that part reacts with the surrounding environment. This description takes the form of input into a mathematical equations, depending on the nature of the problem, which known can be inserted in the form of the material properties, and allow the unknown to be calculated. How the model is discretised dictates the degree of accuracy by which the calculations should occur. A more heavily discretised model will yield more accurate solution yet be more computationally and time demanding. The boundary conditions prescribes reactions or conditions to certain nodes by assigning values of displacement.

### 5.2.1 Material Properties

#### Isotropic material

The materials used for the analysis are modelled as an isotropic elastic materials using the experimentally evaluated material properties. Hooke's law describes the relationship between the stress and strain of a body when the strain is sufficiently small that the stress and strain depend linearly on each other, as with a linear elastic material. It gives the relationship with reference to the stiffness tensor  $C$ , which describes the elastic constants of a medium. Each component of stress  $\sigma$  is linearly dependent on the strain component  $\epsilon$  and vice versa, Equation 5.3. The material properties of an anisotropic are directional whereas an isotropic material is one which has identical material properties in all directions. Isotropy is introduced into a FEA model via the stiffness tensor. This stiffness tensor can be significantly simplified to one with 12 stress values where a material is isotropic (see Equation 5.4) as opposed to one of 81 values for an anisotropic material. With this scenario, there are only two quantities necessary to calculate the relationship between the stress and strain, the Young's Modulus and the Poisson's ratio which represent the resistance to change in volume and shearing deformations respectively.

$$\sigma = -C \cdot \epsilon \quad (5.3)$$

$$\begin{pmatrix} \sigma_{11} \\ \sigma_{22} \\ \sigma_{33} \\ \sigma_{12} \\ \sigma_{31} \\ \sigma_{23} \end{pmatrix} = \frac{E}{(1+\nu)(1-2\nu)} \begin{bmatrix} 1-\nu & \nu & \nu & 0 & 0 & 0 \\ \nu & 1-\nu & \nu & 0 & 0 & 0 \\ \nu & \nu & 1-\nu & 0 & 0 & 0 \\ 0 & 0 & 0 & \frac{1-2\nu}{2} & 0 & 0 \\ 0 & 0 & 0 & 0 & \frac{1-2\nu}{2} & 0 \\ 0 & 0 & 0 & 0 & 0 & \frac{1-2\nu}{2} \end{bmatrix} \cdot \begin{pmatrix} \epsilon_{11} \\ \epsilon_{22} \\ \epsilon_{33} \\ \epsilon_{12} \\ \epsilon_{31} \\ \epsilon_{23} \end{pmatrix} \quad (5.4)$$

For an isotropic linear elastic material, the bulk modulus, shear modulus and density are used to define the longitudinal  $v_l$  and shear wave velocity  $v_s$  as shown in Equations 5.5 and 5.6.

$$v_l = \sqrt{\frac{K + \frac{4}{3}\mu}{\rho}} \quad (5.5)$$

$$v_s = \sqrt{\frac{\mu}{\rho}} \quad (5.6)$$

Representing stone as an isotropic medium is an assumption often used in geophysical applications as the equations are much easier to understand, the computational costs are considerably less and accurate results are obtained. Although most sedimentary rocks are anisotropic, many of the current geomechanical models incorporate isotropic assumptions. In an investigation of the pore pressure and horizontal stress profile, it was found that a model assuming isotropy for sandstone profile showed negligible difference, however pore pressure was underestimated by the use of an isotropic model. Since pore pressure modelling is out-with the scope of the study, the benefits of ease of representation and a decrease in computational cost and time associated with isotropic representation outweigh the costs, making it the most appropriate modelling type.

### Linear elastic material

A linear elastic problem is one where the solution satisfies the equations and boundary conditions at each node for the normal and shear strains. Considering a finite volume of matter, the generated stresses as a result of an external force are identified in Figure 5.1. Here, the subscript 1, 2 and 3 denote the axial direction and a double subscript denotes the axis of the plane, and the axis which it is acting in this direction (for example  $\epsilon_{12}$  is the strain generated in plane 1, in direction of plane 2). For a linear elastic material, the normal stresses, the stresses acting in the direction of the plane ( $\sigma_{11}, \sigma_{22}, \sigma_{33}$ ) and shear stresses, the stresses acting in an axis perpendicular ( $\sigma_{12}, \sigma_{23}, \sigma_{13}, \sigma_{21}, \sigma_{32}, \sigma_{31}$ ) can be represented by the stress matrix in Equation 5.7 and 5.8. Since  $\sigma_{21} = \sigma_{12}$  (etc) we can see that there are a total of 6 independent stress components. Likewise, the corresponding strains generated are shown in Figure 5.8 where there are 6 independent strain components. These stresses are strains as a result of the displacements in the  $x, y$  and  $z$  direction. This gives a total of 15 unknowns in the analysis.

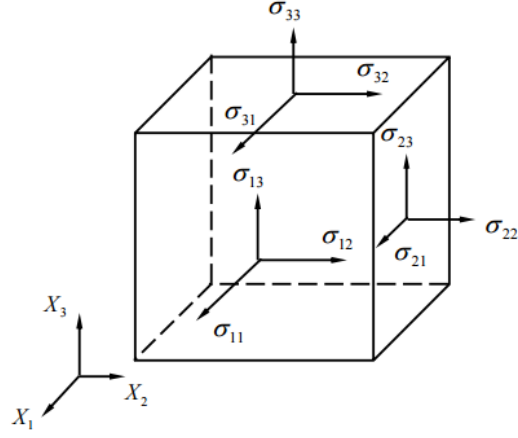


Figure 5.1: Stresses generated on each plane in 3 axis

$$\sigma = \begin{bmatrix} \sigma_{11} & \sigma_{12} & \sigma_{13} \\ \sigma_{21} & \sigma_{22} & \sigma_{23} \\ \sigma_{31} & \sigma_{32} & \sigma_{33} \end{bmatrix} \quad (5.7)$$

$$\epsilon = \begin{bmatrix} \epsilon_{11} & \epsilon_{12} & \epsilon_{13} \\ \epsilon_{21} & \epsilon_{22} & \epsilon_{23} \\ \epsilon_{31} & \epsilon_{32} & \epsilon_{33} \end{bmatrix} \quad (5.8)$$

The normal strains are as described in terms of displacement in the equations below, Equation 5.11, where  $x, y, z$  is the displacement in axis 1, 2 and 3 respectively. The shear strains are shown in Equation 5.12, where  $x, y$  and  $z$  are the displacements in the  $x$  direction and  $u, v, w$  are the axial direction.

$$\epsilon_{11} = \frac{\delta u_1}{\delta x_1} = \frac{\delta u}{\delta x} \quad (5.9)$$

$$\epsilon_{22} = \frac{\delta u_2}{\delta x_2} = \frac{\delta v}{\delta y} \quad (5.10)$$

$$\epsilon_{33} = \frac{\delta u_3}{\delta x_3} = \frac{\delta w}{\delta z} \quad (5.11)$$



$$\begin{aligned}
2\epsilon_{12} = \gamma_{xy} &= \frac{\delta u_1}{\delta x_2} + \frac{\delta u_2}{\delta x_1} = \frac{\delta u}{\delta y} + \frac{\delta v}{\delta x} \\
2\epsilon_{23} = \gamma_{yz} &= \frac{\delta u_2}{\delta x_3} + \frac{\delta u_3}{\delta x_2} = \frac{\delta v}{\delta z} + \frac{\delta w}{\delta y} \\
2\epsilon_{13} = \gamma_{xz} &= \frac{\delta u_1}{\delta x_3} + \frac{\delta u_3}{\delta x_1} = \frac{\delta u}{\delta z} + \frac{\delta w}{\delta x}
\end{aligned} \tag{5.12}$$

Solving for these unknowns takes into account the equations of equilibrium (Eq. 5.13), resulting motion as a result of the strains (kinematics, Eq. 5.14) and the behaviour between the stress and strain (constitutive, Eq. 5.15). These 15 equations can be used to solve for the 15 unknowns. This is the fundamental theory behind Finite Element Analysis.

$$\sigma_{ij} + f_i = 0 \tag{5.13}$$

$$e_{ij} = \frac{1}{2}(u_{ij} + u_{ji}) \tag{5.14}$$

$$\begin{aligned}
e_{ij} &= \frac{1 + \nu}{E} - \frac{\nu}{E} \sigma_{kk} \epsilon_{ij} \\
\sigma_{ij} &= 2G e_{ijj} + \lambda e_{kk} \epsilon_{ij}
\end{aligned} \tag{5.15}$$

The material properties of the sandstone are derived from mechanical testing. These tests were performed due to the wide range of variability of the material properties of this type of sandstone. It also ensured that the sandstone was an appropriate representation of petroleum reservoir rock matter. Water material properties are taken from literature [110] as these properties were not found to vary as widely. The material properties used for the FEA models can be seen in Table 5.1.

## Discretising

In FEA, the model representation of the problem is separated into discrete sections known as elements by a process referred to as meshing. This meshing allows the overall system to

Material	Density $\rho$ ( $g/cm^3$ )	E (GPa)	Poisson's ratio $\nu$
Acoustic Absorber	1.01	2.27	0.3
Aluminium	2.70	69.00	0.3
Sandstone	2.06	2.28	0.2
Water	1.00	2.20	-

Table 5.1: Material properties used in FEA

be divided into subsystems, each with its own set of governing equations. Once the type of mesh has been defined, the suitable size of mesh or degree to which the system is to be meshed must be determined. Smaller subsystems increase the quantity of subsystems, and as a result the computational demand. The degree of appropriate meshing is determined by the required accuracy of solution. Under-meshing will result in inaccurate or even incorrect results whereas over-meshing will cause unnecessarily high processing time.

Each subsystem of the divided model is known as an element, which is essentially a building blocks of the overall model. Nodes are the interconnecting points of adjacent elements, and can be seen as a part of an extremely simplistic 2D model shown in Figure 5.2. At a minimum, nodes must be present in a model at locations where there is a change in geometry or application of a load or boundary condition.

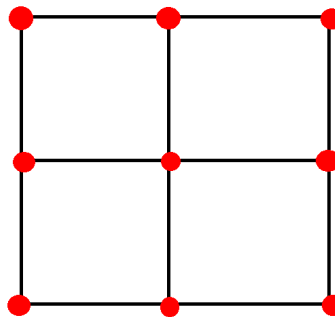


Figure 5.2: Simplistic diagram of 4 elements (black lines) and 9 nodes (red dots)

The use of a standard recommended meshing density of 15 elements per dominant wavelength of acoustic source is applied to the model. Where multiple materials are associated with a model, the material which facilitates the slowest wave speed of the highest frequency of interest

is chosen to calculate the meshing density. This ensures that the analysis is performed to the correct accuracy for the study and yields relevant results. Table 5.2 defines the maximum corresponding mesh size used in FEA for each material.

Material	Element size (m) (15 elements per $\lambda$ )
Acoustic Absorber	0.0050
Aluminium	0.0169
Sandstone	0.0023
Water	0.0049

Table 5.2: Element size used for FEA

### 5.2.2 Boundary Conditions

A boundary condition assigns a known value for a displacement onto a node or group of nodes. Applying a boundary condition specifies a value within the equations of state at that particular node or element in the model, which in turn influences the behaviour of neighbouring nodes in the model. An example of a boundary condition is a fixed wall providing no further displacement or an applied force which provides a displacement to a particular region.

### 2D models

Symmetry allows for substantial simplification to a model and can be applied using an axial or mirror representation, depending on geometry. Axial symmetry can be applied where the geometry is uniform over a revolution, Fig. 5.3(a) whereas a plane of symmetry can be applied where the geometry is mirrored exactly about a plane Fig. 5.3(b). Using this plane of symmetry, it is assumed that the same physical processes are applied on equal sides of the axis. A plane of symmetry was used for all models used in this study to significantly reduce computation time.

Choosing a 2D plane problem is an effective way to simplify a 3D problem where the geometry is symmetrical. It allows all stresses, strains and displacements in the third direction to be

zero, as shown in the equations below. This reduces the number of unknowns from 15 to 10.

$$\sigma_{33} = \sigma_{13} = \sigma_{23} = 0$$

$$\sigma_{11} \neq 0$$

$$\sigma_{22} \neq 0$$

$$\sigma_{12} \neq 0$$

$$F_3 = 0$$

$$\epsilon_{33} = \epsilon_{13} = \epsilon_{23} = 0$$

$$\epsilon_{11} \neq 0$$

$$\epsilon_{22} \neq 0$$

$$\epsilon_{12} \neq 0$$

$$u_3 = 0$$

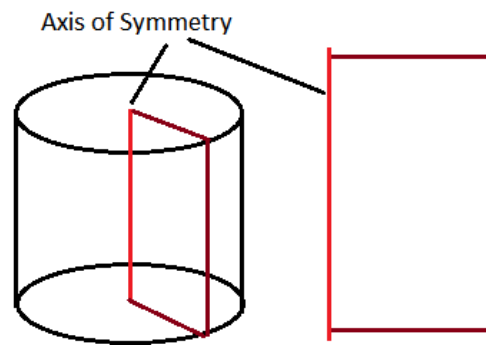
$$u_3 = 0$$

$$u_1 \neq 0$$

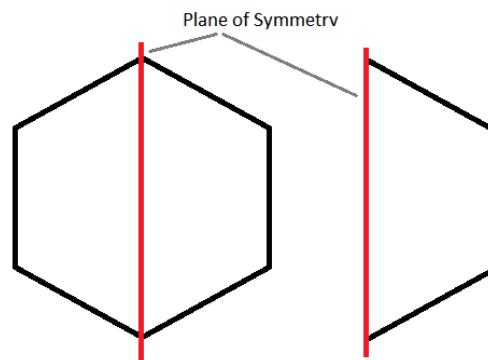
$$u_2 \neq 0$$

### Fixed Surface

To represent the walls of the vessel, an encastre condition was applied to the outer walls of the fluid. The encastre condition constrains nodes against displacement at any direction; displacement of the nodes are equal to zero. The acoustic absorber was represented as an absorbing boundary condition. This boundary absorbs energy at this interface and eliminates reflections from these boundaries.



(a) Axi-Symmetric Boundary



(b) Plane of Symmetry

Figure 5.3: Symmetry boundary conditions

$$u_x x = u_y y = u_z z = 0 \quad (5.16)$$

### Loads

The application of a force, moment, displacement, velocity, acceleration, temperature or heat flux can be applied to prescribed node points of the elements of a model.

A displacement was applied to the surface of the ultrasonic horn in the direction of the radiated source to represent the wave into the model. This was applied as a cyclic displacement at a frequency of 20 kHz to represent the ultrasonic wave field generated from a horn. The amplitude of this displacement was varied to represent the amplitude of the pressure field required within the bulk of the water.

## 5.3 FEA Model Validation

FEA was used to quantify the stress and pressure distribution generated due to the alternating ultrasonic wave field within the sandstone sample and within the surrounding water respectively. Steps were taken to ensure that the model was accurate as follows.

1. Generate a FEA model matching the physical set-up of the characterisation tank filled with fluid.
2. Include material properties from literature or experimental testing
3. Use the FEA model to calculate the pressure field in the fluid of characterisation tank.
4. Measure the pressure field of the fluid in the characterisation tank using hydrophone.
5. Compare the FEA calculated pressure field with experimentally measured pressure field measured using a hydrophone.
6. Modify the input boundary condition of the FEA model of the characterisation tank so that the magnitudes of pressure generated in the fluid matched the experimentally calculated pressure.
7. Using this modelled ultrasonic source, apply to test tank FEA model

8. Include the plaster or sandstone samples into the FEA model with the derived material properties.
9. Using FEA, calculate the pressure fields within the tank and stress fields generated within the sample during testing.

In order to ensure that the FEA results were accurate the models must first be checked against the physical system. Experimental analysis was performed on the characterisation tank. The pressure fields recorded were compared to the calculated FEA pressure trends. Modification of boundary conditions was performed to ensure appropriate matching of the calculated and measured pressure field. Analysis of the pressure field generated for the range of amplitudes of ultrasonic input was calculated for the experimental configuration by changing the amplitude of displacement of the applied sinusoidal displacement (representing hydrophone amplitude) until the magnitude matched that recorded experimentally. Once the pressure calculated from the FEA model matched the experimental pressure recorded, the model can be further progressed with the addition of a sample. This allowed for calculation of the effect of the acoustic pressure field on the samples. The internal stresses as a result of this pressure were also calculated using FEA. This FEA validation allows confidence in the results and calculation of stresses without an invasive experimental setup. At this point they could be deemed appropriate for the more complex analysis with the inclusion of the sandstone samples.

Two tanks were used; the characterisation tank which was used to scan the pressure field using the hydrophone and the test tank, in which the sample was exposed to the acoustic field. The characterisation tank is larger in volume to allow sufficient space for field measurements. The sample test tank was smaller in volume to optimise the ultrasonic field experience by the samples. The characterisation tank measured 540 mm wide and filled with degassed water to 400 mm high. The test tank measured 220 mm wide and was filled with degassed water to 115 mm high.

The FEA models of the characterisation tank and test tank are shown in Figure 5.4. The tanks walls were modelled using an encastre boundary, represented in the the figure as a solid yellow line, to represent the walls of the vessel. Encastre constrains all displacements and rotations at the node which is assigned the encastre condition. A free surface boundary condition was applied to the surface of the water and an axi-symmetric boundary, represented here as a dashed yellow line was applied to the central axis line of the model.

FEA was used to analyse the pressures generated as a result of the oscillating horn. The load was applied as an oscillating sinusoidal load at the surface of the horn, in an amplitude which was varied to ensure the pressure field represents the amplitude measured during pressure

characterisation.

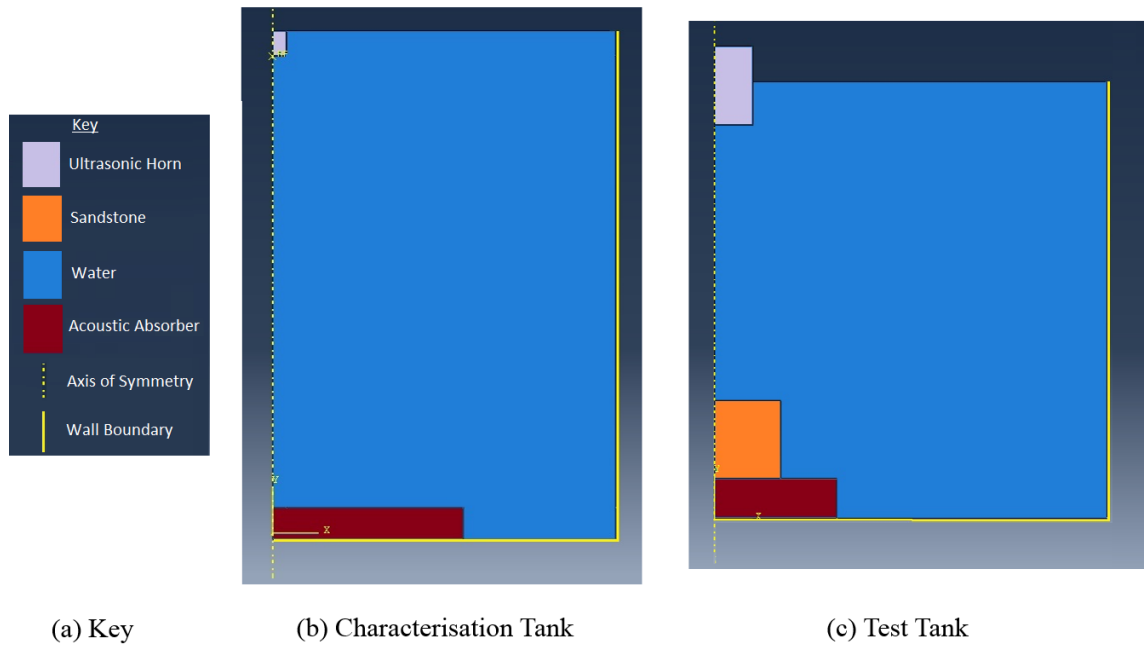


Figure 5.4: FEA model of the Characterisation tank and test tank (not to scale)

Once an FEA predicted pressure field was calculated, validation was performed experimentally using a Hydrophone. The acoustic pressure was measuring along the central axis of symmetry of the experimentation tank. For correct and accurate hydrophone measurements, there are several potential issues which must be considered. These include signal noise, transient emissions, the liquid medium choice and acoustic reflections.

In electronic measurements, noise is defined as a series of irregular fluctuations that accompany a transmitted electrical signal but are not part of it and tend to obscure the true reading. These noise signals could come from ambient sounds and vibrations from surrounding machines which are picked up by the measurement devices. To minimise noise as much as possible, ambient measurements were taken before the equipment was switched on and this noise was subtracted from the hydrophone and cavitation voltage measurements.

When equipment is first switched on the components experience unstable activity due to the sudden change in state. This transient state takes the form of a spike of electrical energy emissions before the equipment has normalised to a steady state. Before settling into a steady state, the frequency spectrum recorded would contain many different frequency components as opposed to the two or three dominant frequencies which are associated with longer, steady beam exposure. The acoustic device was left running throughout the duration of the experimental characterisation tests to allow a steady state field to be achieved to avoid transients.



To minimise the variability between experimental tests the medium used for the experiments was consistent throughout unless where otherwise stated. Water was degassed by boiling before being brought to room temperature in a sealed vessel and used for testing. Although the water was degassed, air bubbles may be introduced into the system when including the sample, horn or hydrophone to the tank. Any air bubbles within the field may disperse or reflect the acoustic wave which is being transmitted, decreasing the effect of the acoustic field and potentially causing damage to the ultrasonic horn. To reduce the chance of this occurring, any visible bubbles within the tank were physically cleared prior to testing.

Acoustic reflections from the side of the tanks should be avoided as they were not considered in the FEA model. A polyurethane rubber acoustic absorber was positioned at the bottom of the tank to minimize direct reflections from the ultrasonic horn. The acoustic absorber possesses an acoustic impedance similar to that of water and a high attenuation so waves are absorbed as opposed to reflected back into the field.

Acoustic reflections can also occur as a result of cavitation activity within the bulk of the fluid, known as cavitation shielding. Cavitation shielding occurs where cavitation bubbles which have been generated at the surface of the ultrasonic horn to prevent the transition of acoustic energy further into the liquid. This has been observed at higher amplitude experiments, as seen in Figure 5.5. These cavitation bubbles absorb the acoustic energy in growing and cavitating in either a stable or transient fashion and prevent the acoustic energy from entering the field where it is required.

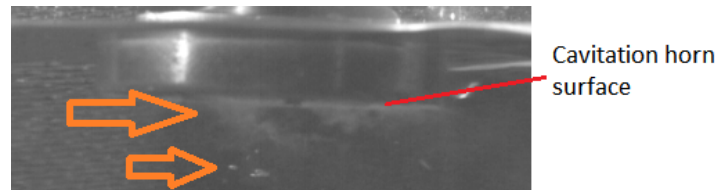


Figure 5.5: Cavitation bubbles generated at the horn surface at high amplitudes with cavitation regions highlighted by the arrow

### 5.3.1 Vibration analysis

#### Mode Shape Confirmation

The first step of pressure field characterisation was to ensure that the horn was vibrating in a longitudinal piston mode at 20 kHz. Experimental modal analysis was performed to confirm that the ultrasonic horn was vibrating in the mode shape predicted by FEA. A laser Doppler

Vibrometer (LDV) was used to validate the vibration mode of the ultrasonic horn. In order for LDV to be well understood, the Doppler effect must be described.

### Laser Doppler Vibrometry

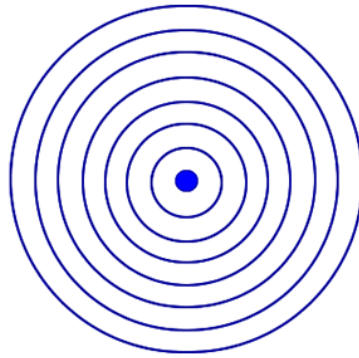
Laser-Doppler vibrometer (LDV) uses the interaction between two coherent light beams and the horn to calculate motion. In order to understand how a LDV measures the behaviour of the ultrasonic horn, the doppler shift must first be understood. The Doppler shift describes how the frequency of a wave changes if the source of the wave is moving relative to the observer. A familiar example of this effect is the change in pitch heard when a vehicle with a siren approaches, passes and continues into the distance from an observer. As the vehicle travels and emits the acoustic sound (the siren), while travelling in the same direction the emission of the sound, the wavelengths are compressed and the waves travelling in the opposite direction are extended. Figure 5.6(a) depicts an the acoustic field generated from a stationary source and travelling toward the acoustic sensor, for example a siren being generated from an ambulance and heard by a pedestrian. Figure 5.6(b) [111] shows how the siren generated by the ambulance is skewed due to the ambulance velocity in the direction of the pedestrian, with the wavelength being shortened in the direction of travel giving a higher pitch of siren than if it was stationary. As the ambulance passes, the siren wavelength lengthens as the source travels in the opposite direction from the pedestrian and the siren has a much lower pitch.

The frequency shift can be calculated depending on the direction of the wave source as described in Equation 5.17 for an approaching wave and Equation 5.18 for a departing wave.

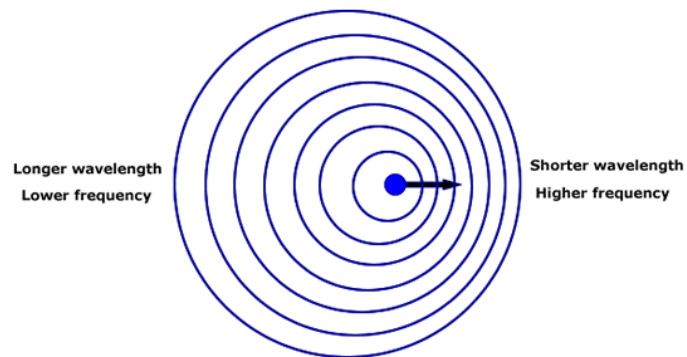
$$f_{observed} = \left[ \frac{v}{v - v_{source}} \right] f_{source} \quad (5.17)$$

$$f_{observed} = \left[ \frac{v}{v + v_{source}} \right] f_{source} \quad (5.18)$$

Applying this same principle to the ultrasonic horn reflecting a laser beam as opposed to the ambulance emitting an acoustic wave we can calculate the speed and therefore amplitude of vibration of the oscillating face. If the object is stationary, the reflected laser beam would be the exact same frequency and wavelength as the radiated beam. If the surface is moving toward the reflected beam, there is a shorter return distance to travel and the wavelength will



(a) Waves radiated from a stationary acoustic wave source



(b) Doppler effect representation of waves radiated from a travelling acoustic wave source

Figure 5.6: The doppler effect

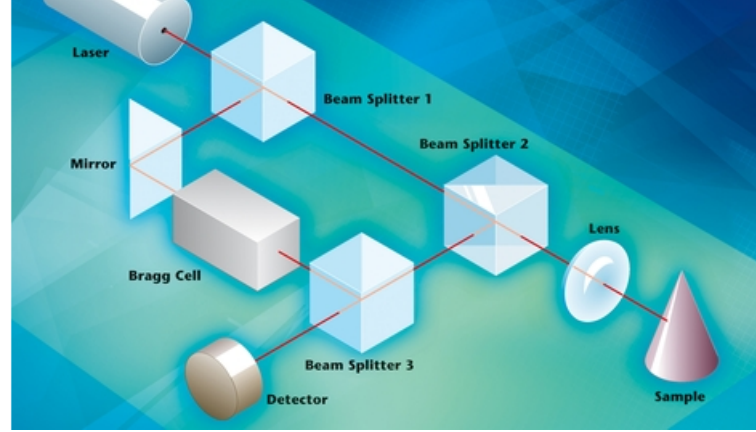


Figure 5.7: Typical LDV configuration

decrease (since the speed is the same). The change in wavelength of the emitting wave and returning wave can be used to calculate the speed of vibration of the horn.

The laser beam configuration of a typical LDV can be seen in Figure 5.7 [112] showing the separation of the laser beam into the reference beam and the measurement beam, using a beam splitter. The measurement beam then passes through a secondary beams splitter before being focused on the test object. The reflected beam is then passed to a third beam splitter, which combines the measurement beam with the reference beam and sent to the detector.

As the path length of the reference beam ( $r_2$ ) is constant over a time, any motion of the target object measured by  $r_1$  generates a dark and light interference fringe pattern on the detector. The complete dark and bright cycle on the detector corresponds to an object displacement of exactly half a wavelength of the light used. To determine the direction of motion, an acousto-optic modulator (Bragg cell) is placed in the reference beam, which shifts the light frequency by 40 MHz (by comparison, the frequency of the laser light is  $4.74 \cdot 10^{14}$  Hz). This generates a modulation frequency of the fringe pattern of 40 MHz when the object is at rest. If the object then moves towards the interferometer, this modulation frequency is reduced and if it moves away from the vibrometer, the detector receives a frequency higher than 40 MHz. This means that it is now possible not only to detect the amplitude of movement but also to clearly define the direction of movement.

The modulation frequency of the interferometer pattern is directly proportional to the velocity of the object. The sensitivity of this process is half the wavelength of the wavelength used. In this case, a Helium-Neon laser of wavelength 632.8 nm, so this process can measure changes as small as 316.4 nm. The total intensity calculated as a result of the two coherent waves of intensities  $I_1$  and  $I_2$  can be calculate using Equation 5.19 where  $r$  is the path length of the beam. The relationship between the two path lengths ( $r_1 - r_2$ ) Is the interference term.

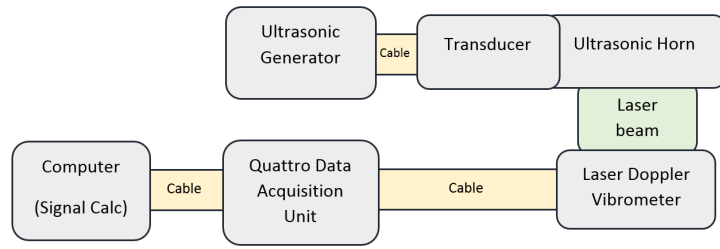
This term describes the relationship between path lengths between the two beams. Where path length  $(r_2 - r_1)$  is a full integer multiple then constructive interference occurs and the intensity is four times that of the single beam. An uneven number of half wavelengths will cause the opposite effect, destructive interference where the intensity of the beam will be zero. The benefit of LDV is that it is a non invasive means of measurement meaning there is no interference resulting from any added accelerometer mass. In addition, measurements are fast and minute amplitudes can be measured with great accuracy.

$$I_{total} = I_1 + I_2 + 2\sqrt{I_1 \cdot I_2} \cdot \cos\left[\frac{2\pi(r_1 - r_2)}{\lambda}\right] \quad (5.19)$$

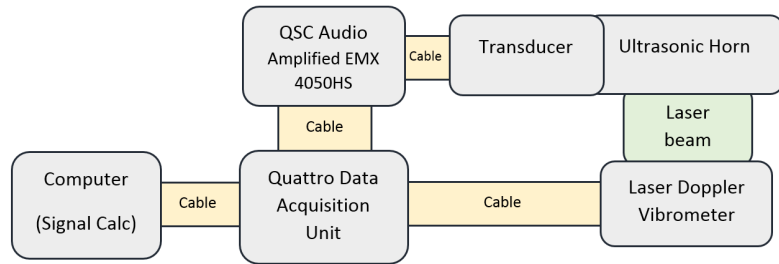
### Laser Experimental Configuration

Similar experimental configurations shown in Figure 5.8 were used for experimental modal analysis (EMA) of the vibrating horn and horn tip amplification measurements using a 3D and 1D laser doppler vibrometer respectively. For EMA, a signal generator (built into a Quattro DP240 data acquisition unit) provides a low power random excitation signal which is sent through a power amplifier (QSC Audio RMX 4050HD) before being sent to the transducer. The transducer vibrates in response to the frequencies of excitation which in turn vibrates the ultrasonic horn. For analysis of the mode of vibration, the horn was driven in free air and the behaviour of the horn at each frequency is measured. A Polytec 3D CLV-3D laser vibrometer measures the response of the ultrasonic horn in 3 axes at a series of pre-defined grid points along the horn. The raw signal measured by the vibrometer is extremely low in magnitude so it is passed through a conditional amplifier before being sent to the data analysis software (Signal Calc) on the PC. This analysed data was then imported to a modal extraction software, ME'ScopeVES, which extract the mode shapes of the ultrasonic horn. Measurements were taken at 60 points on the ultrasonic horn and the mode of vibration analysed. The results at the operational frequency of 20 kHz showed the horn moving in a longitudinal mode, as was expected and predicted in the FEA. The resulting mode of vibration can be seen in Figure 5.9 where the green skeleton shows the resting position of the horn. This confirms that the horn was truly acting as a piston transducer at the frequency of use and that the representation within FEA is appropriate.

Once the mode of vibration of the horn was confirmed to match that applied in the FEA model, the amplitude of the horn representation in FEA was scaled to match the amplitude of vibration of the tip of the horn. The ultrasonic horn is tapered and therefore amplifies the amplitude of the horn. The ultrasonic generator provided input values at the ultrasonic

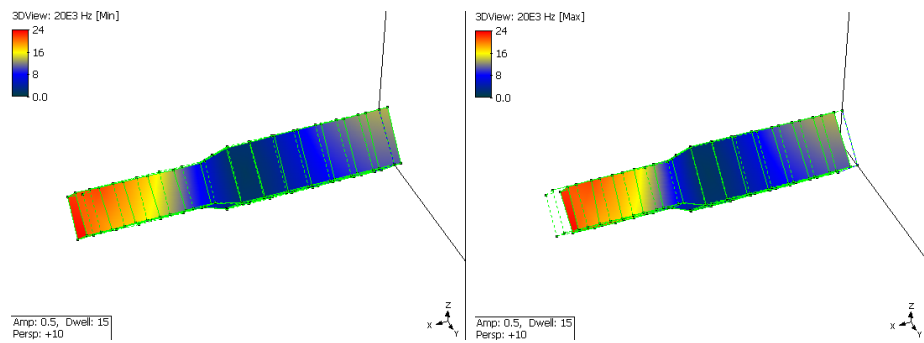


(a) 1D Amplitude Measurement



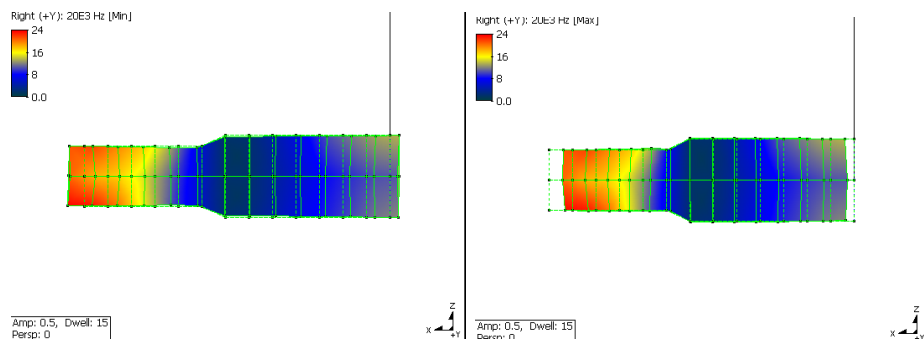
(b) 3D Experimental Modal Analysis

Figure 5.8: Experimental configuration for the 1D/ 3D LDV



(a) Maximum

(b) Minimum



(c) Maximum side view

(d) Minimum side view

Figure 5.9: Displacement of 20 kHz horn showing the longitudinal mode

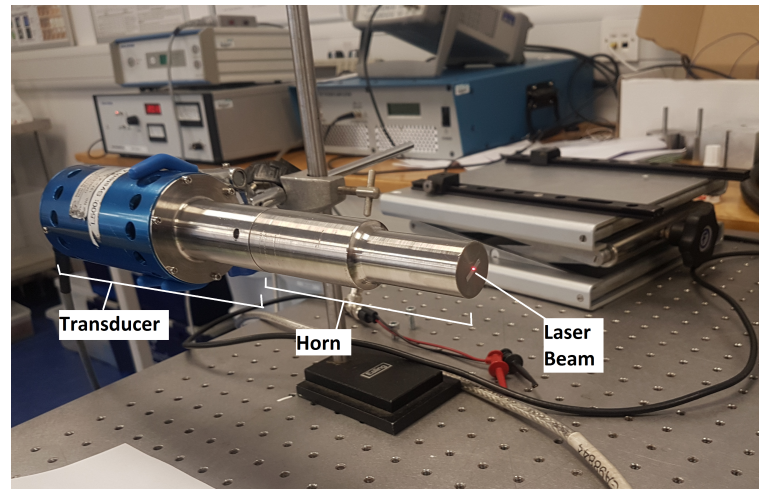


Figure 5.10: Typical LDV configuration

generator of a range from 1 to 10. These values were applied to the transducer and the displacement at the tip of the ultrasonic horn in free air is measured using a 1D laser vibrometer. To determine the precise amplitude of vibration at the tip of the horn, the transducer is driven at each amplitude using the ultrasonic generator and the displacement at the centre of the tip of the horn was measured using a 1D laser doppler vibrometer (Polytec, OFV 3001) with the experimental configuration shown in Figure 5.8(a). The laser was focused on the centre of the front face of the horn. The 1D laser measures the displacement in 1 direction, perpendicular from the face of vibration. The positioning of the 1D Polytec laser during measurements can be seen in Figure 5.10. The arbitrary input values to the transducer system of 1 to 10 with their corresponding displacement at the tip of the ultrasonic horn are shown in Figure 5.11.

### 5.3.2 The Hydrophone

Hydrophones are the most widely used tool for measurement of ultrasound pressure in water due to their high reliability and simplicity of use. A hydrophone is a device which converts acoustic pressure into an electrical signal from which the acoustic field can be calculated. The higher the pressure within the field, the higher the measured electrical response with a relationship defined by the hydrophone manufacturer. A Reson TC4035D needle hydrophone with a usable frequency range of 10 kHz to 800 kHz was used for measuring the pressure in the field. The TC4035D hydrophone is made of a piezoelectric thermoplastic fluoropolymer called polymer polyvinylidene fluoride (PVDF), produced by the polymerisation of vinylidenedifluoride. PVDF can be poled by placing it under a strong electric field to induce a net dipole moment. A net dipole moment occurs in a material where there is a separation of charge

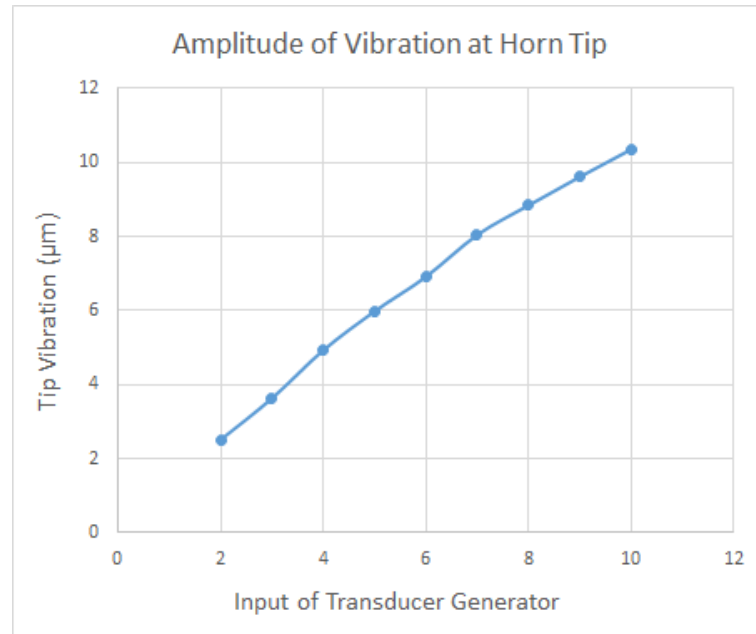


Figure 5.11: Amplitude of vibration at horn tip in relation to the amplitude in at transducer power generator

and atoms share an electron unequally, so one atom is more electronegative than the other. The more electronegative atom pulls more tightly on the shared electron. In a piezoelectric material, the charges are exactly balanced, even if not symmetrically arranged. The effects of the opposing charges cancel each other out leaving no net charge on the face of the material i.e. the electric dipole moments cancel each other out. If you apply a mechanical stress on the material, the charges are forced out of balance. The effects of the charges (dipole moments) no longer cancel each other out and a net positive and negative charge appears on the opposite face and a voltage is produced across these faces. As described in Chapter 2, piezo-electricity is an electric charge that accumulated in certain material in response to an applied mechanical stress. In this scenario, the application of mechanical stress is in the form of an acoustic wave on the surface of the hydrophone. An advantage of using a PVDF hydrophone over alternatives such as a ceramic hydrophone is that it possesses an acoustic impedance which is more closely matched to that of water having less of an influence on the acoustic field.

Needle hydrophones have the advantage over larger membrane hydrophones of measuring the response of a much smaller area allowing for better spatial resolution and less intrusion on the acoustic field. Since the voltage reading from the hydrophone is extremely low, a pre-amplifier was attached between the device and the DPX500MHz Tektronix DPO7054 digital oscilloscope where the voltage readings could be recorded. An average of 20 voltage readings are taken for each point and averaged. The points were taken at 1cm intervals along the axis of symmetry of the experiment tanks. Using the voltage measurements  $V$  and hydrophone



sensitivity  $G$ , a specific property of the hydrophone, the pressure amplitude  $P$  was calculated using Equation 5.20. The Reson hydrophone has a sensitivity of  $-214dB$  re  $1\frac{V}{\mu Pa}$  which translates to a voltage conversion sensitivity ratio of  $1.995 \times 10^{-11}(\frac{V}{\mu Pa})$  or  $1.995 \times 10^{-5}(\frac{V}{Pa})$ .

$$P = \frac{V}{G} \quad (5.20)$$

It is standard practice to refer to the acoustic pressure in logarithmic form of decibels ( $dB$ ), relating the pressure to a reference pressure  $P_{ref}$ . In underwater acoustics it is standard to take the reference pressure as  $1\mu Pa$  so the acoustic pressure values are usually expressed in  $dB$  re  $1\mu Pa$ . Since intensity is proportional to the square of the acoustic pressure the corresponding expression for the acoustic pressure level  $P_a$  is calculated using Equation 5.21.

$$P_a = 10\log\frac{P}{P_{ref}} = 10\log\frac{P}{1 \times 10^{-6}} \quad (5.21)$$

### Near Field

A planar ultrasonic beam propagates as a longitudinal wave from the ultrasonic horn surface into the medium and exhibits two distinct beam patterns. A slight convergence of the acoustic beam occurs at a point in a region known as the near field. After this point the beam diverges in a region referred to as the far field. In the near field constructive and destructive interference of multiple waves are created by the ultrasonic horn. As a result the relative phase of the pressure field and the particle velocity are continually changing with position. This creates a complex and rapidly varying acoustic field closer to the acoustic source. The acoustic field can be unpredictable and non-linear. Once the far field point has been reached the acoustic field pressure and particle velocity are synchronised so the field is stable

Taking the speed of an acoustic waves in water  $v_a$  as  $1497 \text{ m/s}$  [113] the wavelength  $\lambda$  for each frequency  $f$  can be calculated using Equation 5.22. From this the perpendicular distance from the source  $z$  at which the far field initiates can be calculated using the diameter of the acoustic surface  $D$  and wavelength  $\lambda$  using Equation 5.23.

$$\lambda = \frac{v_a}{f} \quad (5.22)$$

$$z = \frac{D^2}{4\lambda} \quad (5.23)$$

The far field distance from the ultrasonic horn was calculated as 18.8 mm for the 74.84 mm wavelength of the 20kHz transducer. An erroneous measurement resulting from the near field interference would result in a mismatch with FEA, to measurements were taken beyond this point. An additional benefit of This also prevents damage of the measurement equipment from being in close contact with the acoustic surface.

### Hydrophone Measurements

Figure 5.12 shows the frequency response of the hydrophone within the pressure field from a 20 kHz transducer and ultrasonic horn. The driving frequency can be seen at 20 kHz as a peak pressure and a harmonic can be observed at 40 kHz. A low sub-harmonic voltage reading at 10 kHz was also detected however is not clear in this graph. Measurements from the 20 kHz horn used for experimentation for this study can be seen in Figure 5.13, showing a pure 20kHz output.

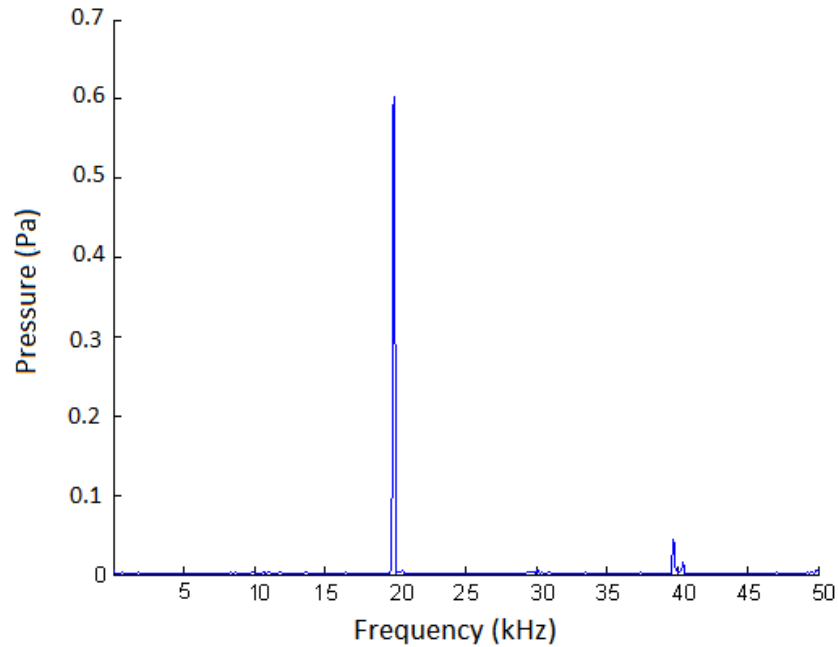


Figure 5.12: Frequency analysis of Pressure measurements from an alternative 20 kHz horn, showing sub-harmonics and harmonic measurements

The face of the ultrasonic horn was positioned 30 mm below the surface of the characterisation tank and driven at a low amplitude of  $0.5\mu\text{m}$  ( $\approx 0.5 \text{ W}$ ) for the initial characterisation

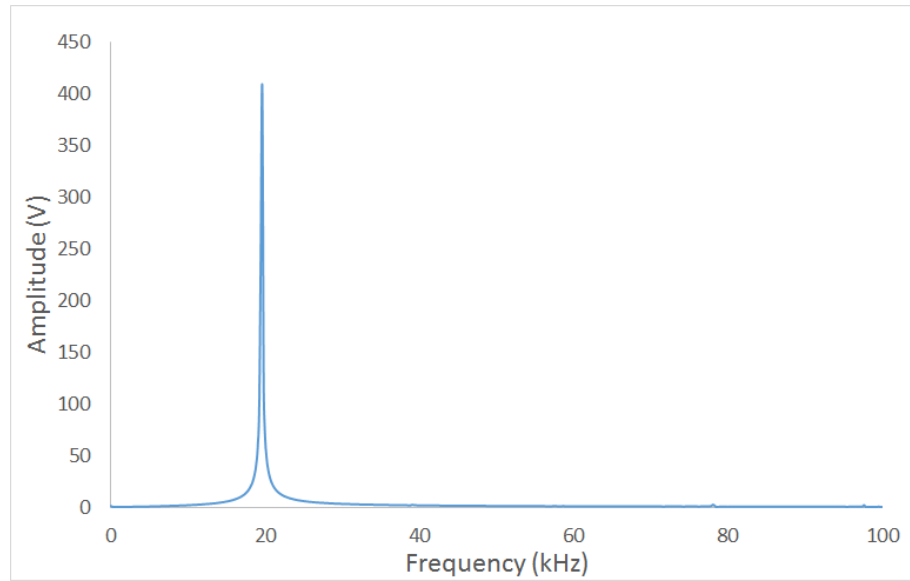


Figure 5.13: Frequency analysis of voltage recorded from the 20 kHz horn

measurements. This low setting was chosen to avoid any unnecessary damage to the hydrophone which may result from prolonged exposure. The face of the ultrasonic horn was wetted so no air bubbles are present to affect the acoustic field emitted from the source. The hydrophone scan was performed across the central plane of the large water tank at 10 mm grid intervals and pressure readings plotted. Measurements were taken from a distance of 20mm from the source of the horn to avoid near field calculations. A 3 axis motorised positioning system was used to increased accuracy and control over measurements. This gave a 2D pressure plot which is compared to the corresponding cross section within the FE results in Figure 5.14. The pressure can be seen to fluctuate as it radiates from the ultrasonic horn, at the bottom of the figure. Discrepancy between the measured and recorded fields shapes of the field are a result of the rougher sampling rate for the measurements preventing a smooth curved field from being observed. An axial scan of the pressure field radiating from the centre of the face of the ultrasonic horn and that measured using FEA is shown in Figure 5.15. These results show similar trends of high pressure closer to the source and low pressure at the regions furthest from the horn face. This shows a trend in agreement with the FE calculated field. Discrepancies between the two pressure fields can be explained by the lower resolution of measurement points with the hydrophone recordings and extrapolation of the pressure field.

### 5.3.3 Acoustic Characterisation

The amplitude of acoustic pressure within the tank was measured using the hydrophone at a fixed distance of 40mm below the ultrasonic horn at a range of amplitudes of vibration between

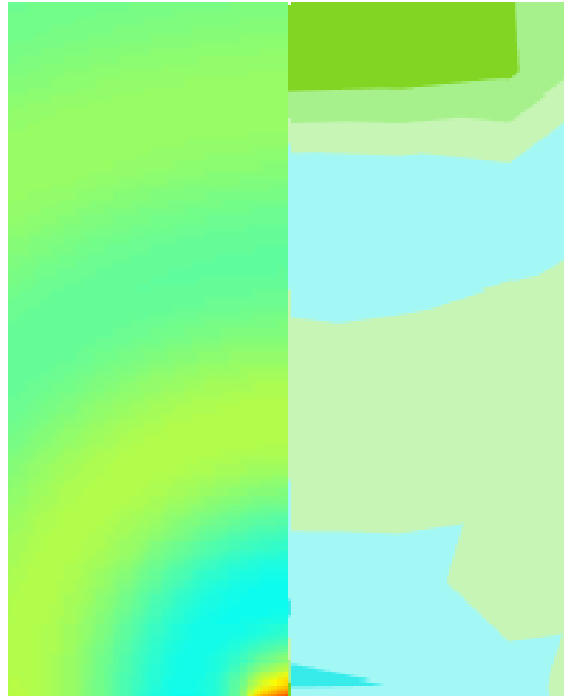


Figure 5.14: Plot of cross section of the pressure field measured using the Hydrophone (right) and calculated using FEA (left)

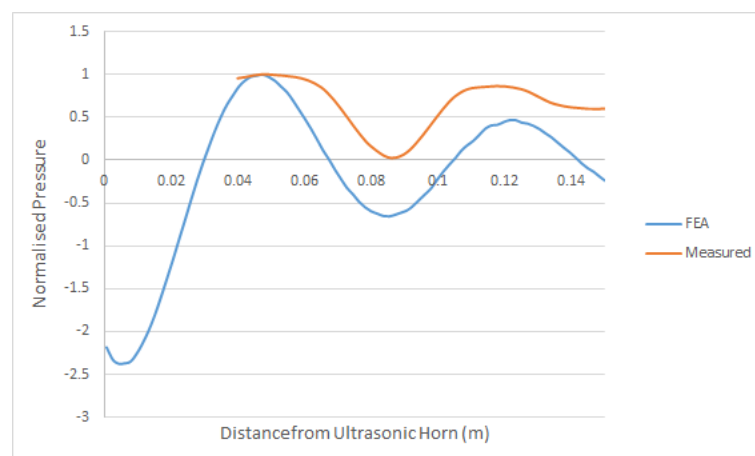


Figure 5.15: Comparison of axial scan of the Pressure field radiated from the centre of the horn calculated using FEA and measured using the Hydrophone

1  $\mu\text{m}$  and 5  $\mu\text{m}$ . This was performed to determine the relationship between the amplitude of vibration and the acoustic pressure. The resulting pressure amplitudes are plotted in Figure 5.16 showing that with an increase in amplitude beyond 2.5  $\mu\text{m}$ , the transmission of the acoustic field into the bulk of the fluid decreases. This was due to significant cavitation activity around the surface of the horn absorbing the acoustic energy and preventing it from reaching the remainder of the fluid. Acoustic streaming absorbs energy within liquids, with various studies being performed into accurately measuring the extent of this absorption [114]. Cavitation bubbles increase local attenuation coefficient of ultrasound by absorbing the energy input to the system. Where a large cluster of cavitation bubbles form near to the horn, the energy does not make it to the bulk of the fluid but is absorbed by the formation of cavitation bubbles [115]. The pressure fields generated within the FEA model was scaled according to these hydrophone measurements of the acoustic pressure. The calculated pressure fields generated for the range of transducer inputs can be seen in Figure 5.17 showing the optimum coupling of vibration from the horn into the water is at 2.5  $\mu\text{m}$  (1W).

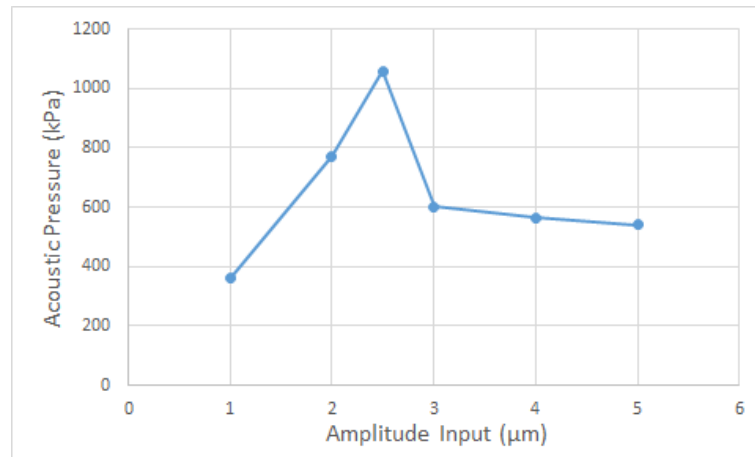


Figure 5.16: Pressure measured at a fixed point of 40 mm from the ultraonic source with increasing amplitude of transducer power source

Calculated pressure fields generated by the 5  $\mu\text{m}$  and 2.5  $\mu\text{m}$  ultrasonic horn displacement were applied to the FEA model of the fluid tank including the sandstone sample, with corresponding maximum pressures within the axial scan of 0.77 MPa and 1.1 MPa respectively. A comparison between these generated pressure fields within the test tank with 2.5  $\mu\text{m}$  and 5 amplitude of horn displacement can be seen in Figure 5.18. The stresses of 285 and 764 kPa respectively generated within the rock samples as a result of these pressure fields can be seen in Figure 5.20, which are plotted in Figure 5.19 and 5.21.

Preliminary testing using exposure times of either 5 or 10 minutes at an amplitude of 5  $\mu\text{m}$  indicated a decrease in tensile strength of a small batch of samples following exposure of ultrasonic wave fields with several of the treated samples fragmenting in a different plane to the control samples. Testing was performed for 30 minutes to attempt to replicate and

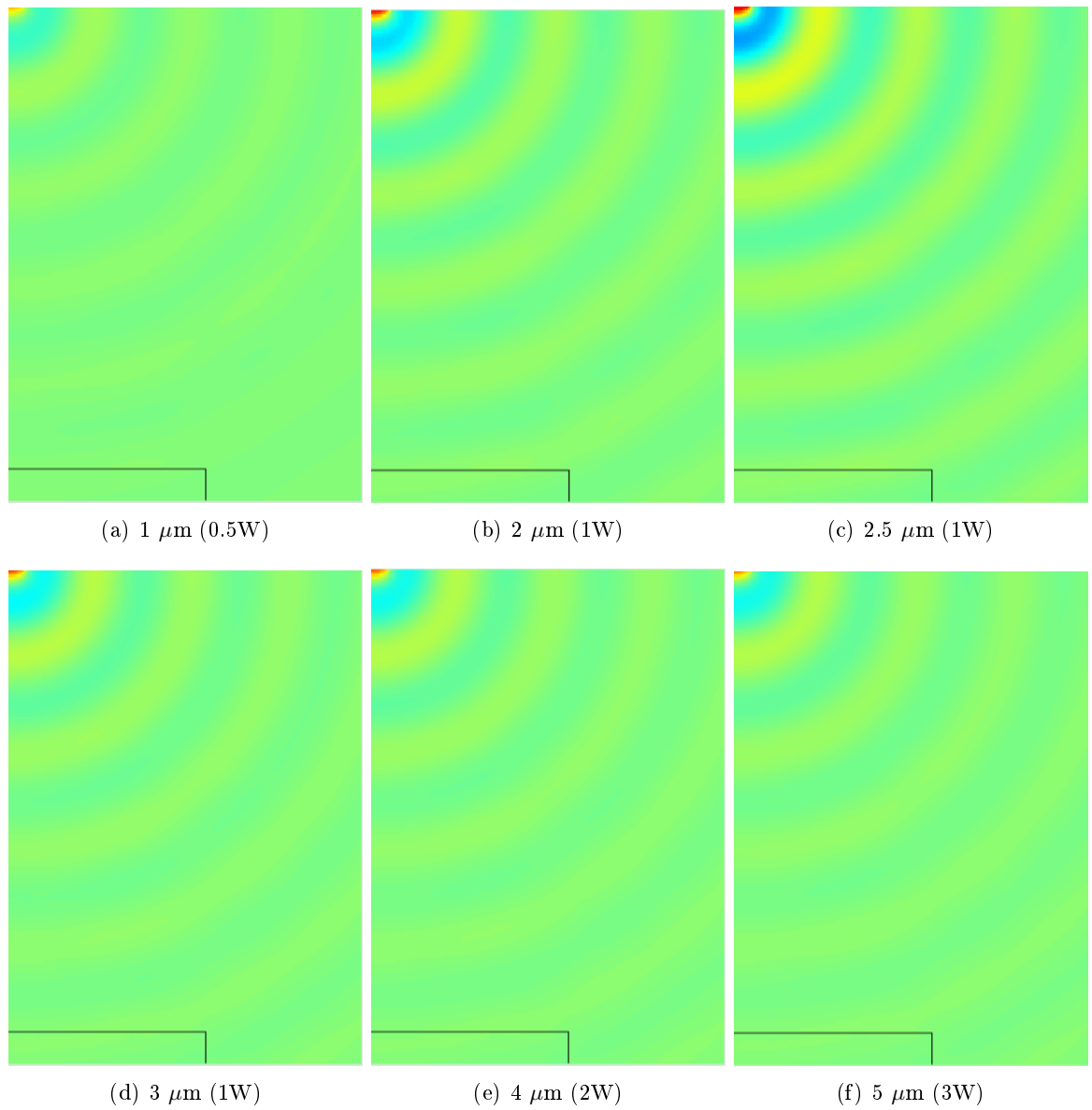


Figure 5.17: Pressure field comparison of the transducer amplitude in the characterisation bath

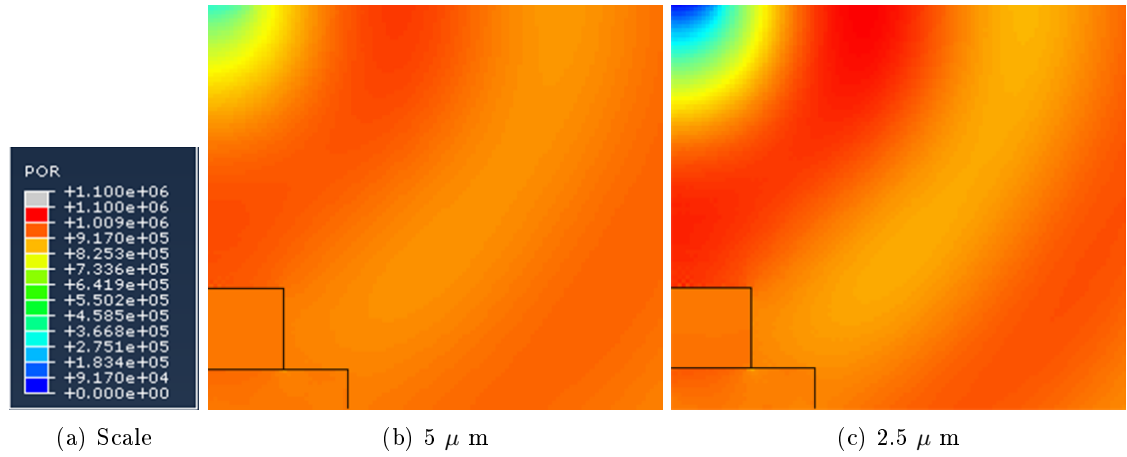


Figure 5.18: Pressure field generated in the fluid of the test tank

enhance the effect which the ultrasonic acoustic field is having on the samples.

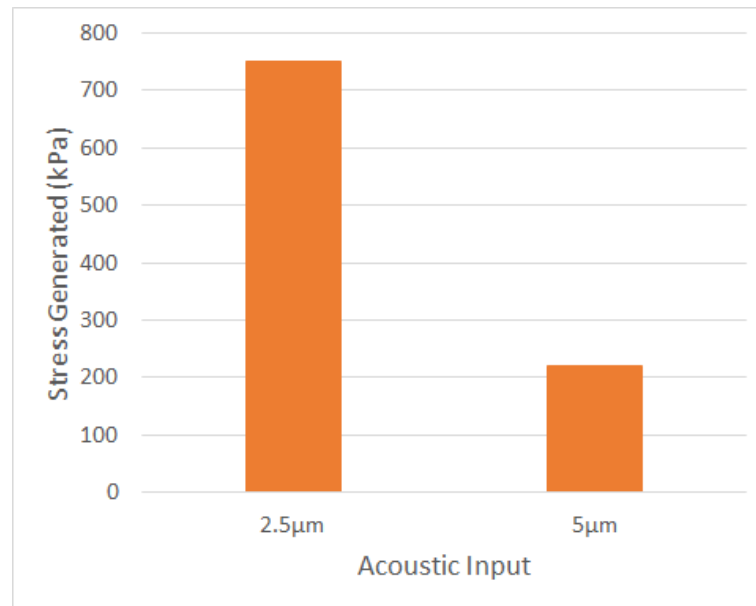


Figure 5.19: Calculated maximum axial stress generated with the sandstone during testing with corresponding maximum axial acoustic pressure generated

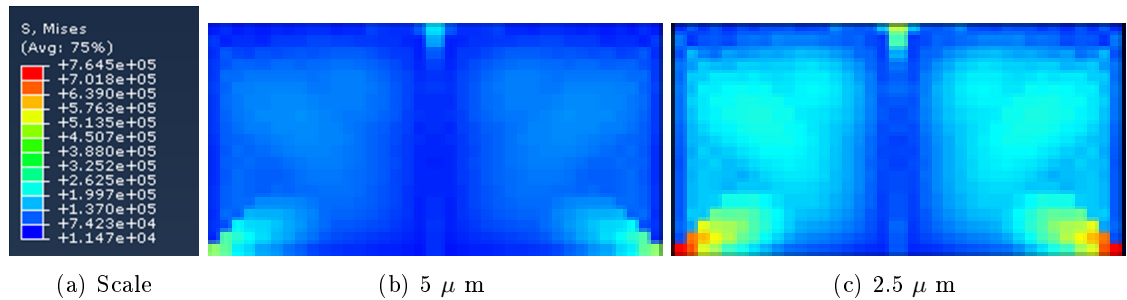


Figure 5.20: Stress field generated in the sandstone as a result of the pressure within the test tank

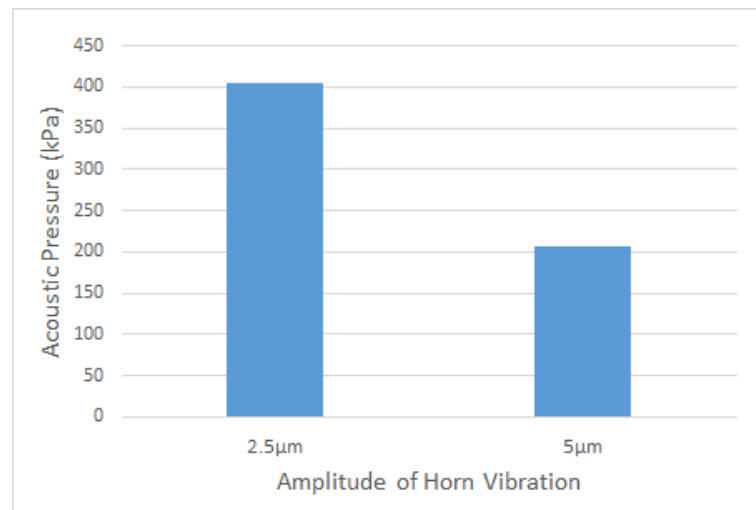


Figure 5.21: Calculated maximum acoustic pressure generated with the test tank for 2.5  $\mu\text{m}$  and 5  $\mu\text{m}$  input

#### 5.3.4 Cavitation

Application of an ultrasonic field to the small cavitation vessel showed clear signs of cavitation activity, Figure 5.22. There are a variety of methods which can be used to confirm the presence of cavitation activity such as recording the electrical current supplied to the ultrasonic system or measuring the displacement of the ultrasonic horn. The problem with these methods is that they do not provide a direct measure of the cavitation activity, but simply provide a measurement of the energy going into the system with an assumed relationship between cavitation activity and supplied current or amplitude of horn vibration.

Besides visual confirmation which may be difficult to consistently observe, another simple and commonly utilised method of confirming the presence of cavitation is by the use of aluminium foil. The foil is placed in the cross section of a cavitating liquid as a target for cavitation erosion. From the onset of ultrasonic activity, cavitation bubbles are observed darting around the foil. Regions of high cavitation activity are identified by a more abundant quantity of cavitation pitting as shown in Figure 5.23. While this method does identify regions of cavitation, an industry acknowledged non-intrusive method of numerically quantifying the cavitation field would be favourable.

#### Cavimeter

The NPL cavitation sensor known as a Cavimeter, shown in Figure 5.24, is a device which contains an internal sensing layer which acts in a similar way to a hydrophone in that it



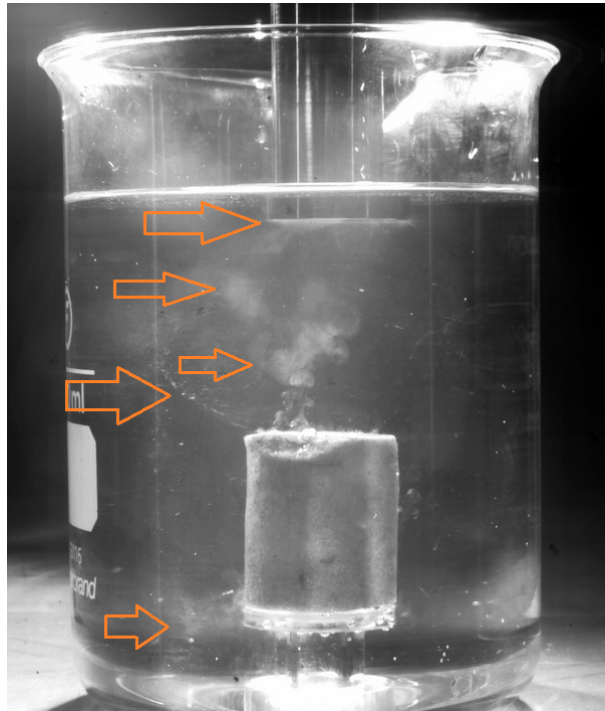


Figure 5.22: Cavitation clusters evident within the Cavitation vessel with regions of cavitation activity highlighted by orange arrows

possesses piezoelectric properties, and converts a mechanical pressure signal to voltage. The sensor consists of an inner strip of piezoelectric polymer film acting as an acoustic receiver. The sensor is shrouded in a 4mm thick layer of polyurethane which acts as a cavitation shield.

The NPL Cavimeter works as a real time measurement of cavitation activity. It operates by measuring the broadband acoustic signal of a localised volume and providing information about the energy associated with transient cavitation bubble collapse. The broadband acoustic signal measured relates to the magnitude of transient cavitation. A cavitation bubble exposed to an acoustic source absorbs and emits the acoustic energy, acting as a secondary acoustic source. These secondary acoustic emissions hold a lot of information related to the dynamics of the cavitation process. As opposed to cavitation sensors which focus on the low frequency emissions from cavitation fields to measure the cavitation activity, the Cavimeter measures the broadband noise emissions which focus on transient cavitation activity signals. A wide range of signals can be observed as a result of the application of an acoustic source; the fundamental frequency, harmonics, sub-harmonics, ultra-harmonics and the broadband signal.

As well as being a result of the acoustic source, the recorded voltage at the fundamental frequency  $f_o$  can also have contributions from linear bubble oscillations from stable cavitation bubbles as they fluctuate in size with the acoustic field absorbing and emitting acoustic energy.

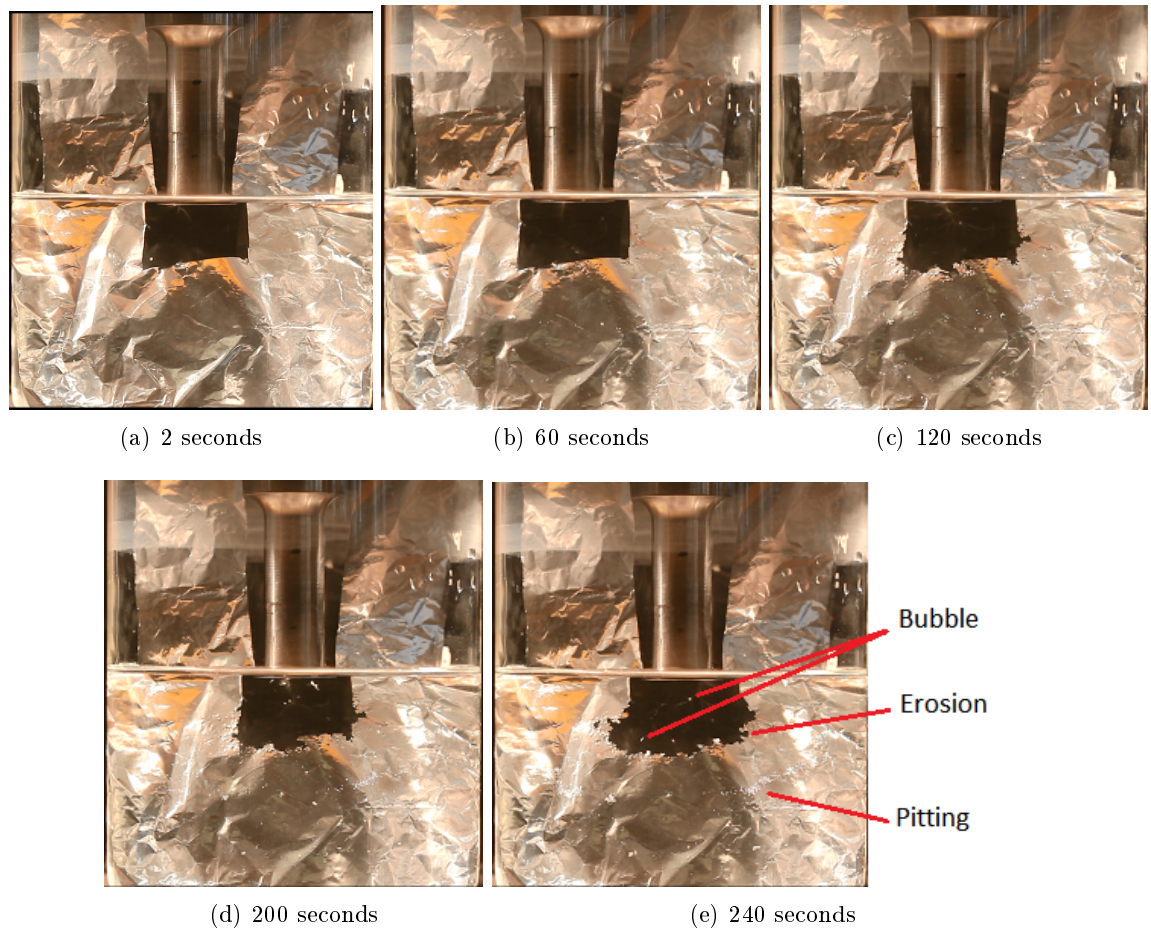


Figure 5.23: Cavitation erosion of aluminum foil

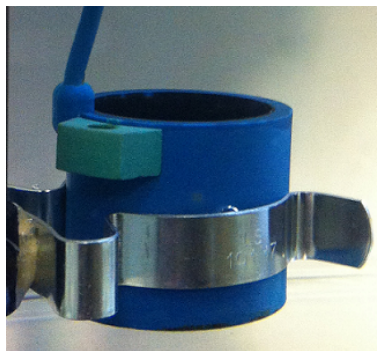


Figure 5.24: NPL Cavimeter

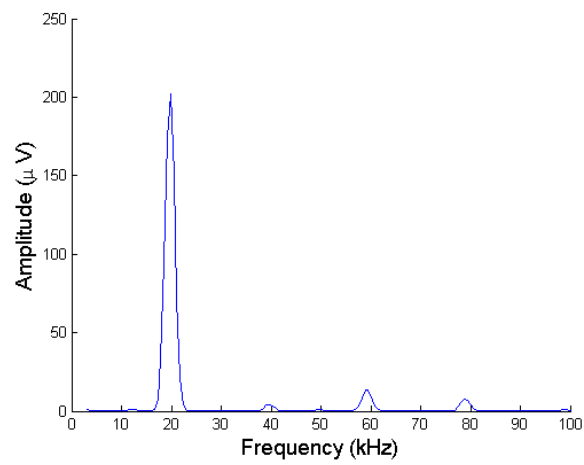
Harmonics occur at full integer  $n$  multiples of the fundamental frequency,  $nf_o$ . These harmonics are a result of direct readings from the ultrasonic horn due to harmonic signals in the electrical waveform, non-linear bubble oscillations and possibly non-linear propagation in the medium between the acoustic source and Cavimeter. Sub-harmonics occur at the inverse of full integer multiples of the fundamental frequency,  $\frac{f_o}{n}$ .

A bubble possesses a resonant radius at which it resonates with the applied frequency. When a bubble of double this radius is excited, or where a bubble takes more than a single acoustic period to reach critical size before collapse, sub-harmonic signals can be seen. Ultra-harmonics of the fundamental frequency are present at  $\frac{mf_o}{p}$  where  $m$  and  $p$  are integers,  $m > p$  and  $\frac{m}{p}$  is non integral. These ultra-harmonic frequency signals are present at bubble events similar to those that occur at sub-harmonic frequencies. In addition to these signals, a broadband signal is observed at all frequencies. This broadband signal is generated by the shock waves emitted by collapsing bubbles of a wide range of sizes.

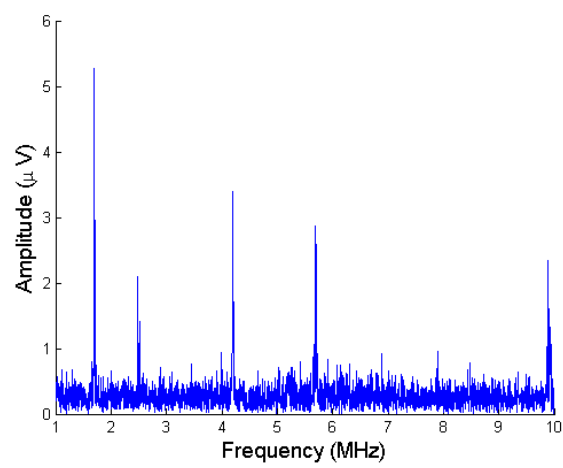
The Cavimeter measurements can be separated into three main ranges of frequency referred to as the low, sub harmonic and high frequency range. The low frequency of 20 - 60 kHz corresponds to the direct field of interest, that of the acoustic driving frequency, in this case 20 kHz. The sub-harmonic low frequency of 10 - 30 kHz detects sub-harmonics of the driving frequency to identify the onset of cavitation activity. The high frequency 1.5 -7 MHz range to measures transient cavitation effects is referred to as the broadband signal which we are interested in for cavitation quantification.

Figure 5.25(a) shows a lower range frequency response recorded using the Cavimeter in the cavitation bath at the operating fundamental frequency of 20 kHz. Sub-harmonics and harmonics can be seen as spikes in voltage response. In contrast to the lower range frequency response, the voltage readings of frequencies above 1 MHz and up to 10 MHz can be seen in Figure 5.25(b).

The broadband acoustic signals can be seen clearly in 5.25(b) as a voltage reading for the range of frequencies. In a cavitation field this signal contains information about the cavitation field as a result of shock waves emitted on the collapse of transient bubbles of a wide range of sizes so they can be attributed to the occurrence of violent transient cavitation [116,117]. The Cavimeter voltage reading for this violent transient cavitation can be used to calculate the broadband integrated power (BIP), the measurement of cavitation. The recorded power refers to the rate of energy within the measured volume of fluid, averaged over a time period as opposed to the total power in the acoustic beam or produced by cavitation activity throughout the vessel volume.



(a) Low range frequency readings



(b) Broadband range of frequency readings

Figure 5.25: Recordings from the Cavimeter

$$BIP = \int_{f_2}^{f_1} V_c(f)^2 df \quad (5.24)$$

The BIP can be calculated using Equation 5.24 where  $V_c(f)^2$  represents the frequency spectral squared magnitude recorded by the Cavimeter.  $f_2$  is the highest frequency considered, in this instance 10 MHz as it is the optimum limit at which the piezoelectric film can be used.  $f_1$  is the lowest frequency, in this case 1 MHz which corresponds to the frequency above which the acoustic spectrum is least affected by harmonic signals.

## 5.4 Chapter Summary

Finite element analysis of the experimental configurations was performed. The experimental arrangements were modelled using the appropriate dimensions of the equipment and the material properties calculated using experimental analysis and literature review. In order to get an appropriate representation, the ultrasonic horn performance was characterised using the hydrophone and applied to the model. Once the pressure was estimated, the boundary conditions of the FEA model were adjusted accordingly to match the pressure fields.

At this point a sample of the dimensions and material properties of the sandstone samples were included in the FE model and the generated stresses analysed. This allowed the stress generation as a result of each applied ultrasonic field can be observed.

## Chapter 6

# Results

### 6.1 Statistical Significance

In probability theory, Normal (or Gaussian) distribution is the most commonly used distribution method in statistics as it provides a suitable description of the spread of most natural occurrences. This distribution describes a set of data using the mean,  $\mu_m$  and spread of values about this mean, generally expressed in terms of variance,  $s^2$  or standard deviations,  $s$ . The probability density of the normal distribution is described using Equation 6.1 . Graphical representation of this probability density function surrounding the mean value can be seen in Figure 6.1 . The standard distributions from the mean captures a specific volume of the data range. For example 68.26% of the data falls within 1 standard deviation, 95.44% of the data falls within 2 standard deviations and 99.73% of the data falls within 3 standard deviations from the mean. The mean and standard deviation can be calculated used Equation 6.2 and 6.3, where  $N$  is the number of samples.

$$F(x | \mu, (s^2)) = \frac{1}{\sqrt{(2\pi s^2)}} e^{\frac{(x-\mu)^2}{2s^2}} \quad (6.1)$$

$$\mu_m = \frac{\sum x}{N} \quad (6.2)$$

$$s = \sqrt{\frac{\sum \mu_m z^2}{N}} \quad (6.3)$$

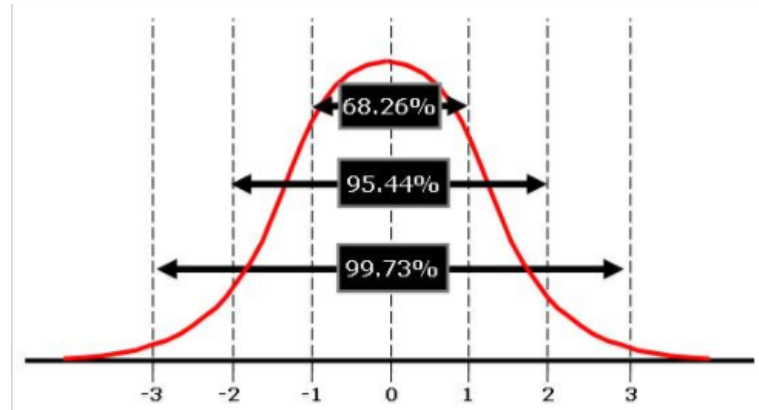


Figure 6.1: Normal distribution of standard deviations around the mean

### 6.1.1 Significance Testing

The spread of distribution of tensile strengths measured for the control batch of samples has a standard distribution as shown in Figure 6.2. It is the assumption of this normal distribution of data which allows statistical analysis in the form of significance testing to be performed on the batch of samples. Where the number of samples is sufficient to display a standard distribution of data, the t-test can be applied to determine statistical significance.

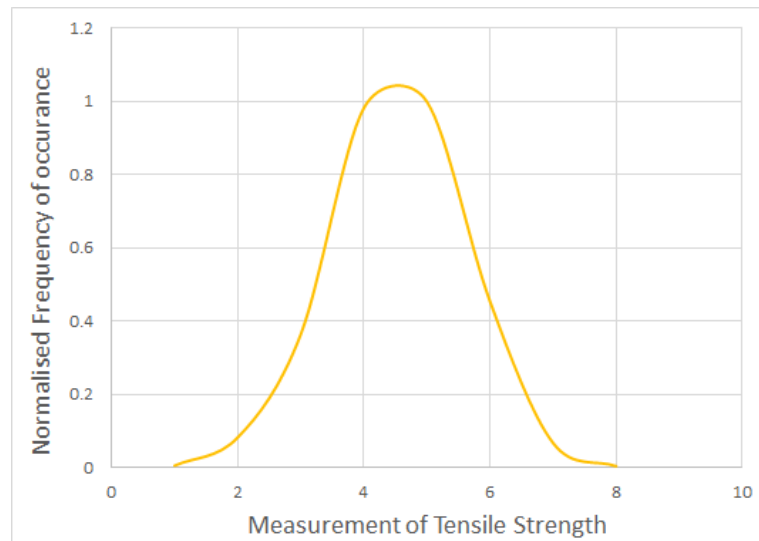


Figure 6.2: Distribution of normalised tensile strength measurements for the Control Batch 1 samples

Significance testing calculates the probability that the relationship between the two set of variables is by chance. It helps answer questions of whether you could duplicate the results

accurately in further research by using probability at the normal distribution curve. There are several steps involved in significance testing.

The first step to determining statistical significance is to clarify the study objective. This is done by stating the Null hypothesis  $H_0$ , which the investigation aims to disprove. The null hypothesis for this investigation claims that there is no significant difference between the mean of the experiment group,  $\mu_A$  and the mean of the control group,  $\mu_C$ . If the mean falls into a region showing a significant difference, to a pre-determined level of significance, then the null hypothesis can be rejected.

The tensile strength of samples treated with ultrasound is not significantly different to the untreated, control samples.

$$H_0 : ControlSamples = TreatedSamples \quad (6.4)$$

In this case:

$$H_0 : \mu_C = \mu_A \quad (6.5)$$

Once the null hypothesis is clear, the Alternate hypothesis  $H_1$  is stated. The alternative hypothesis directly rivals the Null hypothesis and must be true if the null hypothesis is rejected. A statistical hypothesis test will be used to determine which hypothesis can be rejected and is supported.

$$H_1 : ControlSamples \neq TreatedSamples \quad (6.6)$$

In this case:

$$H_1 : \mu_C \neq \mu_A \quad (6.7)$$

Proceeding to claim significance of a result requires a level of significance to be selected prior to analysis, depending on how confident we want the results to be. The level of significance ( $\alpha_s$ ) used is 0.05 for the null hypothesis, giving 95 % confidence (shown in Fig 6.3) [118] in all statistical analysis throughout this thesis as is the generally accepted threshold for publication confidence.

Once the null, alternative hypothesis and level of confidence have been assigned, the t-test



can be performed. The t- test is performed on the sets of data to find the mean and spread taking the number of samples and the variance of the data into consideration.

### **T-Test**

Before performing the t-test, it must be decided if the samples are paired or unpaired and if the variances are equal. An example of paired samples occurs when the populations are dependent on one another. Consider testing the performance of the same group of runners after drinking two types of energy drink. Since the group of runners remains the same, the results depend on each other therefore the samples are paired. Considering our groups of samples, different samples are used for each test. They are independent from one another and an unpaired t-test is chosen.

An unpaired t-test can take two forms, that of equal or unequal variances. The F-test (or Fisher's Test) can be used to determine if the variances of the sample are equal. The F-Test itself requires a specific standard null and alternate hypothesis to be set as in Equations 6.8 and 6.9. The F value is the ratio of the variances of the two sets of data putting the largest variance as a numerator, meaning values are always higher than 1 as shown in Equation 6.10. A larger F value denotes a greater difference in variance and leads to a rejection of the null hypothesis. The critical F value depends on the number of degrees of freedom used (corresponding to the quantity of samples) and the level of significant which is required. F-tests are performed prior to t-testing for each set of data analysis and compared to the critical F-value to determine if unequal or equal variance t-testing is necessary.

Null Hypothesis: The variance of sample 1 is not equal to the variance of sample 2

$$H_0(F) : s_1^2 = s_2^2 \quad (6.8)$$

Alternate Hypothesis: The variance of sample 1 is equal to the variance of sample 2

$$H_1(F) : s_1^2 \neq s_2^2 \quad (6.9)$$

$$F = \frac{s_1^2}{s_2^2} \quad \text{where } s_1 > s_2 \quad (6.10)$$

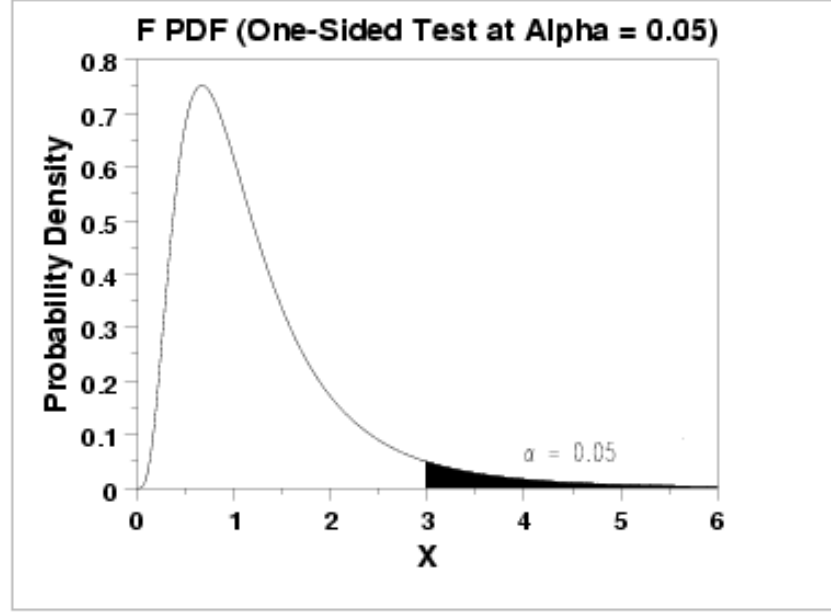


Figure 6.3: Fisher distribution of variances, highlighting the 0.05 level of significance in which the data must sit in to be considered valid

Depending on if the variances for each analysis has been determined equal or unequal, the t-test analysis is applied to the data using Equation 6.11.

$$t = \frac{\mu_{m1} - \mu_{m2}}{s_e} \quad (6.11)$$

Where the standard error ( $s_e$ ) has to take into account the variances of the two samples shown in Equation 6.12 , and the pooled estimate of the standard deviation  $s_p$  is calculated as in Equation 6.13 where  $n_1$  and  $n_2$  is the quantity of samples in group 1 and group 2 respectively.

The P value calculated using the t-test determines whether the null hypothesis can be accepted. Provided that the 'P value' is below 0.05 (giving 95% confidence in the result) then the null hypothesis can be rejected. The higher the P value, the more confident the results are.

$$s_e = s_p \sqrt{\frac{1}{n_1} + \frac{1}{n_2}} \quad (6.12)$$

$$s_p^2 = \frac{(n_1 - 1)s_1^2 + (n_2 - 1)s_2^2}{n_1 + n_2 - 2} \quad (6.13)$$

## 6.2 Discussion

There were two key areas of investigation with this study. The first was the effect of the ultrasonic wave field on the tensile strength of the sandstone samples. The second was the effect of the ultrasonic wave field on the fluid within the sample pores.

Four separate statistical t-tests are performed to analyse the results of the tensile strength and mass loss of samples following ultrasonic treatment. The t-tests are set to disprove the below hypotheses stating that all tested samples are equal to their respective control samples. The hypotheses are in terms of the tensile strength values  $TS_{5\mu m}$  and  $TS_{2.5\mu m}$  and the masses lost from the samples exposed  $ML_{5\mu m}$  and  $TS_{2.5\mu m}$  following exposure to the 5  $\mu m$  and 2.5  $\mu m$  amplitudes of pressure fields respectively.  $TSC_{5\mu m}$  and  $TSC_{2.5\mu m}$  are the control batch values of tensile strength and  $MLC_{2.5\mu m}$  and  $MLC_{5\mu m}$  are the control batch values for the mass lost for each amplitude. The control batches were intended for direct comparison to the corresponding amplitude only and differ due to the quantity of saturation time of the control samples. These four null hypothesis are listed below and are the results of which are discussed individually:

- $TS_{5\mu m} = TSC_{5\mu m}$
- $TS_{2.5\mu m} = TSC_{2.5\mu m}$
- $ML_{5\mu m} = MLC_{5\mu m}$
- $ML_{2.5\mu m} = MLC_{2.5H}$

### Tensile Strength

#### 5 $\mu m$ Amplitude Acoustic Pressure Field

Figure 6.4 shows the average and spread of tensile strength measurements for the samples exposed to the 5  $\mu m$  ultrasonic field. A description of the spread of data are compared in Table 6.1 with corresponding t-test analysis results are shown in Table 6.2. The most important value in this table is the significance status, which for this data shows that there the tensile strengths of the set of samples which were exposed the the acoustic pressure field did not differ significantly to the control batch of samples.

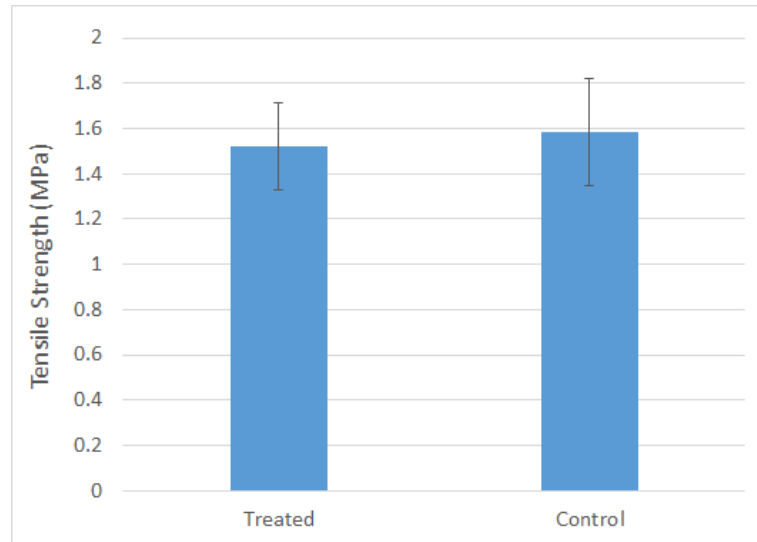


Figure 6.4: Comparison of Average Tensile Strengths and 95% confidence levels between samples treated with  $5\ \mu\text{m}$  ultrasonic field compared to the control batch

	Tested	Control
Mean	1.52	1.59
Variance	0.16	0.25
No. Samples	17	17

Table 6.1: Data Analysis for Tensile strength of the samples treated with  $5\ \mu\text{m}$  ultrasonic pressure field compared to the control

Statistical Characteristic	Value
Critical value for 95% confidence	1.17
Calculated t value	-0.43
Significance status	32.676% : Not Significant

Table 6.2: Statistical Output for Data Analysis for Tensile strength of the samples treated with  $5\ \mu\text{m}$  ultrasonic pressure field compared to the control

### 2.5 $\mu\text{m}$ Pressure Field Exposure

Figure 6.5 shows the average and spread of tensile strength measurements for the samples exposed to the  $2.5\ \mu\text{m}$  amplitude ultrasonic pressure field. A description of the spread of data are compared in Table 6.3 with corresponding t-test analysis results are shown in Table 6.3. The most important value in this table is the significance status, which for this data shows

that the tensile strengths of the set of samples which were exposed to the acoustic pressure field did differ significantly to the control batch of samples with a confidence level of 97.35 %. What was unexpected which is clearer in Figure 6.5, is that the samples exposed to the 2.5  $\mu\text{m}$  acoustic wave field showed an increase in tensile strength when compared to the control.

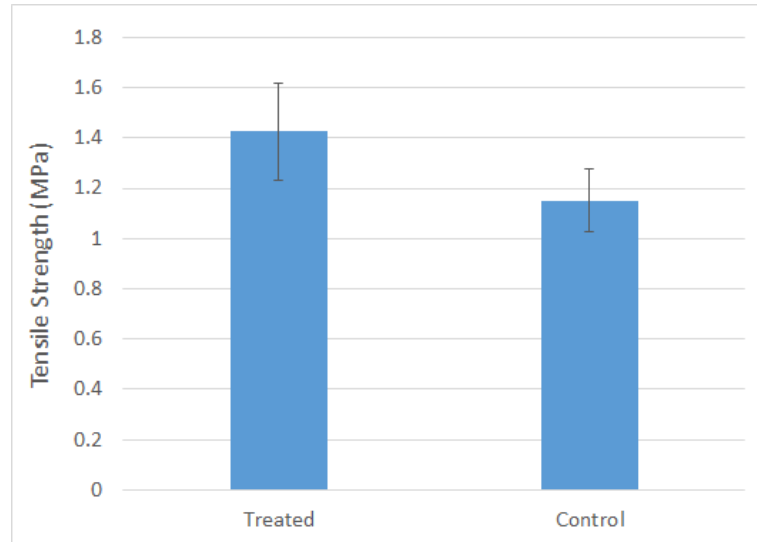


Figure 6.5: Comparison of Average Tensile Strengths and 95% confidence levels between samples treated with 2.5  $\mu\text{m}$  amplitude ultrasonic pressure field and the control batch

	Tested	Control
Mean	1.43	1.15
Variance	0.16	0.06
No. Samples	17	14

Table 6.3: Data Analysis for Tensile strength of the samples treated with 2.5  $\mu\text{m}$  amplitude ultrasonic pressure field compared to the control

Statistical Characteristic	Value
Critical value for 95% confidence	1.17
Calculated t value	2.24
Significance status	97.35% : Significant

Table 6.4: Statistical Output for Data Analysis for Tensile strength of the samples treated with 2.5  $\mu\text{m}$  amplitude ultrasonic pressure field compared to the control

### 6.2.1 Mass Lost

#### Mass change during testing with 5 $\mu\text{m}$ Ultrasonic Pressure Field

Figure 6.6 shows the average and spread of mass loss measurements for the samples exposed to the 5  $\mu\text{m}$  amplitude ultrasonic pressure field. A description of the spread of data are compared in Table 6.5 with corresponding t-test analysis results are shown in Table 6.6. For this data, the significance status shows that the mass gain of the set of samples which were exposed to the acoustic pressure field did differ significantly to the control batch of samples with a 99.93 % confidence level. The samples exposed to the 5  $\mu\text{m}$  acoustic pressure field lost between 60 and 100 mg during exposure to the ultrasonic wave field. In comparison, the control sample mass measurements varied from between 36 mg of loss and a mass gain of 38 mg.

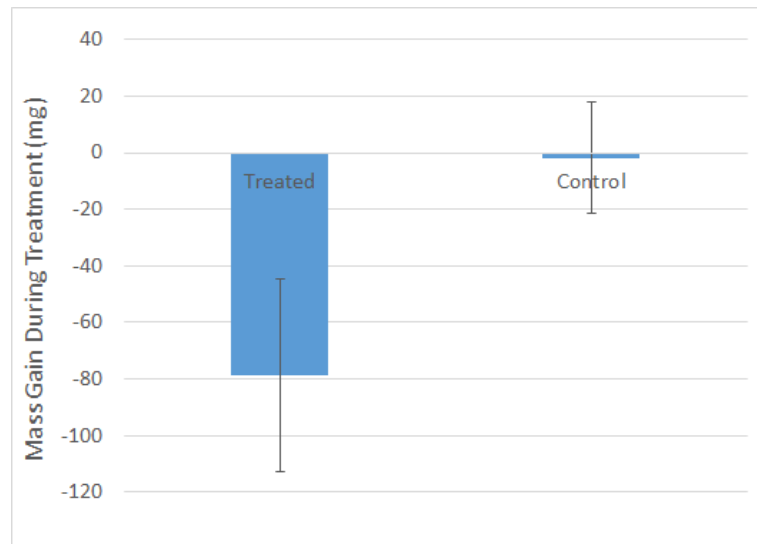


Figure 6.6: Comparison of Average Mass Gain and 95% confidence levels between samples treated with with 5  $\mu\text{m}$  amplitude ultrasonic pressure field ultrasonic field and the control batch

	Tested	Control
Mean	0.0788	0.0018
Variance	0.0051	0.0017
No. Samples	17	17

Table 6.5: Data Analysis for Mass Lost of the samples treated with with 5  $\mu\text{m}$  amplitude ultrasonic pressure field compared to the control

Statistical Characteristic	Value
Critical value for 95% confidence	1.17
Calculated t value	3.85
Significance status	99.931 % : Significant

Table 6.6: Statistical Output for Data Analysis for Mass Lost of the samples treated with with 5  $\mu\text{m}$  ultrasonic pressure field compared to the control

### Mass change during 2.5 $\mu\text{m}$ Ultrasonic Pressure Field

Figure 6.7 shows the average and spread of mass gain measurements for the samples exposed to the 2.5  $\mu\text{m}$  ultrasonic pressure field. A description of the spread of data are compared in Table 6.7 with corresponding t-test analysis results are shown in Table 6.8. For this data, the significance status shows that mass gain of the set of samples which were exposed the the acoustic pressure field did differ significantly to the control batch of samples with a 99.9998 % confidence level. The samples exposed to the 2.5  $\mu\text{m}$  pressure acoustic pressure field gained between 120 and 170 mg during exposure to the ultrasonic wave field. In comparison, the control sample mass gain varied from between 23 mg and 70 mg during the controlled process.

### Fluid Behaviour Compared

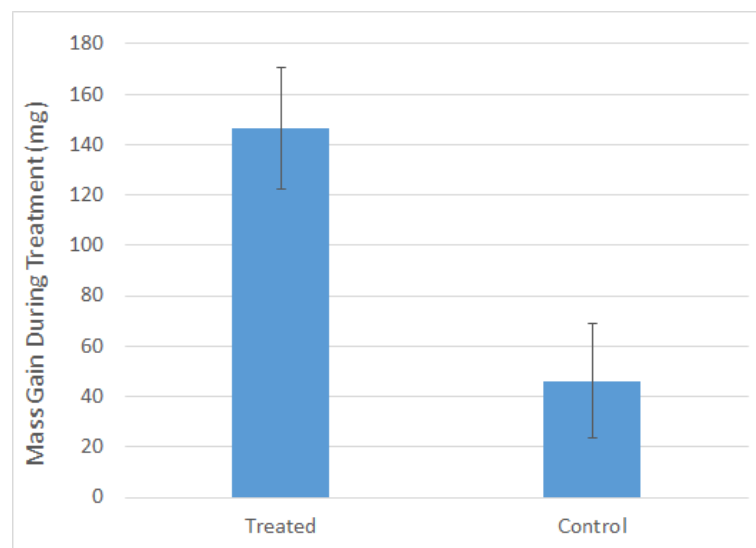


Figure 6.7: Comparison of average mass gain and 95% confidence levels between samples treated with 2.5  $\mu\text{m}$  amplitude ultrasonic pressure field and the control batch

	Tested	Control
Mean	0.1460	0.0460
Variance	0.0026	0.0023
No. Samples	17	16

Table 6.7: Data Analysis for mass gain of the samples treated with 2.5  $\mu\text{m}$  amplitude ultrasonic pressure field compared to the control

Statistical Characteristic	Value
Critical value for 95% confidence	1.17
Calculated t value	-5.81
Significance status	99.9998% : Significant

Table 6.8: Statistical Output for Data Analysis for Mass gain of the samples treated with 2.5  $\mu\text{m}$  amplitude ultrasonic pressure field compared to the control

## 6.3 Conclusions

### 6.3.1 Tensile Strength Measurements

Measurements showed a variation in tensile strength between the two batches of control samples. This is caused by the difference in moisture content between the two sample batches at the time of testing. The samples for the 2.5  $\mu\text{m}$  acoustic field tests had been left to soak at an ambient environment for 21 days. In contrast, the samples for the 5  $\mu\text{m}$  acoustic field test had been soaked for 35 days. It is thought that after 35 day duration, the sample pores are essentially filled with the saturation fluid (i.e. almost fully saturated) whereas the samples soaked for 21 days are partially saturated. As outlined in Figure 3.8 (Chapter 3) the increased moisture content results in a lower tensile strength of the sample.

To consider the tensile strength of the samples following exposure to an ultrasonic field, the treated samples are compared to the corresponding control batch only. It was expected that the alternating acoustic field would generate stresses within the sample which enhance micro-cracks, decreasing the strength resulting in a lower tensile strength. In contrast to what was expected, statistical analysis confirmed what was indicated through graphical representation - that there was an insignificant difference between the tensile strength of samples exposed to a 5  $\mu\text{m}$  acoustic pressure field when compared to the corresponding control batch. Further



unexpected results were measured for the samples exposed to the 2.5  $\mu\text{m}$  acoustic pressure field showed a statistically significant increase in strength of the samples when compared to the control batch.

Calculated peak stresses generated in the samples as a result of the 5  $\mu\text{m}$  and 2.5  $\mu\text{m}$  amplitude acoustic field reached 285 and 764 kPa respectively. The compressive and tensile strengths of the sandstone samples was measured as 36.3 and 71.2 MPa respectively. These stresses generated within the samples were below that calculated within the samples as a result of the acoustic field, however it should be noted that the stress generated within the sample as a result of an acoustic field was not intended to directly exceed the strength of the sample, but the application of the cyclic acoustic wave field to weaken regions within the sample. It is this cyclic load on the sample which is proposed to cause a strength decrease during oscillating loading would cause an effect on the rock matrix resulting in a decrease in strength.

Research has shown that in contrast to metals, the fatigue life of geo-materials is affected by the frequency of loading. Application of an oscillating force in granite samples showed that a higher frequency field (5 Hz as opposed to 1 Hz) resulted in an increase in fatigue life and decrease in rock propagation rate [119]. It has also been shown that the dynamic strength of the rock depends on loading rate, where fatigue life increases with increasing frequency [120]. Studies on intact sandstone show a decrease in fatigue strength within the frequency range of 0.1 - 3 Hz, however at a frequency of 10 Hz the rock showed an increase in strength and deformation properties. Investigations based on the high dependence of micro-structure on sample properties concluded that a redistribution of grains occurs during exposure to the cyclic load, making the rock more compact and the sample stiffer. They found that the cyclic loading response is sensitive to geometry and mineralogy [121]. It is proposed that low frequency loading enabled the brittle behaviour of the rock to develop, where crack growth has enough time to coalesce and generate a failure at the maximum load [119].

Investigations have been performed on the dependence of the frequency of the applied load at low frequencies and with a variety of wave shapes [122], however there were no similar investigations performed at an ultrasonic frequency.

Based on research performed at low frequencies, it is suggested that the lack of difference in tensile strength observed with the 5  $\mu\text{m}$  amplitude may be explained by the existence of a threshold stress under which there is no significant change to the rock matrix. It is clear that the behaviour exhibited here is extremely complex, and further thorough experimentation and investigation is necessary before any conclusions are drawn regarding these results. Further to the changes in tensile strength, cavitation erosion was evident throughout testing which in sufficient amplitudes could cause a decrease in sample strength, the breakdown of

blockages or change of properties of the pore wall.

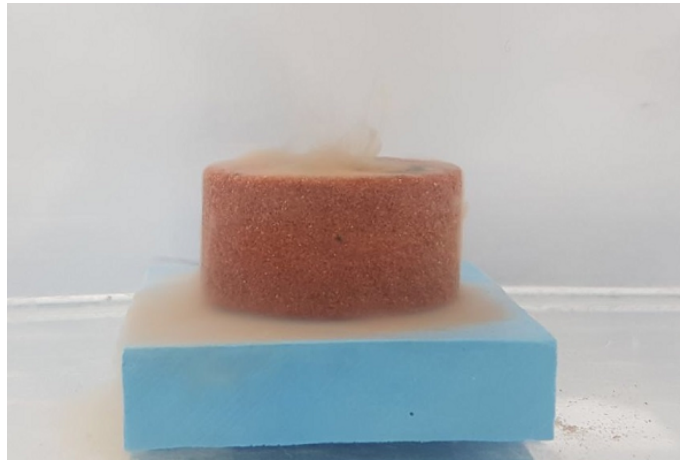
### 6.3.2 Pore Fluid Loss

Mass measurements of the sample before and after testing was used to determine how much fluid was contained within the sample pores. An increase of mass signifies the displacement of air within the sample pores by the fluid within the cavitation bath. The difference between the mass gain for the control treatment can be explained by the duration of the saturation period prior to testing. As highlighted, the control samples for the 5  $\mu\text{m}$  amplitude test had a higher moisture content than the control samples for the 2.5  $\mu\text{m}$  amplitude test following soaking durations of 35 and 21 days respectively. Control samples were intended for comparison with the tested samples only. Excluding the duration of saturation the control samples experienced the same conditions throughout testing.

Samples exposed to 5  $\mu\text{m}$  acoustic field experienced a loss in mass compared with the control. This indicates a significant loss of mass of the rock and containing fluid during the test. The measured mass loss can be accounted for by cavitation erosion of the external surface, as shown in Figure 6.8. Eroded rock could be seen at the bottom of the tank and dispersed within the fluid. Significant cavitation erosion was also observed surrounding samples exposed to the 2.5  $\mu\text{m}$  acoustic field, however any decrease of mass measured due to erosion was shielded by the displacement of gas bubbles within the pores with surrounding fluid of greater density and therefore increasing the mass. This was observed by bubble formation at the pore surface during ultrasonic exposure.

The relative gain in mass observed for the samples exposed to the 2.5  $\mu\text{m}$  acoustic field indicates an exchange of air within the sample pores with the surrounding fluid. Air bubbles were observed forming at the mouth of the pores during the 30 minutes of exposure before detaching and rising to the surface. The gas within the pores is displaced by the heavier fluid resulting in the mass change. This effect would make a larger impact for these samples as opposed to those exposed to the 5  $\mu\text{m}$  due to the difference in air content of the pores prior to testing. The 5  $\mu\text{m}$  samples had been soaked longer therefore had less pore air content to displace. On the other hand, the 2.5  $\mu\text{m}$  amplitude acoustic field may also be a more effective amplitude to cause this displacement. The displacement of fluid as a result of the acoustic field is clear, however the exact reason for the 2.5  $\mu\text{m}$  amplitude having a more pronounced effect needs further investigation with consistently saturated samples to be confirmed.

Figure 6.8: Cavitation erosion evident during testing



### 6.3.3 Conclusion

The inconsistent and unexplained variation of reservoir recovery following nearby seismic activity is the source of this investigation. Evidence shows the generation of ultrasonic wave fields at a range of frequencies up to 150 MHz within a saturated, porous media due to seismic waves travelling through. The investigation looked to potential mechanisms brought about by these ultrasonic field within the fluid saturated porous rock within the reservoir. This study is intended as a preliminary stage of research performed at atmospheric conditions, where any observed effect would need further investigation to see if the specific type of wave field had the potential to be generated within a reservoir.

The two main mechanisms of investigation can be separated into the decrease of strength of the reservoir rock with subsequent fracture and modification of the properties of the pore walls, pore fluid or interaction between the two. These mechanisms were studied following investigations into these changes in reservoir activity supported by research into other effects brought about due to ultrasonic wave fields.

Firstly, we remind ourselves of the ways in which the recovery of reservoir fluid can be enhanced. Petroleum is prevented from being recovered either by sedimentary rock providing a barrier to fluid flow or the physical properties of the fluid making it immobile. Increasing the pathways between where the petroleum is held and where it is readily recovered is proposed by acoustic wave interactions with the rock matrix or with the fluid held within the rock matrix. The acoustic waves generate internal stresses within the rock matrix. In addition, the acoustic wave causes cavitation bubbles to be generated at the fluid to pore wall interface and within the pore fluid itself. This cavitation acts on a microscopic level to erode the wall of the rock matrix and increase the number or volume of pathways.

Recalling the material balance, Equation 1.1 in Chapter 1.1, we know that increasing the efficiency of a reservoir can be caused as a result of the following processes:

- Increasing the free gas within the reservoir
- Increasing the free oil within the reservoir
- Increasing the free water within the reservoir
- Increasing the free pore volume of the reservoir
- Increasing fluid mobility

The goal of increasing the free pore volume and therefore fluid mobility by decreasing the strength of the rock following ultrasonic exposure did not yield expected results. While cavitation was observed eroding the walls of the sample, a significant decrease in sample strength was not measured following the tested conditions. Cavitation erosion effects could be implemented within reservoir conditions to increase the pore volume or to erode barriers to the fluid motion between pores which can arise during reservoir recovery. This is a preliminary investigation and will need significant and extensive further research into the feasibility of implementation with real reservoir fluids and conditions using a more realistic representation of the ultrasonic wavefields which have been postulated to be generated within the reservoir.

Where petroleum exists within a reservoir, it is likely that there is a considerable quantity of accompanying dissolved gas and water. Behaviour of the test fluids within the pores as a result of the interacting acoustic field showed an exchange of gaseous content of the pore fluids with the degassed surrounding fluid. This gas fluid exchanged caused by bubble generation could bring about localised perturbations within a reservoir increasing the free gas content and modifying recovery. Although the presence of gas bubbles within the rock samples would be significant compared to the dispersed gas molecules within a saturated reservoir, the state exchange poses a promising driving mechanism for enhanced reservoir recovery. Separating the states within the petroleum replicates the effects coming into play with naturally occurring drive mechanism such as gas cap drive and water drive. Where these mechanisms could be implemented at the wave fields generated due to seismic wave dispersion, they would exist as a secondary recovery mechanism which utilises the natural processes. This is supported by the exchange of fluids observed with the core investigation. Analysis into the range of frequencies and amplitudes for which this interaction of differing states occurs would be beneficial to determine the best method of application to a reservoir.

It is proposed that in extension to this research, investigation into a more localised pore fluid

interaction be progressed with regard to reservoir recovery to determine what is happening at this level to cause the gas-fluid exchange. Regarding the strength increase observed, additional supporting research would need to be performed to get a better understanding of what is happening at the rock matrix level. Results indicate at a threshold value at which an increase in rock strength occurs below which there is no influence. This should be investigated and could be implemented along with reservoir recovery to increase strength in alternative fields or for alternative uses such as increasing the integrity of porous rock.

## Chapter 7

# Further Work

Basic investigation into a variety of potential further mechanisms of porous rock fracture as a result of ultrasonic wave fields was performed, however due to time and sample quantity limitations no statistically significant analysis was carried out. A brief summary of these findings which may be further investigated to support the investigation are highlighted in this chapter with a brief description of the background to the study.

In the core investigation, increasing permeability as a result of enhancing pathways for fluid flow or modifying the behaviour of the fluid within the pores was considered. Water saturated samples only were used for the core investigation, however to get a better understanding of the changes of the fluid properties in response to the acoustic field, a variety of saturation fluids are compared here.

### 7.1 Fluid behaviour with a Cavitation Field

#### 7.1.1 Background

Modification of the way in which different pore fluids interacts with each other and the rock matrix under an ultrasonic wave-field is explored. Possible enhancements of fluid flow within pores is proposed by:

- Encouraging peristaltic movement of the pore fluid

- Enhancing pore pathways by eroding blockages or generating new pathways
- Stimulating fluid motion

Peristaltic movement occurs when a mechanical wave travels along the surface of material. It is the same method by which the oesophagus transports food from the mouth to the stomach by generating a wave of compression which forces food down the tract. In sandstone it is the acoustic wave travelling along the pore walls of the samples which causes the fluid to flow through. Any blockages within the pores such as sediment build up during fluid migration through a reservoir could be unblocked by this mechanical vibration providing the material with enough energy to move. For example, asphaltene deposits are a common problem in reservoirs following recovery which clog the well-bore tubing and valves, as well as coating the surface safety and process control equipment.

In addition to this mechanical vibration, cavitation erosion of the pore walls will increase the pathways available for fluid to flow in porous rock. As mentioned in the core investigation, cavitation bubbles can stimulate fluid flow by generating localised high pressures and temperatures, or erratic pressure fields at the fluid interface stimulating flow.

Sandstone samples of 52 *mm* in length and 36 *mm* diameter are saturated with one of three types of saturation fluid, exposed to an ultrasonic wave field and then dried. The cavitation field was applied to determine how bubble collapse affects sample strength, the interaction between saturation fluid and sample and the interaction between the saturation fluid with the surrounding water.

Investigation into the relationship between a range of saturation fluids and the pore walls as a result of ultrasound exposure would be useful to determine if the material properties between the imbibing water and saturation fluid can be modified to enhance saturation fluid mobility.

### 7.1.2 Reservoir Fluids and Saturation Fluids

The wide range of fluid types and states present within a reservoir comes about as a result of the conditions the petroleum experiences throughout its generation, migration and storage. As described in Chapter 1, oil within reservoirs can range from light [21] or heavy [89]. With this range of oil comes a range of properties, as shown in Table 7.1.

Water, kerosene and rapeseed oil were used as saturation fluids. They were chosen due to

Fluid	Density $g/cm_3$	Viscosity cP	Surface tension Dynes/cm	Interfacial Tension (w/water) Dynes/cm
Light Mineral Oil	0.8383	35.5	32	51.0
Heavy Mineral Oil	0.8508	167	46.2	61.8

Table 7.1: Fluid properties of light and heavy mineral oils

their differing densities, viscosities, surface tensions and interfacial tensions which are listed in Table 7.2. This allows the effect of the acoustic fields on the interaction between the rock and the differing fluid properties to be considered. The range of properties allows comparison of the effect of the ultrasonic treatment upon these to be isolated. Water provides the control fluid and also represents water which would be present within a reservoir.

Fluid	Density $g/cm_3$	Viscosity cP	Surface tension Dynes/cm	IFT (w/water) Dynes/cm
Water [21, 123]	1	1.0038	72.86	1
Kerosene	0.768	2.9	27	48
Rapeseed oil [124–127]	0.9073	78.8	35.7	30

Table 7.2: Fluid properties of the saturation fluids used for testing at room temperature

## 7.2 Visual Observations

As previously described, cavitation bubbles generates extreme localised pressures and temperatures on collapse which is thought to erode the surface of the rock and modify the interaction between the pore walls and saturation fluid to enhance fluid flow. Samples were saturated with one of the three saturation fluid using the wicking method. The fluid absorbed during the saturation process is referred to as the 'Saturation fluid'. To remove the variability associated with commercial cavitation baths, increase visibility and for greater control over the parameters, a cavitation bath was mad using a vessel, degassed fluid and acoustic source.

A 20 kHz piston transducer was placed in a cavitation bath, consisting of a transparent cylindrical water vessel of 100 mm diameter and 110 mm in height of relatively low volume at room temperature and atmospheric conditions. The low volume vessel was used to maximise the acoustic pressure field within the area and increase the cavitation activity. The amplitude of vibration of the ultrasonic source and exposure time were varied in order to observe how this affected the cavitation field created. The setup along with a pictorial representation (for clarity) can be seen in Figure 7.1. The Samples were placed in the cavitation bath bath



containing degassed, deionised water and a 20kHz planar transducer was applied to the surface to generate a cavitation field. The degassed, deionised water was used to yield more consistent and repeatable cavitation activity under the ultrasonic wave field due to the higher level of control of the fluid. The cavitation field was quantified by measuring the Broadband Acoustic Power (BIP) using the Cavimeter (as described in Chapter 5) to measure emissions which are generated during cavitation bubble collapse [128–130]. This is measured in cavitation meter units of  $10^{-6}V^2Hz$  or  $\mu V^2Hz$ .

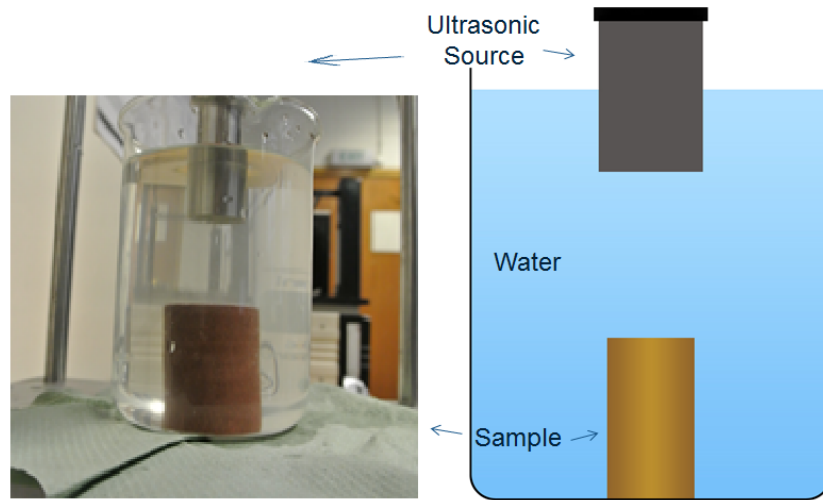


Figure 7.1: Experimental set-up for an optimum cavitation field

A high speed camera was used to observe the response of rapeseed oil saturated samples within a cavitation field with an amplitude of 1, 2 and 3  $10^{-6}V^2Hz$ . As expected, increasing the amplitude of cavitation activity from 1 to 3 increases the aggression of response of the saturation fluid of the samples. A comparison of the response of rapeseed oil saturated samples to the acoustic field can be seen in Figure 7.3.

The high speed camera captured the interaction between a cavitation field of amplitude of 3  $\mu V^2Hz$  BIP and sandstone samples saturated with the three saturation fluids. The fluid behaviours compared in Table 7.4. This amplitude was chosen to enhance the observed effects and for ease of visibility.

For water saturated samples the cavitation activity can be seen as a cloud of eroded sediment dispersed in the surrounding fluid. Within 1 second of switching on the acoustic field, cavitation erosion can be seen at the bottom of the samples in contact with the stand and at the top surface of the sample. As time progresses, this sediment cloud grows as more of the sample is eroded. The top surface of the sample closest to the acoustic source is the main cavitation erosion site as seen at 60 seconds.


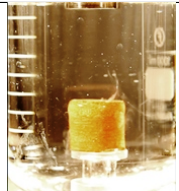
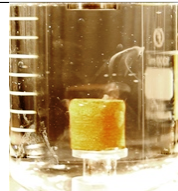
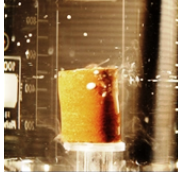


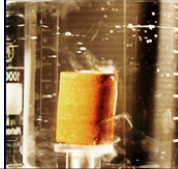
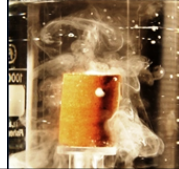

Time (s)	10	30	60
$1 \mu V^2 Hz$			
$2 \mu V^2 Hz$			
$3 \mu V^2 Hz$			

Table 7.3: Rapeseed oil saturated sandstone sample behaviour when exposed to a cavitation bath over time

For kerosene saturated samples, cavitation erosion can be recognised at 1 second as a mixture of saturation fluid and eroded sediment in a cavitation cloud at the top surface of the sample. At 5 seconds, this cloud has grown and begun to develop at the bottom of the sample in contact with the stand. Further cavitation erosion can and what appears to be kerosene removal from the sample pores from the top of the sample. At 40 seconds the kerosene which has been removed from the sample and eroded sediment has spread significantly from the sample into the surrounding cavitation bath and additional areas of cavitation activity are identified at the sides of the sample. For the 60 and 80 second pictures the sample can be barely seen through a cloud of kerosene and sediment as the sediment spreads further.

For the rapeseed oil saturated samples, cavitation activity can be observed from 1 second as the fluid and eroded sediment is seen emerging from the pores at the top surface of the sample. As transient activity continues, more pronounced bulbous accumulations of the oil can be seen being draw outwards from the pores of the sample. In contrast to the kerosene, the rapeseed oil spreads upwards and remains in a more globular form.

Following cavitation testing, the fluid from the bath was filtered to identify any sediment which eroded from the samples. These filters can be seen in Figure 7.2 and are used for discussion of erosion activity between the samples. The highest quantity of sediment erosion was observed for the water saturated sandstone samples with an increase of sediment observed following exposure to higher amplitudes of cavitation amplitude. Kerosene saturated samples show the next largest quantity of sediment erosion, also producing an increased quantity of sediment with increased amplitude of BIP during cavitation. The filtered water from the test


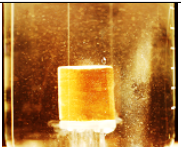
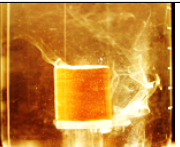







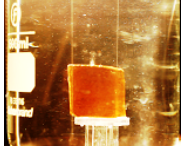




Time (s)	1	5	40	60	80
Water					
Kerosene					
Rapeseed Oil					

Table 7.4: Comparison of response of various fluid saturated samples with time

of rapeseed oil saturated sandstone showed the least filtered sediment. This may be a result of mixing between the sediment and rapeseed oil itself making an emulsion which was observed on the surface of the sample following testing as opposed to being dispersed within the water due to the inter-facial tension forces between the two fluids. It must be noted however, that since the samples were not flushed out after treatment, this filtered water will only contain the sediment which is eroded from the outer circumference of the sample which were capable of detaching from the rock and fluid. Any sediment eroded from within the pores of the sample, or where the sediment is unable to adhere from the fluid or rock interface would not be accounted for.

To confirm that cavitation erosion was occurring at the surface of the rock, plaster samples were exposed to the cavitation bath to compare a uniform, non-porous material to the sandstone samples. Following exposure to the cavitation bath, erosion was also visible on surface of the plaster samples. The outer surface of a plaster which had been exposed to a transient cavitation field is shown alongside a sample which had not been exposed to a cavitation field in Figure 7.3. This confirms that the field facilitates cavitation activity at the surface of the sample.

When a dry sample is placed within the cavitation bath, bubbles are observed growing and detaching from the pore mouth at a constant rate as water naturally displaces the air within them. When the ultrasonic field is applied to the bath, bubble formation stops. Vibration of the sandstone pores due to the ultrasonic field appears to inhibit the flow of fluid into the sample to displace the air at this amplitude. A further increase in amplitude of acoustic field saw the return of this bubble formation, however at a less consistent rate.

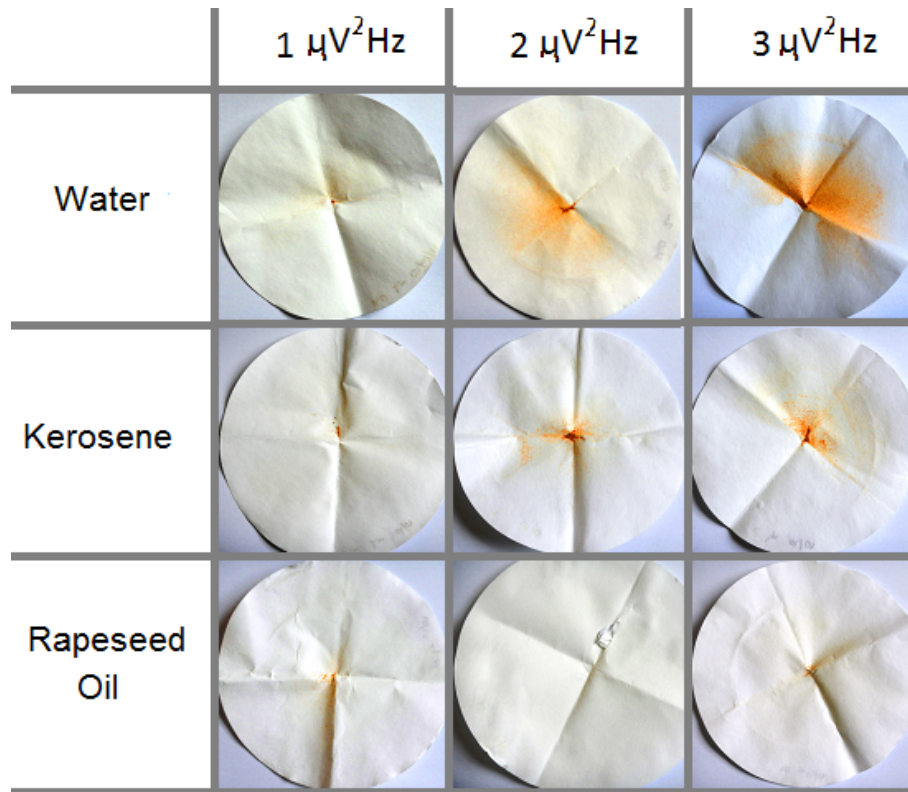


Figure 7.2: Filter from transient cavitation exposure of sandstone samples saturated with the three saturation fluids, after three amplitudes of BIP

As the sample is placed in the fluid the displacement of air at the pore surface of the sample with the surrounding fluid occurs naturally. Once the acoustic field is switched on, this natural displacement is upset, potentially due to vibration of the pore walls or agitation of the fluid at the mouth of the pore. As the amplitude of the acoustic field is increased, the displacement of gas with fluid returns. It is thought that this is the acoustic field causing mechanical agitation within the sample providing peristaltic motion to allow the flow of the fluid into the sample.

Dry samples in contrast to the samples with saturation fluid have a saturation fluid to cavitation water interface preventing the natural displacement. When the rapeseed oil and kerosene samples are placed in the water without the acoustic field being switched on, no bubbles are observed at the surface of the pores. It is not until the acoustic field is initiated that displacement of fluids occurs. Research has shown that an acoustic field provides the change in pressure necessary to overcome the capillary and gravitational forces which holding fluid in place [131]. The peak droplet rate of a fluid under an acoustic field has been found to be proportional to the fluid viscosity and inversely proportional to the interfacial tension. The peak droplet rate is shown to be higher with increasing amplitude and frequency of ultrasonic wave field [89].



(a) Side view



(b) Top view

Figure 7.3: Control vs Transient Cavitation bath exposure of Plaster samples. Note: control sample is on the left

### 7.3 Findings

The cavitation field was used to look for a change of fluid properties, rock matrix or permeability using the localised high pressure and temperature generated at bubble collapse. Again, looking at the material balance equation of Chapter 1.1, we know that the recovery of petroleum or water from a reservoir can be controlled by modifying the free volume of the oil, gas or water, increasing the pore volume or water influx. In changing the fluid properties, a change in available or 'free' fluid can be made. Changing the pore volume of the matrix is another method of increasing reservoir recovery.

**Fluid properties**

Literature tells us that the temperatures and pressures generated as a result of the cavitation bubble could be used to lower the viscosity of the fluids, provide enough energy for the fluid to overcome the surface tension properties holding it in place, erode the rock matrix to change rock wettability or increase the amount of pores and therefore permeability. These tests have showed that the cavitation field caused relative motion and dispersion of fluid from saturated pores with the effect being more pronounce with increasing cavitation amplitude. The cavitation bubbles were observed drawing gas from the saturation fluid at the pore surface. Additionally, bubbles were observed drawing the fluid within the pores under the ultrasonic field.

The highly viscous rapeseed oil was observed dispersing within the fluid as a result of the ultrasonic wave field. This shows a change in state of the fluid making it more susceptible to flow. An example of this is where cavitation was shown in lab conditions to cause cracking of petroleum into lighter constituents [132] which are more easily obtained. The effects which are involved in this cracking from one state of oil to another could be occurring here, and implements within a reservoir to ease the rate at which the oil can be recovered.

Increasing fluid mobility can also take the form of pore wall modifications by changing the wettability of the pore to the fluid. Wettability is dictated by cohesion and adhesion which has been showed to altar from one form to another using cavitation [133]. The surface of the rock changes from oil wet to water wet would release the strong pull of the rock wall to the oil, making it more easily recovered.

Separating the gas from the saturation fluid could be used to modify the capillary pressure within reservoir pores, which could be used to enhance gas cap reservoir recovery at the primary stages.

This fluid agitation could also be applied in conjunction with other enhanced recovery mechanism which drive fluids into the reservoir to enhance recovery. For example, the pumping down of carbon dioxide which is sometimes performed would increase the amount of cavitation opportunity to decrease the petroleum resistance to flow.

### Rock Matrix Properties

Literature shows that the ultrasonic wave field used to generate the cavitation bubbles can cause peristaltic movement of the pore walls which drives the fluid, with optimum acoustic amplitude relating to the pore fluid viscosity and inter-facial tension of the fluid. Peristaltic motion of the pores in a reservoir would be extremely beneficial to enhancing oil recovery and could cause trapped residual oil droplets to combine making them more mobile. Investigation of the amplitude necessary for an effect within a pore channel should be investigated along with research into what is achievable amplitudes within a real reservoir conditions.

### Permeability

As identified in the previous chapter, cavitation erosion is occurring under the ultrasonic field, which could be manipulated to expand micro-cracks and enhance pore pathways, increasing the pore volume and thereby the permeability. This could be used to break down asphaltene deposits within a reservoir which are generated throughout recovery. It must also be noted, that this erosion could also cause the opposite effect if implemented incorrectly by eroded sediment generating a new blockage.

#### 7.3.1 Further Work

Based on this investigation, the following avenues of further research are suggested:

- Develop a means of testing permeability of samples to kerosene and rapeseed oil would be beneficial to the study to determine if the wettability of the rock is being changed during ultrasound exposure. This could heavily enhance reservoir recovery changing from oil to water wet rock. Real time in pore analysis such as x-ray scanning, or using a slice of porous rock against a transparent vessel would also aid in understanding what is happening under the effects of the ultrasonic wave fields. The real time effect of the ultrasonic wave field on the capillary forces can be observed using this method.
- Given the complexity of the cavitation process and the abundance of parameters, an investigation into the feasibility of generating cavitation at the high pressures and temperatures experienced within a reservoir would be the next step toward utilising cavitation as an effective reservoir recovery mechanism.

- Regarding the relative motion of the fluid, the relationship between the optimum amplitude and frequency to promote motion of fluids at the range of viscosities and densities relevant to reservoir oil should also be considered for two reasons. Firstly, to determine if they are realistically generated waves within a reservoir and secondly to ensure that the reduction of relative motion measured as a result of the ultrasonic wave field at certain frequencies does not decrease the recovery.
- More complex FEA of the multi-physics relationship at the pore- fluid interface would benefit further study by allowing the wave dispersion to be more accurately measured. Using this model, the pore wall properties, pore fluid properties and relationship between the two could be further analysed.
- Modification of the wave delivery method, such as the dual-shock lithotripsy method which has been a recent cause of interest within the profession could provide a more efficient form of wave delivery for reservoir recovery methods.



## References

- [1] C. E. Brennen, *Cavitation and Bubble Dynamics*. Oxford University Press, 1995.
- [2] R. W. Allmendinger, *A structural geology Laboratory manual for the 21st century*. Richard W. Allmendinger, 2015.
- [3] A. Yamaji, *An Introduction to Tectonophysics Theoretical Aspects of Structural Geology*. Terrapub and Tokyo, 2007.
- [4] “Compressive strength of rocks,” June 2015.
- [5] “Pore fluid effects on rock mechanics,” June 2015.
- [6] BP, “Bp energy edition: 2017 edition,” tech. rep., BP, 2017.
- [7] BP, “Bp statistical review of world energy june 2016,” tech. rep., BP, <http://www.bp.com/content/dam/bp/pdf/energy-economics/statistical-review-2016/bp-statistical-review-of-world-energy-2016-oil.pdf>, 2013.
- [8] E. Tzimas, A. Georgakaki, C. G. Cortes, and S. Peteves, “Enhanced oil recovery using carbon dioxide in the european energy system,” tech. rep., Institute for Energy, 2005.
- [9] T. Ehmed, *Reservoir engineering handbook and second edition*. Gulf Professional Publishing, 2000.
- [10] R. Stoneley, *An introduction to petroleum exploration for non geologists*. OUP Oxford, 1995.
- [11] P. H. Nelson, “Pore-throat sizes in sandstones and tight sandstones and and shales,” *The American Association of Petroleum Geologists*, vol. 93, pp. 329 – 340, 2009.
- [12] Walsh and M. P., “A generalized approach to reservoir material balance calculations,” *Petroleum Society of Canada*, vol. 34, p. 1, 1995.
- [13] Walsh and M.P., “New and improved equation solves for volatile oil and condensate reserves,” *Oil and Gas Journal*, vol. 72, p. 1, 1994.

- [14] Walsh, M.P., Ansah, J., , Raghavan, and R., "The new and generalized material balance as an equation of a straight line: Part 2 - applications to saturated and non-volumetric reservoirs," *Permian Basin Oil and Gas Recovery Conference and Midland and Texas*, vol. 1, p. 1, 1994.
- [15] Walsh, M.P., Lake, and L.W., *A Generalized Approach to Primary Hydrocarbon Recovery*. Amsterdam: Elsevier, 2003.
- [16] Muskat and M., *Physical Principles of Oil Production*. McGraw-Hill Book Co. Inc., 1949.
- [17] Tsiklauri, David, Beresnev, and Igor, "Properties of elastic waves in a non-newtonian (maxwell) fluid-saturated porous medium," *Transport in Porous Media*, vol. 53, no. 1, pp. 39–50, 2003.
- [18] B. D., *Statistical Analysis of Crude Oil Recovery and Recovery Efficiency and second edition*. API, 1984.
- [19] E. Alhomadhi, M. Amro, and M. Almobarky, "Experimental application of ultrasound waves to improved oil recovery during waterflooding," *Journal of King Saud University - Engineering Sciences*, vol. 26, no. 1, pp. 103 – 110, 2014.
- [20] Beresnev, I.A., and P. Johnson, "Elastic-wave stimulation of oil production: A review of methods and results.," *Geophysics*, vol. 59, pp. 1000–1017, 1994.
- [21] T. Hamida and T. Babadagli, "Analysis of capillary interaction and oil recovery under ultrasonic waves," *Transport in Porous Media*, vol. 70, no. 2, pp. 231–255, 2007.
- [22] Simkin and E. M., "Oil will return in three months," : *Energy (Energiya)*, vol. e, pp. 44–47, 1985.
- [23] Odeh and A. S., "Mathematical modeling of the behavior of hydrocarbon reservoirs-the present and the future," *Advances in transport phenomena in porous media: Martinus Nijhoff Publ.*, vol. 128, pp. 821–848., 1987.
- [24] Nikolaevskiy and V. N., "Mechanism and dominant frequencies of vibrational enhancement of yield of oil pools:," *Transactions (Doklady) of the USSR Academy of Sciences and Earth Science Sections*, vol. 308, pp. 570–575, 1989.
- [25] A. Abedini, F. Torabi, and N. Mosavat, "Oil recovery and asphaltene precipitation and permeability damage during immiscible and miscible cyclic co2 injections in light oil systems," *International Journal of Oil Gas and Coal Technology*, vol. 9, p. 265, 2015.
- [26] J. M. Hunt, 1996. *Petroleum Geochemistry and Geology*. New York:. W. Freeman and Co., 1996.

- [27] Parker, P.G, Stringfield, and V.T, "Effects of earthquakes and trains and tides and winds and atmospheric pressure changes on water in the geologic formations of southern florida," *Econ. Geology*, vol. 45, pp. 441–460, 1950.
- [28] Raju, V. R., Neidhardt, and T., "Pore pressure changes in soft clays due to dynamic excitations (manuscript)," tech. rep., Institut fur Bodenund Felsmechanik der Universitet Karlsruhe., 1991.
- [29] Dobry, R, Elgamal, A. W, Baziar, M. Vucetic, and M., "Pore pressure and acceleration of wildlife site during the 1987 earthquake," *Dobry and R. and Elgamal and A. W. and Baziar and M. and and Vucetic and M. and 1989 and Pore pressure and acceleration of wildlife site during the 1987 earthquake: Proc. 2nd US-Japan Workshop on Liquefaction*., vol. 2, pp. 145–160, 1989.
- [30] Simkin, E. M., Lopukhov, and G. P., "Vibro-wave and vibro-seismic methods of oil reservoirs stimulation (a review), ser. oil industry," *Union Research Institute of Organization and Management and Economics of Oil and Gas Industry (VNIOENG) (in Russian)*, vol. 15, p. 1, 1989.
- [31] Steinbrugge, K. V, Moran, and D. F, "An engineering study of the southern california earthquake of july 21 and 1952 and its aftershocks," *Bulletin of the Seismological Society of America*, vol. 44, pp. 201–462, 1954.
- [32] Zhang, L. H., Ho, P., Yun, L., Shengning, and H, "Low frequency vibration recovery enhancement process simulation," in *Society of Petroleum Engineers*., 1999.
- [33] Campbell, M., Greated, and C., *The Musician's Guide to Acoustics*. OUP Oxford, 1994.
- [34] Christensen and T., *Rameau and Musical Thought in the Enlightenment*. Cambridge Studies in Music Theory and Analysis, Cambridge University Press, 2004.
- [35]
- [36] T. M. MÃijller, B. Gurevich, and M. Lebedev, "Seismic wave attenuation and dispersion resulting from wave-induced flow in porous rocks - a review," *GEOPHYSICS*, vol. 75, no. 5, pp. 75A147–75A164, 2010.
- [37] T. BourbiÃl and O. Coussy, *Acoustics of Porous Media*. Editions TECHNIP, 1987.
- [38] H. Rossmannith, *Fracture and Damage of Concrete and Rock*. CRC Press, 1992.
- [39] A. L. Krylov, V. N. Nikoayeskii, and G. A. El, "Mathematical model of non-linear generation of ultrasound by seismic waves," *Doklady Akademii Nauk SSSR*, vol. 318, pp. 1340–1344, 1991.

- [40] D. Johnston, M. N. Toksoz, and A. Timur, "Attenuation of seismic waves in dry and saturated rocks: II. mechanisms," *Geophysics*, vol. 44, pp. 691–711, 1979.
- [41] V. N. Nikolaevskii, "Rock vibration and finite oil recovery," *Fluid Dynamics*, vol. 27, pp. 689–696, 1992.
- [42] e. a. J.F. Thimus, *Poromechanics: Proceedings of the 1st Biot conference*. CRC Press, 1998.
- [43] V. N. Nikolaevskiy, *Geomechanics and Fluidodynamics: With Applications to Reservoir Engineering*. Springer Science & Business Media, 2013.
- [44] N. G. Mazur, V. Nikolayevskii, and G. El, "Energy exchange between seismic and ultrasonic vibrations in an elastic medium with a microstructure," *Journal of applied math mechanics*, vol. 61, pp. 325–328, 1995.
- [45] Santos, J.E., Ravazzoli, C.L., Gauzellino, P.M., Carcione, and J.M., "Numerical simulation of ultrasonic waves in reservoir rocks with patchy saturation and fractal petrophysical properties," *Computational Geosciences*, vol. 9, no. 1, pp. 1–27, 2005.
- [46] Duhon and R. D., *An investigation of the effect of ultrasonic energy on the flow of fluids in porous media*. PhD thesis, Univ. of Oklahoma., 1964.
- [47] V. Nikolaevskiy, G. Lopukhov, L. Yizhu, and M. J. Economides, "Residual oil reservoir recovery with seismic vibrations," *Society of Petroleum Engineers*, vol. 11, 1996.
- [48] K. W. Winkler and W. F. Murphy, *Acoustic Velocity and Attenuation in Porous Rocks*, pp. 20–34. American Geophysical Union, 2013.
- [49] Zamora, M, Sartoris, G, and C. W, "Laboratory measurements of ultrasonic wave velocities in rocks from the Campi Flegrei volcanic system and their relation to other field data," *Journal of Geophysics*, vol. 99, pp. 13552 – 13561, 1994.
- [50] A. Wulff and H. Burkhardt, "Mechanisms affecting ultrasonic wave propagation in fluid-containing sandstones under high hydrostatic pressure," *Journal of Geophysical Research*, vol. 102, pp. 3043–3050, 1997.
- [51] Fairbanks, H.V, Chen, and W. I, "Ultrasonic acceleration of liquid flow through porous media," *Chemical Engineering Progress Symposium*, vol. 67, pp. 260–262, 1971.
- [52] N. V. Cherskiy, V. P. Tsarev, V. M. Konovalov, and O. Kusnetsov, "The effect of ultrasound on permeability of rocks to water," *Transactions (Doklady) of the USSR Academy of Sciences and Earth Science Section*, vol. 57, pp. 1000 – 1017, 1977.
- [53] Noltingk, B.E., Neppiras, and E.A., "Cavitation produced by ultrasonics," *Journal of the Acoustical Society of America*, vol. 57, pp. 1379–1396, 1975.

- [54] H. S. Al-Hadhrami and M. J. Blunt, "Thermally induced wettability alteration to improve oil recovery in fractured reservoirs,," *SOC PETROLEUM ENG*, pp. 179–186, 2001.
- [55] A. Aarts, G. Ooms, K. Bil, and E. Bot, "Enhancement of liquid flow through a porous medium by ultrasonic radiation," *SPE Journal*, vol. 4, pp. 321–327, 1999.
- [56] A. Shedid, "An ultrasonic irradiation technique for treatment of asphaltene deposition," *Journal of Petroleum Scien*, vol. 42, pp. 57–70, 2003.
- [57] Neretin, V. D., Yudin, and V. A., "Results of experimental study of the influence of acoustic treatment on percolation processes in saturated porous media and in topics in nonlinear geophysics," *All-Union Research Institute of Nuclear Geophysics and Geochemistry*, vol. 122, pp. 132–137, 1981.
- [58] Nosov and V. A., "Soviet progress in applied ultrasonics ultrasonics in the chemical industry:," *Consultants Bureau and New York*, vol. 2, p. 1, 1965.
- [59] Johnston and H. K., "Polymer viscosity control by the use of ultrasonics," *Chem. Eng. Progr. Symp*, vol. 67, pp. 39–45, 1971.
- [60] E. M. Simkin, "Creation and industrial realization of the technology of controllable acoustic treatment for mineral production stimulation in wells," tech. rep., Krylov Research Institute of Oil and Gas (VNII), 1990.
- [61] Johnson, D.O., Edgar, D.E., Wilkey, M.L., Paulsen, P.D., and A. Greer, "âĀĬsonication stimulation of stripper well production in east gilbertown field and west-central alabama,âĀĬ," tech. rep., The Pennsylvania State University and Stripper Well Consortium,, 2004.
- [62] A. Daehnke, "Thesis stress wave and fracture propagation in rock," Master's thesis, Vienna University of Technology, 1997.
- [63] Y. Ju, L. Sudak, and H. Xie, "Study on stress wave propagation in fractured rocks with fractal joint surfaces," *International Journal of Solids and Structures*, vol. 44, no. 13, pp. 4256 – 4271, 2007.
- [64] Y. Li, Z. Zhu, B. Li, J. Deng, and H. Xie, "Study on the transmission and reflection of stress waves across joints," *International Journal of Rock Mechanics and Mining Sciences*, vol. 48, no. 3, pp. 364 – 371, 2011.
- [65] Z.-X. Zhang, "Chapter 3 - rock fracture and rock strength," in *Rock Fracture and Blasting* (Z.-X. Zhang, ed.), pp. 69 – 88, Butterworth-Heinemann, 2016.

- [66] Weinberg, Kerstin, Ortiz, and Michael, “Kidney damage in extracorporeal shock wave lithotripsy: a numerical approach for different shock profiles,” *Biomechanics and Modeling in Mechanobiology*, vol. 8, no. 4, pp. 285–299, 2009.
- [67] D. M. Newman, *Shock Wave Lithotripsy 2: Urinary and Biliary Lithotripsy*. Springer US, 1989.
- [68] Cleveland, R. O., McAteer, and J. A., *Physics of Shock-Wave Lithotripsy*, pp. 527–558. Wiley-Blackwell, 2012.
- [69] Yamaji and A., *An Introduction to Tectonophysics: Theoretical Aspects of Structural Geology*. Terrapub, 2007.
- [70] Chaussy, Christian, Schmidt, Egbert, Jocham, and Dieter, “Extracorporeal shock wave lithotripsy: a new aspect in the treatment of kidney stones,” in *Current Status of Clinical Organ Transplantation* (Abouna, GeorgeM., White, and ArthurG., eds.), vol. 5 of *Developments in Surgery*, pp. 305–317, Springer Netherlands, 1984.
- [71] O. A. Sapozhnikov and M. R. B. et al., “Advantage of a broad focal zone in swl: Synergism between squeezing and shear,” *AIP*, vol. 351, pp. 351–355, 2007.
- [72] Mota, Alejandro, Knap, Jaroslaw, Ortiz, and Michael, “Three-dimensional fracture and fragmentation of artificial kidney stones,” *Journal of Physics: Conference Series*, vol. 46, pp. 299–303, 2006.
- [73] R. O. Cleveland and J. A. McAteer, *Smith’s Textbook of Endourology*. Blackwell Publishing Ltd, 2012.
- [74] Y. A. Pishchalnikov, J. A. McAteer, R. J. VonDerHaar, I. V. Pishchalnikova, and J. C. Williams, “The characteristics of broad and narrow focal zone lithotripters,” *AIP Conference Proceedings*, vol. 1049, no. 1, pp. 238–242, 2008.
- [75] W. Eisenmenger, “The mechanisms of stone fragmentation in eswl,” *Ultrasound in Medicine & Biology*, vol. 27, no. 5, pp. 683 – 693, 2001.
- [76] Eisenmenger, W., Du, X. X., Tang, C., Zhao, S., Wang, Y., Rong, F., Dai, D., Guan, M., Qi, and A., “The first clinical results of “wide focus and low pressure” eswl,” *Ultrasound in Medicine & Biology*, vol. 28, pp. 769–774, 2002.
- [77] S. Suslick, Y. Didenko, and M. M. F. et. al., “Acoustic cavitation and its chemical consequences,” *Philosophical Transactions of The Royal Society B Biological Sciences*, vol. 357, pp. 335–353, 1999.
- [78] L. A. Crum, “Cavitation microjets as a contributory mechanism for renal calculi disintegration in eswl,” *The Journal of Urology*, vol. 140, pp. 1587–1590, 1988.

- [79] D. Lee, Koizumi, N., Ota, K., Yoshizawa, S., Ito, A., Kaneko, Y., Matsumoto, Y., Mitsuishi, and M., "Ultrasound-based visual servoing system for lithotripsy," in *Intelligent Robots and Systems and 2007. IROS 2007. IEEE/RSJ International Conference on*, pp. 877–882, Oct 2007.
- [80] Y. Matsumoto and J. S. A. and Shin Yoshizawa, "Medical ultrasound with microbubbles," *Experimental Thermal and Fluid Science*, vol. 29, pp. 255–265, 2005.
- [81] W. Sass, M. Braunlich, H.-P. Dreyer, E. Matura, W. Folberth, H.-G. Priesmeyer, and J. Seifert, "The mechanisms of stone disintegration by shock waves," *Ultrasound in Medicine & Biology*, vol. 17, no. 3, pp. 239 – 243, 1991.
- [82] Delius, M., Brendel, W., Heine, and G., "A mechanism of gallstone destruction by extracorporeal shock waves," *Naturwissenschaften*, vol. 75, no. 4, pp. 200–201, 1988.
- [83] R. Apfel, "Acoustic cavitation series: part four -. acoustic cavitation inception," *Ultrasonics*, vol. 22, pp. 167–173, 1984.
- [84] Frenkel and J., *Kinetic Theory of Liquids*. Dover Publications and New York, 1955.
- [85] E. Herbert, S. Balibar, and F. Caupin, "Cavitation pressure in water," *Physical Review E*, vol. 74, p. 041603, 2006.
- [86] Frederick and J.R., *Ultrasonic Engineering*. John Wiley & Sons, 1965.
- [87] "Standards for ultrasound equipment."
- [88] M. S. Plesset, "Bubble dynamics and cavitation," *Annual Review of Fluid Mechanics*, vol. 7, pp. 145–185, 1977.
- [89] T. Hamida and T. Babadagli, "Effects of ultrasonic waves on the interfacial forces between oil and water," *Ultrasonics Sonochemistry*, vol. 15, no. 4, pp. 274 – 278, 2008.
- [90] Mettin, R., Akhatov, I., Parlitz, U., Ohl, C. D., Lauterborn, and W., "Bjerknes forces between small cavitation bubbles in a strong acoustic field," *Phys. Rev. E*, vol. 56, pp. 2924–2931, Sep 1997.
- [91] Graham, D. R., Higdon, and J. J. L., "Oscillatory flow of droplets in capillary tubes. part 1. straight tubes," *Journal of Fluid Mechanics*, vol. 425, pp. 31–53, Dec. 2000.
- [92] Salamon, M.D.g., Orowecz, and K.I., "Mathematical analysis of the stress and displacement distributions around bord and pillar workings.," in *Proc. 1st Intl. Cong. on Rock Mechanics. Lisbon.*, 1966.
- [93] *Comparison Of Griffith's Theory With Mohr's Failure Criteria. American Rock Mechanics Association.*, The 3rd U.S. Symposium on Rock Mechanics (USRMS), 20-22, American Rock Mechanics Association, April 1959.

- [94] N. Ezekwe, *Petroleum Reservoir Engineering Practice*. Prentice Hall, 2010.
- [95] G. Survey, "The geologic basis for appraising undiscovered hydrocarbon reseources in the national petroleum reserve of alaska by the play appraisal method," *U.S. Geological Survey*, vol. 1399-1988, p. 105, 1988.
- [96] E. Fjar, R. Holt, A. Raaen, R. Risnes, and P. Horsrud, "Appendix a rock properties," in *Petroleum Related Rock Mechanics 2nd Edition* (E. FjÃr, R. Holt, P. Horsrud, A. Raaen, and R. Risnes, eds.), vol. 53 of *Developments in Petroleum Science*, pp. 435 – 441, Elsevier, 2008.
- [97] "Standard test method for compressive strength and elastic moduli of intact rock core specimens under varying states of stress and temperatures."
- [98] Mao, X. Zhang, L. Liu, and R, "Mechanical and thermal damage properties of sandstone at high temperatures," *Electronic Journal of Geotechnical Engineering*, vol. 19, p. 3137, 2014.
- [99] R. Berenbaum and I. Brodie, "Measurement of the tensile strength of brittle materials," *Journal of applied physics*, vol. 10, pp. 281–287, 1959.
- [100] M. Mellor and I. Hawkes, "Measurement of tensile strength by diametral compression of discs and annuli," *Engineering Geology*, vol. 5, no. 3, pp. 173 – 225, 1971.
- [101] M.Diederichs and G.Grasselli, eds., *Numerical modelling of a Brazilian Disc test of layered rocks using the combined finite-discrete element method; O. K. Mahabadi & G. Grasselli and A. Munjiza*, Proceedings of the 3rd CANUS Rock Mechanics Symposium and Toronto, May 2008.
- [102] Chen, C. S., Pan, E., Amadei, and B., "Determination of deformability and tensile strength of anisotropic rocks using brazilian tests," *Int. J. Rock Mech.*, vol. 35, pp. 43–61, 1998.
- [103] J. C. C. N. W. Jaeger and J. Zimmerman, *Fundamentals of Rock Mechanics*. Chapman and Hall and London, 1976.
- [104] U. R, *The ISRM Suggested Methods for Rock Characterization and Testing and Monitoring: 2007-2014*. Springer, 2015.
- [105] "Standard test method for splitting tensile strength of intact rock core specimens d3967 - 08."
- [106] F. G. Bell, *Engineering properties of Soils and Rocks*. Wil, 1999.



- [107] Knox, RW, Burgess, WG, Wilson, KS, Bath, and AH;, “Diagenetic influences on reservoir properties of the sherwood sandstone (triassic) in the marchwood geothermal borehole and southampton and england.,” *Clay Minerals*, vol. 19, pp. 441 – 456, 1984.
- [108] P. G. J. Yates, “The material strength of sandstones of the sherwood sandstone group of north staffordshire with reference to microfabric,” *Quarterly Journal of Engineering Geology and Hydrogeology*, vol. 25, pp. 107 – 113, 1992.
- [109] M. Safiuddin, H. B. Mahmud, and M. Z. Jumaat, “Efficacy of astm saturation techniques for measuring the water absorption of concrete,” *Arabian Journal for Science and Engineering*, vol. 36, pp. 761–768, 2011.
- [110] D. A. Malhotra, *Steam Property Tables: Thermodynamic and Transport Properties*. reateSpace Independent Publishing Platform, 2012.
- [111]
- [112] Polytec, “Basic principles of vibrometry.”
- [113] *CRC Handbook of Chemistry and Physics 90th*, 1978.
- [114] L. Rozenberg, *High-Intensity Ultrasonic Fields*. Springer US, 1971.
- [115] S. Netherlands, *Cavitation in Biomedicine: Principles and Techniques*. Springer Netherlands, 2015.
- [116] Neppiras and E.A, “Measurement of acoustic cavitation,” *Sonics and Ultrasonics and IEEE Transactions on*, vol. 15, pp. 81–88, 1968.
- [117] M. Hodnett, R. Chow, and B. Zeqiri, “High-frequency acoustic emissions generated by a 20 kHz sonochemical horn processor detected using a novel broadband acoustic sensor: a preliminary study,” *Ultrasonics Sonochemistry*, vol. 11, no. 6, pp. 441–454, 2004.
- [118] N. I. of Standards and Technology, “Engineering statistics handbook.”
- [119] A. Momeni, M. Karakus, G. Khanlari, and M. Heidari, “Effects of cyclic loading on the mechanical properties of a granite,” *International Journal of Rock Mechanics & Mining Sciences*, vol. 77, pp. 89–96, 2015.
- [120] Y. Ishizuka, T. Abe, and J. Kodama, “Fatigue behaviour of granite under cyclic loading,” in *ISRM International Symposium, 10-12 September, Mbabane,*, 1990.
- [121] M. Bagde and V. Petros, “The effect of micro-structure on fatigue behaviour of intact sandstone,” *Manoj N. Bagde, Vladimir PetroÁq*, vol. 2, pp. 240–247, 2011.

- [122] M. N. Bagde and V. Petros, "Waveform effect on fatigue properties of intact sandstone in uniaxial cyclical loading," *Rock Mechanics and Rock Engineering*, vol. 38, pp. 169–196, 2005.
- [123] A. W. Adamson, *Physical chemistry of surfaces*. Wiley, 1997.
- [124] Nouredдини, H., Teoh, B.C., D. Clements, and L., "Densities of vegetable oils and fatty acids," *Journal of the American Oil Chemists Society*, vol. 69, no. 12, pp. 1184–1188, 1992.
- [125] H. Nouredдини, B. C. Teoh, and D. Clements, "Viscosities of vegetable oils and fatty acids," *Journal of the American Oil Chemists Society*, vol. 69, no. 12, pp. 1189–1191, 1992.
- [126] OMeara, M., Farkas, B.E., Dungan, and S., "Determination of oil/steam and oil/air interfacial tension at elevated temperatures. paper 077-62," in *National IFT Annual Meeting and Las Vegas and NV and USA and June 25-June 28*, 2012.
- [127] A. Tuteja, "Robust omniphobic surfaces," *Proceedings of the National Academy of Sciences*, vol. 47, pp. 18200–18205, 2008.
- [128] N. A. Chang and S. L. Ceccio, "The acoustic emissions of cavitation bubbles in stretched vortices," *Journal of the Acoustical Society of America*, vol. 130, pp. 3209 – 3219, 2011.
- [129] S. R. Haqshenas and N. Saffari, "Multi-resolution analysis of passive cavitation detector signals," *Journal of Physics: Conference Series*, vol. 581, no. 1, p. 012004, 2015.
- [130] Salgaonkar, V. A., Datta, S., Holland, C. K., . Mast, and T. D., "Passive cavitation imaging with ultrasound arrays," *The Journal of the Acoustical Society of America*, vol. 126, pp. 3071–3083, 2009.
- [131] I. A. e. a. Beresnev, "Elastic waves push organic fluids from reservoir rock," *Geophysical Research Letters*, vol. 32, 2005.
- [132] A. I. Nesterenko and Y. S. Berlizov, "The possibility of cracking hydrocarbons with cavitation. a quantitative energy assessment," *Chemistry and Technology of Fuels and Oils*, vol. 43, no. 6, pp. 515–518, 2007.
- [133] V. Belova, D. A. Gorin, D. G. Shchukin, and H. MÃ¼hlwald, "Controlled effect of ultrasonic cavitation on hydrophobic/hydrophilic surfaces.," *ACS Appl Mater Interfaces*, vol. 3, pp. 417–425, 2011.